Real Time Mining (RTM)

Integration of Fast Data into the updating and estimation of resources through a portable XRF sensor

Eliane da Silva Soares

Thesis to obtain the Master of Science Degree in

Mining and Geological Engineering

Supervisors:

Prof. Amílcar de Oliveira Soares

Dr. Nelson Bruno Monteiro Ferreira Pacheco

Examination Committee

Chairperson:	Prof. Maria Teresa da Cruz Carvalho
Supervisor:	Prof. Amílcar de Oliveira Soares
Members of the Committee:	Prof. Maria João Correia Colunas Pereira

April 2018

This page was intentionally left blank.

"***Resource scarcity is also likely to encourage creativity and innovation by imposing some stimulating challenges to the economy***." ***(Van Neuss, 2015)***

This page was intentionally left blank.

ACKNOWLEDGMENTS

This thesis could not be done without the support of the people who surrounded me with their knowledge, patience and inspiration. I would like to take this opportunity to express my deep gratitude to:

Evergreen Foundation for their contribution throughout the last years in the pursuit of my graduation.

To Somincor, in special to Dr. Nelson Pacheco who welcomed me to Somincor facilities and guided me during the campaign. To the Engineers Sandra Santos, Sofia Menezes and all the professionals I met during the time I was visiting the Neves Corvo mine. Thanks for providing me with the necessary data and for your availability whenever I needed it.

To my mentor Prof. Dr. Amílcar Soares for approaching me with this emergent topic! His support helped me to answer this challenge.

To Prof. Dr. Leonardo Azevedo who was always available to help me and whose suggestions were always very straightforward.

The research team on Real Time Mining, Engineers Cristina Araújo and João Neves for their patience. You are hard working professionals and Ruben Nunes, your suggestions were always very useful.

To all the professors, staff and colleagues I met in Instituto Superior Técnico.

To my beloved ones. My mother, Delfina Carvalho, who offers me unconditional support and my grandmother, Beatriz Marques de Carvalho. For their understanding and caring.

Happily, I met a set of interesting people along these years who taught me amazing things about sharing and passion for life. To my closest friends with whom I shared good moments of joy and friendship.

To Denis de Oliveira, for his friendship during the last years. Your encouragement made the future prospect bright and light.

To the folks who had the patience to review these pages with me.

ABSTRACT

The aim of this work is to reinforce the advantages of obtaining real time data which would save significant time, effort and money, thus, allowing companies to guide operations much more quickly while making informed decisions.

The future panorama in the mining industry forecast the decrease of enriched ores and the need to access deeper mineral deposits. Thus, the coming challenges are to access depleted and deeper deposits while improving the safety standards and reducing the environmental impact.

To accomplish the proposed, this work contributes to the sampling procedures frontline while integrating the concepts of Real Time Mining (RTM) and Geostatistics applied to a portable X-ray fluorescence device (**hXRF**). The hXRF is an instrument easily managed in the field and responsible to provide a fast-geochemical analysis regarding the materials of interest at the mining stopes. This exercise was performed in the case study of Neves-Corvo Mine and it shows the advantages of considering the fast data provided by the hXRF device, which expresses a significant utility once applied between the drilling core sampling campaigns (ALL) and the face chip sampling (UGS), both herein considered as slow data providers.

To compare the fast data with the slow data, the statistical analysis for both data were performed. From the bivariate analysis, the correlation created a new dataset (hXRF2) which was a forecast of the possible data that could be obtained through the hXRF device regarding the traditional laboratorial assays reference. The geostatistical ordinary kriging algorithm was responsible for the mineral resource estimation and verified the advantages of integrating fast data in the campaigns.

KEYWORDS: Real Time Mining (RTM); Geostatistics; Portable X-rays fluorescence (hXRF**);** Slow data; Fast data; Mineral Resources estimation.

This page was intentionally left blank.

RESUMO

O objectivo deste trabalho visa reforçar as vantagens na obtenção de dados em tempo real, minimizando o tempo, esforço e custos ao permitir que as empresas operem de forma rápida, assegurando a tomada de decisões baseadas em mais informação disponível.

O futuro panorama da indústria mineira prevê a diminuição de minérios enriquecidos e a necessidade de se aceder a depósitos cada vez mais profundos. Consequentemente, o desafio que se segue diz respeito ao acesso a esses depósitos melhorando os padrões de segurança e reduzindo os impactos ambientais.

Para realizar o proposto, este trabalho vem prestar a sua contribuição nos atuais procedimentos de amostragem ao integrar os conceitos de *Real Time Mining* (RTM) e Geostatística aplicados a um aparelho de fluorescência de raios -X (hXRF). O hXRF é um instrumento facilmente manuseado em campo e responsável por prover uma rápida análise geoquímica considerando materiais de interesse nas frentes de trabalho.

Este exercício foi realizado através do caso de estudo da mina de Neves-Corvo e expõe as vantagens da aquisição de *Fast data* proporcionado pelo aparelho hXRF, o qual presta uma utilidade significativa quando aplicado entre as campanhas de amostragem através de sondagens (ALL) e de chips colhidas nas frentes de trabalho (UGS), ambas consideradas como provedoras de *Slow data*.

Para comparar os dados Fast com Slow, a análise estatística para ambos foi realizada. A partir da análise bivariada, a correlação observada permitiu a criar uma nova base de dados (hXRf2), a qual prevê os possíveis resultados que poderiam ser obtidos através do hXRF considerando-se as referências providenciadas pelo laboratório.

A estimação geostatística por krigagem normal foi responsável pela estimação dos recursos e reservas minerais, verificando-se deste modo as vantagens de integrar *Fast data* nas campanhas.

Palavras-chave: *Real Time Mining* (RTM); Geostatística, Aparelho de fluorescência raios-x (hXRF); *Slow data*; *Fast data*, Estimação de recursos minerais.

OUTLINE

LIST OF FIGURES

LIST OF FIGURES IN ANNEXES

LIST OF TABLES

LIST OF SIMBOLS AND ABBREVIATIONS

$\boldsymbol{\lambda}$	Wavelength (m)
$\boldsymbol{h}$	Plank's constant
$\boldsymbol{c}$	Speed of light (m/sec)
$\boldsymbol{E}$	Radiated energy per unit volume
g	Grams
$\boldsymbol{t}$	Tonne

A	
ALL	Drill Core Sampling Data
B	
BGS	British Geological Survey
E	
E&P	Exploration and Production (upstream) in oil and gas industry
F	
FC	Stockwork of copper
H	
hXRF	Handheld/portable X-rays fluorescence device
hXRF1	Handheld/portable X-rays fluorescence collected data
hXRF2	Handheld/portable X-rays fluorescence predicted data within the UGS coordinates
I	
ICSG	International Copper Study Group
ID	Identification
IDW	Inverse Distance Weighting
L	
LAB	Face Chip Sampling reference for the hXRF1
M	
m	Meter
MC	Massive of Copper
MCZ	Massive Copper and Zinc
MRE	Mineral Resource Estimation
MZ	Massive of Zinc
MZP	Massive of Zinc and Lead
R	
RTM	Real Time Mining
S	
sec	Second
T	
TIN	Triangular Irregular Network
U	
UGS	Face chip Sampling collected in the surrounding area where the hXRF1 was taken

This page was intentionally left blank.

CHAPTER I. THESIS OVERVIEW

This thesis was elaborated under the Master of Geological and Mining Engineering in Instituto Superior Técnico with cooperation of the Portuguese Mining Company of Somincor – Sociedade Mineira de Neves Corvo S.A. The different datasets used throughout this study were provided by Somincor.

1.1 PURPOSE OF THE PROJECT

The aim of this thesis is to contribute to the Real Time Mining (**RTM**) framework as an additional documented experiment that gives support to the Face Chip Sampling (**UGS**) and the underground Drill Hole Sampling (**ALL**) campaigns, all herein considered as Slow Data providers. Thus, this experiment lies in a sampling method for material characterization through a handheld X-rays fluorescence device (**hXRF**) that enables the acquition of Fast Data and is expected to give a reliable geochemical analysis regarding the elements of interest, copper (Cu) and zinc (Zn), at the stope mining face.

Considering the option of adding data in real time, it contributes to a short-term planning that will certainly result in a minimization of the waste material, increase the safety and promote fruitful discussions. Moreover, it would enhance the control of productivity by linking the fast modelling update and estimation of resources.

To achieve the purposed, this work was organized through two main work fronts applied to a real case study in the Neves -Corvo mine: the RTM concept, approaching the sensor-based material characterization through the hXRF device and Geostatistics as a field of science that is able to integrate the uncertainty while characterizing the natural resources phenomena.

Regarding the metals of interest, is it possible for the hXRF technique to readily identify these minerals? Can the data provide valid and accurate results? Is it a reliable tool that would contribute to a reduction in the number of samples sent to the laboratorial assays while executing the fast track of ore concentrations?

This thesis expects to obtain qualitative and quantitative considerations about the sampling technique with hXRF. The exploratory data analysis and the mineral resources estimation (MRE) was carried out through the software GEOMS developed by CERENA, Center of Environmental and Natural Resources, in Instituto Superior Técnico and SGEMS for Stanford Geostatiscs Modelling Software. To organize the data, it was also used Microsoft Excel and to obtain the parametric curves for the MRE, a numerical calculus was performed through the Matlab software.

1.2 MOTIVATION

The 2017 Revision of World Population Prospects denotes an increase in global population, approximately up to 9 billion people in 2050 (United Nations Department of Economic and Social Affairs, 2017). Hence, the fast growth in world population and the continuous technological advances require a higher mineral consumption due to the achievement of better standards of living. Reliable information revised from previous studies (Kesler, 2002) underlines that the high standards of living in developed countries overshadows the increase in world population as the main influence in this higher mineral consumption. The combination of these two factors has led to predictions of 1% total increase in global mineral demand per year. Thus, this forecast undoubtedly summarizes the reasons to expect a higher demand of commodities in the next 50 years. Notwithstanding, the future global production of raw materials may face new challenges due to the decline of ore grades. Underlying this statement is Benndorf, J. (Benndorf, J. et al., 2015) who warned of about the industry going towards highly complex settings which, indeed, is due to the depletion of known and stablished mineral reserves.

If in the past centuries the exploration and production of enriched ores and near surface mineral deposits was a relatively easy affair, in the coming future access to constrained deposits seems to be a complex long-term challenge. Thus, the uncertainties due to the geological settings and its quantification to characterize the natural phenomena requires an increased synergy between geostatistics and technology for data management, strengthening the process of resources estimation within the fast updating of data.

The industrial revolution between the 18^{th} - 19^{th} Century was dependent on the existence of a large, readily available supply of natural resources (coal, copper, zinc, iron, lead, etc.). Thereupon, the statism in the following years promoted the compilation of the national mineral production statistics by some countries worldwide such as the compiled documents provided by the British Geological Survey, BGS (Brown, Idoine et al, 2014). Since then, the mineral resources and reserves estimates have been documented, enabling an understanding of today's high-grade content deposits deficit for the coming centuries.

Regarding the metals in study throughout this project, Cu and Zn, the following references will always be considered for both metals. Indeed, they are still the second most required elements within the non-ferrous metal industry (Moya, J., Boulamanti, A., 2016).

From the primordial mineral and metal resource activities managed by the first human beings to nowadays availability of deposits, it has been a concern to balance the world's demand with the natural recovery regime performed by the Nature.

Western Europe was and still is heavily exposed to Zn and Cu imports to satisfy a wide range of industrial goods and the progress of industries and technology, most notably concerning the high- technology developments (Brown et al., 2014).

A recent study regarding the scarcity of minerals estimates the exhaustion of Zn within several decades to a century if its extraction continues at the same velocity (Henckens, Ierland et al. , 2016).However Zn is already considered to be a scarce mineral while Cu is moderately scarce since its exhaustion time is estimated to be between 100 to 1000 years. According to the same study by these authors, both exhaustion estimates are predicted to occur after the year 2050.

In 2008, the European Union stipulated a set of policies and strategies to encourage and ensure sustainable trade, fiscal transparency and to decrease the environmental impact (Eurostat, 2009). New approaches can establish a continuous commitment to accomplish a sustainable development, management and efficient use of the natural resources. Furthermore, the availability of raw materials constitutes one the main pillars to sustain the economy. For instance, at least 30 million jobs worldwide are dependent on this industry (United Nations Department of Economic and Social Affairs, 2017) .

In the future, the exploration expenditure levels over time are expected to increase due the complexity of the geological settings and the access to remote mines. Consequently, it is predictable that companies will face operational and processing equipment costs. For instance, the recovery of the low grade ores in the processing plants will generate additional costs (energy, electricity, consumables, operations, maintenance, etc.), especially considering the tonnage that are necessary to process in order to achieve lucrative concentrate standards.

If in the previous years the technology contributions created a lower cost structure of tradeoffs in a variety of fields and operations, a future increase in the demand for metals could be held by new technological proposals and ensure safety improvements under more geologically complex settings? How could we prepare the future mineral and metal industry and answer to stricter environmental and safety regulations?

The mining companies must invest in research to optimize costs of exploration, production and processing while improving the available technologies. It is urgent to continue working towards expedited analytical methods that enhance the safety and reviews the environmental conditions.

To reply to all these concerns, the European Mineral Industry is implementing the RTM framework. The RTM is exploring and validating new approaches to obtain a continuous process monitoring within the quality management system and towards highly selective mining operations (Benndorf, J. and Osterholt, V., 2015).
It aims to decrease the environmental impact while increasing resource efficiency and enhancing the onsite safety standards (Benndorf, J. and Osterholt, V., 2015). Indeed, the actual research purposes also visualize the optimization of repetitive procedures that would imply significant time for manual execution. Within the sampling procedures, the possibility of obtaining remote data acquired in real time would save significant time, effort and money. The mining companies would be allowed to guide operations much more quickly while discussing results and making informed decisions.

According to Minnitt, R. (2007), some of the main challenges to be overcome in the ALL operations:

- The loss of sample (cuttings) in the hole, or while the collection is taking place, may lead its results to be based on unrepresentative samples,
- The hidden costs from the sampling errors evolve the loss of a significant percentage of the financial input (Figure 1),
- The time needed between the measurements and the report of the results, leading in a delay of the decisions to be taken.

The author also referenced the optimization of costs within the drilling hole sampling campaigns stablishing an optimal point where the marginal gains in information through additional drilling does not compensate the extra cost (Figure 1). Here, the additional data provided by the hXRF could provide a valuable support.

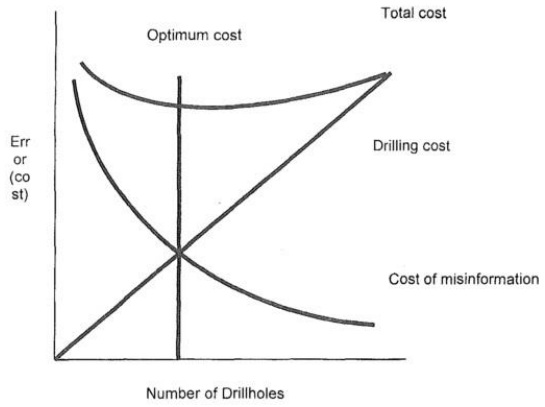

Figure 1 - The cost of drilling and the cost of misinformation at the optimal number of drill holes (Minnitt, R., 2007).

Herein, is tested the viability of the hXRF for data acquisition while measuring the content grades of copper and zinc directly at the stope face. Then, is evaluated the introduction of the Fast data to support the Underground Drill Hole Sampling campaigns saving the time, driving the operations more efficiently, preserving the safety standards, minimizing the expenditure levels, increasing the profitability and avoiding the generation of waste material (Figure 2).

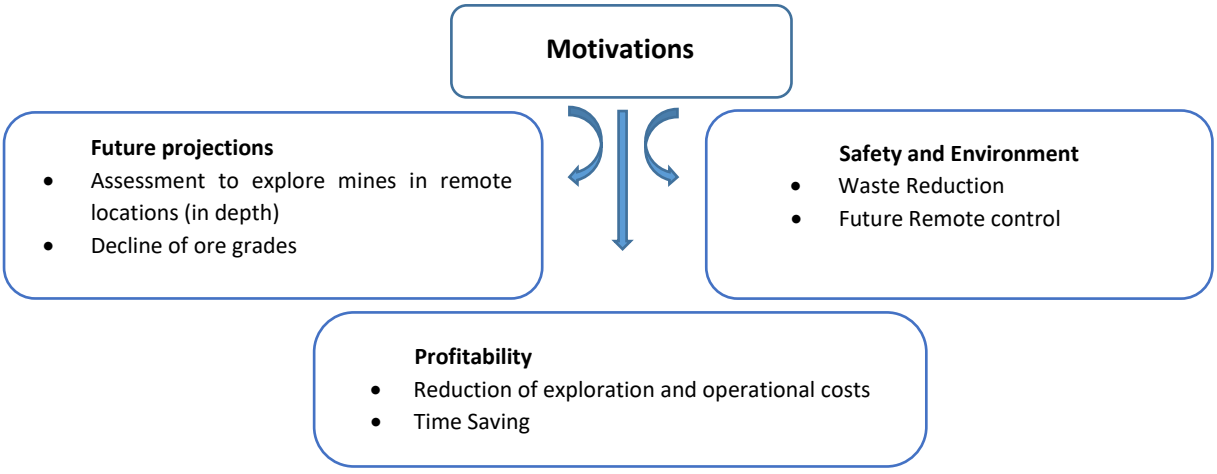

Figure 2 - Schematic Representation of the motivational aspects.

1.3 STRUCTURE OF THE THESIS

The framework for this thesis is basically divided into two major parts. **The first one** integrates the Chapters I, II, III and IV and addresses the topics of study as well as the respective theoretical concepts and tools for the further development. It also includes the presentation of the real -case application and the description of the various types of data. **The second part** deals with the discussion of the results and presents the advantages while using hXRF to support the underground drilling campaigns. Finally, it comprises the conclusions and suggestions for the future works that could be possibly done.

Chapter I – Introduction

The Chapter I presents the scope that led to this research project and the purposes to be achieved.

Chapter II – State of art

The Chapter II provides the state of art covering the RTM concept and the background on geostatistics and how it deals with the earth science data, specifically within the problematic of nature phenomena. Then, the review on the portable X-ray fluorescence equipment is performed: the instrumental and analytical considerations as well as the documented studies using this type of equipment. Finally, it covers the resources and reserves classification.

Chapter III – Methodology:

The Chapter III describes the adopted framework to organize and execute the appropriate tasks towards the problematic herein presented. It also introduces the various types of data that were integrated within the study and its treatment. Finally, it presents the NITON XL3t 600 device which was the equipment used in the previous campaigns and throughout the campaign carried out for this work.

Chapter IV – Real - Case Application:

This chapter introduces the real- case application to the Neves-Corvo Mine. It is reviewed the Neves COrvo geological and mineralization settings. This chapter also describes the data provided by the geological department (Slow data) and the generated data from the hXRF (Fast data).

Chapter V – Discussion of the results

The Chapter V covers the representative sampling data collected through the hXRF device, which was integrated in the GEOMS and SGEMS softwares for the statistical analysis and geostatistical estimation. It is presented the uni, bivariate analysis and the spatial variability. Then, it is commented the output results from the ordinary kriging estimation process and the obtained recovery curves by average content grade/ cut-off, tonnage/cut-off and metal content/cut-off. It also includes an analysis of the recovery curves given by the sampled data by the same parametric functions.

Chapter VI – Conclusions

This chapter presents the final remarks, summing up an overall view of the study. In addition, the recap of the strengths and limitations that covered this project will also be discussed. Then, it is presented the conclusions based on the comparison between both sampling procedures: the Fast Data given by the hXRF device and the Slow Data given by UGS and ALL.

Chapter VII – Way Forward:

It is suggested the possible future works and the considerations to be taken in the future approaches regarding the automated sampling method for material characterization through the hXRF devices.

CHAPTER II. THEORETICAL APPROACH

Sinclair and Blackwell described the technological investments and the drill planning of the production targets as reliant variables for a good approach to the mineral features. Thus, the estimate on the best ore grades and its locations (in situ resources) must be known with an acceptable degree of confidence(Sinclair & Blackwell, 2004).

The inclusion of the uncertainty must be integrated along the process of MRE due to its influence on the acknowledgment of the distribution grades, volumes and some other constrains such as the selection of the best recommended equipment (Emery, Ortiz et al., 2004). Accordingly, it is imperative to forecast its overall impact within the financial model structure of any project. Hence, the confidence of the stakeholders within the mining investments are conditioned to a competent classification of mineral resources and reserves.

Throughout this thesis the concepts of Real Time Mining (RTM) and Geostatistics aim to produce results regarding the fast upgrading of resources. Therefore, to conceptualize the proposed exercise a legit literature research was performed.

The state of the art first stresses the paradigm shifts on RTM through the projects that have been studied and executed throughout the last three years. Then, it includes the application of the handheld x-rays fluorescence device (hXRF) to obtain the elemental geochemical analysis for the fast upgrade of resources, providing henceforth a better understanding of the methodology herein used.

2.1 REAL TIME MINING (RTM)

In the future onward, it is expected to find new ways to extract the ore towards the minimization of the environmental impact on mining operations. The European Project on RTM emerged in the year of 2015 sponsored by the European Union's Horizon 2020 research and innovation programme (Benndorf, J. and Osterholt, V., 2015).

Concerning the underground mines, to list some of the main challenges to be developed:

- Accurate real-time localization through positioning systems,
- To reduce unnecessary energy consumption expenditures,
- Material's track through the management of large number of tags and the autonomous operation of vehicles and machines,
- Better effective material characterization methodology with fast upgrade to the system,
- Optimization of the resource and reserve estimation process.

After solved and implemented, these different work fronts could be also storage in a virtual system that would be extended to all over the mine (Fisher & Schnittger, 2012). The RTM framework (Figure 3) includes in-time feedback control loop that rapidly links online data acquired from material handling, its extraction at the mining face to the further processing, considering a sequentially up-datable resource model. This will allow a better managing and optimization on decision making from the short-term sequencing and production control to the long-term planning (Benndorf, J., 2016, realtime-minig.eu).

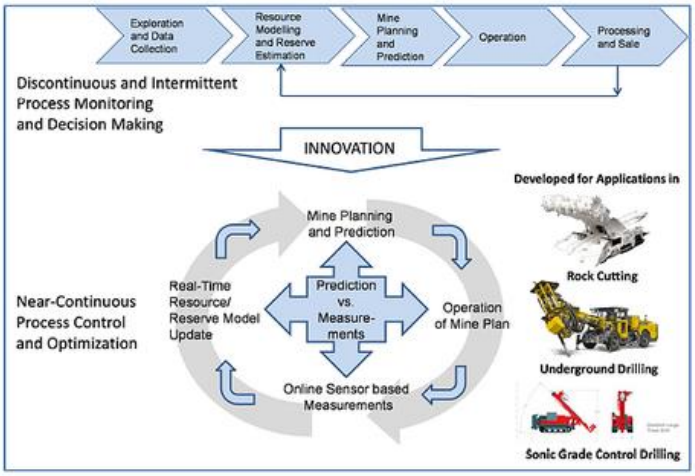

Figure 3- RTM framework (Benndorf, J., 2015).

The hXRF device could present a significant utility once applied in remote locations where the given safety conditions to access certain ore type deposits are especially highly constrained for human activities. Projects of such challenging constrains are associated to costly economic variables and the application of material's characterization through these devices prevent the operator to be exposed for long periods of time in risky conditions. Furthermore, it would be able to cover more stopes within the mine and it could be remotely operated considering its consistent development towards the future technological panorama.

The ability to incorporate online sensor data derived from the production process into the upgrade of resources or reserves integrates a subsequent optimization of short-term planning and production control in which the decisions may represent a large potential for improvement at any given type of mining operations (Benndorf J. and Soares A., 2016).

According to the RTM project two space environments are being tested under the RTM working model: the Neves-Corvo Mine located in Alentejo (Portugal) and Reiche Zeche Mine in Freiberg (Germany). The research phase aim to achieve the technology readiness (TRL) level 7 from the NASA scale, which requires a demonstration of the system prototype in a space environment (Benndorf, 2015; nasa.gov).

2.1.1 Mine Automation and Positioning Systems

The new generation of the automation systems applied in the mining operations can provide mapping and monitoring in underground or under water sites, opening a new cost-effective opportunity and gathering important data from these environments (Thrybom et al., 2015; Freiberg,B. et al., 2017).

The future conditions, forecast the need to access hazardous small deposits within extreme conditions where the autonomous systems will play a privilege role. Furthermore, the mining activity relies on the development of high availability of truthful positioning systems. Taking an example of *The Underwater Explorer for Flooded Mines (UNEXMIN*) on the RTM framework, this project aims to develop a multi-platform robotic system for the autonomous exploration and mapping of flooded underground mines. However, to bring new geological data that could not be obtained through other methods and with no significant costs and safety risks, some other drawbacks are also included such as the risk of damaging the equipment or the mine itself (Lopes L., 2017).

The future demands for underground loaders and trucks equipped with sensors that are able to integrate a vehicle's monitoring system as well as for innovative remote-control systems, increasing the efficiency and enhancing the production. Some of the ongoing projects addressed by Fisher B. (Fisher & Schnittger, 2012) in the *Autonomous and Remote Operation Technologies in the Mining Industry* use an extensive application of positioning systems. As examples, it was presented the El Teniente Mine placed in Chile and the Kiruna iron ore mine in Sweden.

El Teniente projected mine control rooms that are located 50 km from the mine and nearby the city. From the mine control rooms is possible to operate remotely the LHD's traffic flow within the mine. More specifically, one remote operator can control three LHD'S in the various operations. For this type of projects, an extensive wireless network is required for the monitoring and communication between the various integrated operations in order to maximize the benefits and minimize costs (Fisher & Schnittger, 2012) .

Karas H.(2015), presented a study stressing the percentage of the improvement potential after introducing a Mining Operational Center (between 10-20%) and by applying autonomous machines (40-80%) in 24 hours of execution (Figure 4).

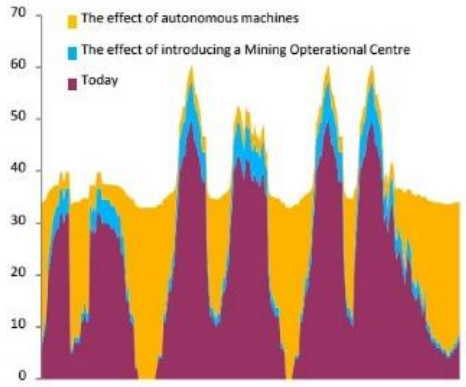

Figure 4 - Improvement potential through autonomous machines and introducing a mining operational center (Whlquist, H., Mobilaris AB Sweden).

The development of autonomous machines in the industry results in a substantial and continuous investment. However, it must be considered the long-term timetable for the automation systems maturation, which evolves a considering time interval until their implementation.

2.1.2 Personnel and safety

The mining companies struggle to remove people from hazardous areas and still increase the safety standards for their personnel, while working towards an optimization of time and productivity (Thrybom et al., 2015). Health and safety has been a major concern since the late 18th - 19th Century due to the industrial revolution and as consequence of more activity in an industrial scale.

Although some authors confirm that fatalities have decreased since the beginning of the 20th Century, the major number of fatalities occurs in underground mining related activities. The rates of injury, occupational respiratory diseases such as pneumoconiosis and fatal accidents remains significant.
Nowadays, the present regulation from the respective authority stresses how important is to improve the workforce safety on hostile mining environments. Thus, the safety is placed in the frontline as the main concern while executing the various mining operations. Some of the main hazardous environments that represents very dangerous situations for the workers are presented as it follows.

- The visibility within the underground sites due to the blind spots,
- The interaction with very large and industrial equipment either these are parked or moving,
- Exposition to gases and dust,
- The extreme temperatures and lack of natural ventilation,
- Height exposition,
- Failures of pillars and the possibility of unexpected rock falls, since the removing of material in the earth crust creates voids that may produce non- expected reactions,
- Explosions, chemicals handling, etc.

The development of the autonomous machinery and the application of the real-time framework through the positioning system assures better safety standards within the mining operations. Future intelligent systems will optimize the ventilation features according the number of equipment and personnel working in each site of the mine. To control the rock mass behavior, new systems are developed for monitoring through sensors in real-time. Also, there is new systems of rock bolts absorbing the rock mass energy and reducing the collapses of stopes (Charles, C. 2017).

Some other systems like the automated process of blasting, robot's explosives handling or the automated systems on drilling equipment provides support with an accurate precision at each mining site or drill rig location (Ficher, B., Schnittger, S.,2012.

Taking the example of La Herradura gold open pit mine in Mexico, anti-collision systems in real time were added in each vehicle to avoid accidents which optimizes the traffic within the mine in a more effective way. The operators are alerted to the presence of any other type of vehicles in the surrounds and within a certain radius of influence (Soares, E., 2017). Finally, the future trends are also towards the cyber security. The systems need to be developed with robustness since this field evolves the integrity of the personal and other conflicting interests in a mine (Thrybom et al., 2015).

2.1.3 Material characterization and Fast Data acquisition

As known, the distribution of the valuable minerals throughout a full rock mass is not uniform since they are commonly segregated or characterized by discontinuous or narrow patrons. To achieve better representativeness, the best solution would be to analyze samples in tonnage so a big part of the full rock mass could be evaluated, of course this is not possible. Despite this, some situations require the obtaining of reliable information which takes more than collecting a few samples due to the hidden costs of sampling errors (Minnitt, 2007). To overcome this challenge is presented one way to get a large quantity of information that can be added to the traditional sampling procedures and provide sufficient information for the validation of the deposit.

To plan a drilling program, it is defined the total number of drills that better insure representativeness. However, this may be very expensive. Furthermore, it is common to not achieve the desired number of samples due to financial constraints, for example, if the budget is not flexible enough to cover possible technical damages and loss of the bit. Hence, considering these types of Slow Data and the day intervals between the previous results given by the previous drilling campaign in day 1 until the next campaign to be executed in 10 days, how many quantities of information could be provided through the hXRF between? Herein, it is considered that the acquisition of the data in a readily format through the real-time upgrade with hXRF (Fast Data) from day one to tenth day, might provide additional information once compared with the drilling sampling data outputs (Sow Data).

2.2 PORTABLE X-RAYS DEVICES

The X-ray spectrometer is a fast and non-destructive measurement technique applied, among other areas, to sampling methods. Through a chemical analysis is possible to have an overview of the constituents present in a sample within a ppm order. Kelsey E. et al. (2016) referred the portable XRF instruments (hXRF) as viable devices that produce a reliable geochemical analysis during field mapping exercises. Its results are comparable with the traditional laboratorial X-ray assays. Regarding its limitations, the portable instrument has been constantly developed to solve a variety of operational needs.

The beginning of the developments in the laboratorial X-ray fluorescence spectrometers have origins in 1895 with the first discovered X-rays by Wilhelm Conrad. His first applications were directed to natural sciences and medical treatments. Later in 1948, Abbott built the first commercial X-ray fluorescence spectrometer based on the Freidman and Birk's work (Beckhoff, B. et al., 2006). Nowadays, a variety of X-rays instruments have been developed for measuring purposes and have been constantly improved to provide better accuracy. There are plenty of fields exploring the portable XRF instruments in order to optimize the operational strategies and gain the maximum information on qualitative chemical data.

The hXRF devices were applied in large compositional multi-element geochemical data set analysis on planetary investigations, specifically in Mars remote operations (Kelsey E., Evans C. et al. ,2016). The improvements over the past decades enabled the portable XRF to be functional in biology, industrial applications (production settings), quality control under alloys manufacturing, controlling the nature of scrap metal, analyzing artifacts, drill rigs under upstream E&P, environmental pollutants studies, ore grade control and geometallurgy (Gazley M. and Fisher L. ,2002).

In the previous years, the X-rays fluorescence (XRF) manufacturers increased the mobility of this type of equipment extending its application within the mining related activities. The ability to make an objective assessment and take a decision depending in the traditional framework can take days to months through a commercial laboratory while the sample is being prepared, analyzed and the results are divulgated (Brand, N. and Brand, C., 2014). Although, the hXRF instruments have limitations to overcome. The further improvements will allow the extended use of this type of data collector into the real-time purpose.

A study from Thermocientif (2013) documented an experiment while testing the hXRF analyzer, which showed up to 95% of correlation between the data and the laboratorial fluorescence assays procedures for Mn-Fe elements in mining exploitation. According with this study, these devices are reliable tools to analyze any type of sample either in the exploration stage or in the ore granding stage.

Somarin A. K. (2013) studied the data acquisition from the hXRF Niton XL3t GOLDD device to measure Molybdenite (MoS_2) concentrate samples, which generally contains between 25 to 65% of Mo. To evaluate the accuracy of the data, the calibration curves were plotted based on known values of the concentrations given by the laboratory. The result has shown correlation between the hXRF instrument and the laboratorial

data references while stating a coefficient of determination,R^2, about 97%, 99% and 97% regarding the values for Mo, Cu and Fe respectively. The author also specified that due to the wide range of the limit of detection intervals, LOD, it is possible to analyze either low or high ore grades.

In 2014, Brand, N.W., and Brand, C.J., presented a study comparing the performance of hXRF instruments within the mineral exploration industry perspective. The study compared their precision and limitations while measuring the same elements between multiple units from the same manufacturer and between similar instruments from different manufacturers. The results obtained from different manufacturers units were shown as consistent and the margin of the errors fell around 10% of the measured values. Furthermore, the precision between the units from the same manufacturer was presented as uniform, despite the small variations induced by operational issues.

Marques, R. (2016) presented a real case study towards the ore quality control and the allocation of mined blocks in a limestone mine using an hXRF device. The author stated some benefits such as the reduction of the waste material, production costs minimization and the increase of profitability.

2.2.1 Equipment's Introduction

The handheld XRF excites the atoms composing a sample while discharging X-rays. In its turn, when the ionization of the atoms is occurring, the ejection of one or more electrons from the sample's inner atoms orbital is induced. The structure of the atom is instable and the electrons within the sample move from the higher to the lower orbitals to fill the empty place left. Then, it produces energy that is equivalent to the difference in energy between the two electronic orbitals, this process is called fluorescence. The instrument is composed by the X-ray tube and the detector (Figure 5), both specifically developed to deploy the instrument in the field (Beckhoff, B. et al.,2006).

The released rays from the sample's composition are captured by the detector and evaluated by the instrument's hardware. The detector generally uses a silicon drift configuration with a sufficient area and resolution to distinguish between the broader X-rays peaks as well as to detect and measure lower energy X-rays (Longoni et al., 1998).

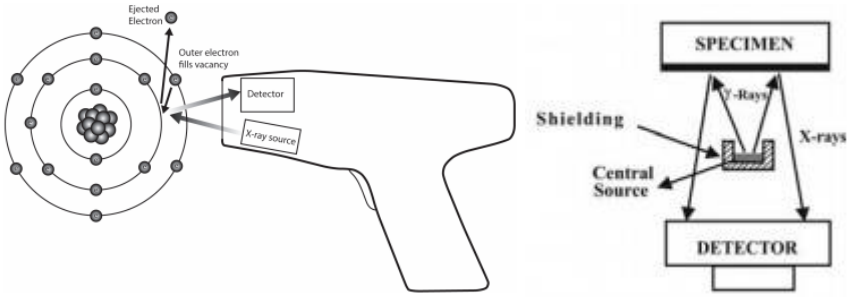

Figure 5 - a) Illustration of the hXRF analyzer b) Geometry applied in radioisotope-induced XRF analysis using X-ray tube or central source (X-ray Fluorescence (XRF) and Particle - Induced X-ray Emission (Gasley, M., and Fisher, M.,2002).

The characteristic wavelength or energy produced by the difference between the energy of the initial and final orbital is calculated through the Planck's Law:

$$\boldsymbol{\lambda}\,(\boldsymbol{m}) = \frac{\boldsymbol{hc}}{\boldsymbol{E}} \qquad \textbf{(2.1)}$$

Where $\boldsymbol{h}$ is the Plank's constant $6.626 * 10^{-34}\, J/\, sec$, $\boldsymbol{c}$ is the speed of light $2.997925 * 10^{8}\, m/\, sec$,and **E**, the radiated energy per unit volume in the wavelength interval$\boldsymbol{\lambda}$.

2.2.2 Instrumental and analytical considerations

To begin a campaign is important to outline a few procedures. Some of the main factors to be considered before and after the readings are herein reviewed.

The following factors may impact the reliability of the data: the unit's window, the short and long-term drifts, calibration, the origin and nature of the standard reference material, the format of the sample against the unit's window (flat or curved surface), the representativeness of the sample, the humidity content (dry or pulverized), the thickness of the sample being analyzed (in the case of using a sample container) , the reading time, the chosen locations for the campaign, the chip sample identification (whether the analysis is collected from cores, pulps or hand specimens) and the further treatment of the data under appropriate statistical analyses.

The traditional laboratory assays are made through approximately 50-100 W of energy against the lower power available in the portable x-ray instrument. This may affect the precision due to the decrease of the signal which has a very important influence in the beam energies and the returning secondary X-rays, as well as in the possible gaps within the detection and the measurement of lighter elements (Longoni et al., 1998, Gazley M. and Fisher L., 2002).

Generally, the precision of a measurement through X-ray technique can also be predicted by the intensity of the beam. As an example, an accumulated intensity of 1,000 000 counted x-ray photons may reach a standard deviation of 0.1%, while 100,000 000 counts 0.01% of standard deviation (Brand N.W., Brand C.J., 2014).

The accuracy of an instrument is determined by the calibration procedures and the quality of the standard materials. To enhance the accuracy of the measurements is recommended to prepare the samples and consider the duration of readings, which can vary from site-to-site conditional on the purpose of the campaign (Brand, N. and Brand, C., 2014). The yield of a greater accuracy depends on the characteristics of the site, its material composition and respective need for bulk media preparation (ex-situ) to obtain more homogenous particles. Considering this, there is a specific sample protocol for preparing and testing samples that must be followed to obtain the best comparison towards the laboratory results (Niton user's guide).
The differences between the types of material being tested considering different degrees of heterogeneity affects the accuracy of the results. Despite this, the results (considered as approximations) from *In situ* analysis and regarding an heterogeneous type of material may express a good correlation.

Gazley M. and Fisher L., (2002) also demonstrated the meaning of the short-term analytical drift given from the portable X-rays fluorescence through the following Figure 6. First, the results were collected and then the analyses were repeated at a constant temperature showing the types of analytical drift within the data.

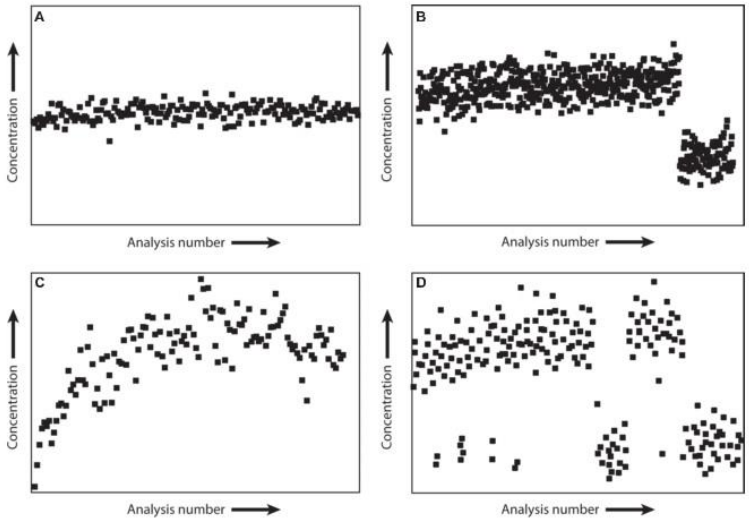

Figure 6 - Examples of short-term analytical drift: A-Ideal data, B- Change potencially caused by the sample moving or step change in the internal calibration of the device, C- Gradual drift after start-up of the unit before it is warmed up, D- Random flutuation (Gazley, M., Fisher, L., 2002).

Some of the drift patterns can be caused by the increase of the unit's internal temperature**.** Subsequently, some elements readings may increasingly be overrated and others underrated. Is less likely the occurrence of this in new devices since they are now equipped with thermometers and can integrate autonomous corrections into the software and its hardware. In addition, the switching of batteries in the unit and its restandardization may produce a random fluctuation between two values not easily detected when the analysis is running. However, this can be identified through a routinely analysis of the standards (Gazley, M., Fisher, L., 2002).

Concentrating now on the energy released as an individuality of a given element, it is stressed that certain pairs of elements present peaks that overlap each other. Although, this is not the case considered within this thesis since it is applied to certain elements such as e.g. As, Zn, Ba, Au and Fe.

Other instrumental and analytical consideration is the instrument's window which may have the size of $1cm^2$. It means that each measured point is an average read through that available small surface area (Figure 7).

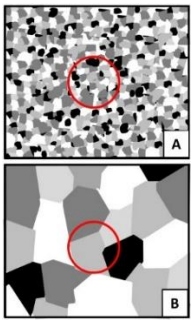

Figure 7 - Example of the sampling analysis through the hXRF device regarding different granulometries from the rock matrix (Gazley, M., Fisher, L., 2002).

Furthermore, there are limitations regarding the X-rays penetrations since they are not able to penetrate more than the material in the surface of the stope. Some other factors, such as the humidity, may affect the readings. Because the sample to be analyzed in situ is not completely dry, the X-rays electromagnetic waves are attenuated producing an underestimation of the true values. The humidity factor in the field should be considered, however, it is possible to apply a post-processing correction or stress the need for a further verification sampling.

Finally, if the hXRF device readings were obtained from the sample's container, an analysis of the SiO2 indicates the influence of contaminants derived from the plastic bags. The most known elements presented in the sample containers are Cu, Zn, As, Zr and Ca. This factor may be corrected subtracting any added concentrations presented in the dataset.

2.3 EXPLORATORY DATA ANALYSIS

The basic descriptive statistical data analysis is the first approach to characterize an ensemble of samples. Statistics is a powerful tool to explore the overall data collection (Rossi, M.E. et al. ,2014) before to perform the MRE. The data collected by the hXRF was organized and interpreted before proceeding with the geostatistical kriging estimation process. The next pages describe the adopted parameters to better characterize the obtained distribution of populations through the hXRF datasets.

The uncertainty is due to the incomplete knowledge from the observer rather than an intrinsic property of the geological systems (Olea, R., 2008). The search for summary information on the attributes of interest underpins the need to do a first approach through the characterization of the distribution functions. Also, the graphical user interfaces from modern computers such as the histograms, box-plots and scatterplots optimize

the extraction of significant information data. To analyze the data ensemble provided by the hXRF device, the statistical concepts of maximum, minimum, mean, outliers, standard deviation, variance, percentile were approached. Under the RTM update, after the automated sampling procedures the new information would be integrated into the system by adding the new statistical parameters.

The dataset is divided into k subsets with the continuous acquisition of data regarding a certain region. The total count of k subsets or the sum of data follows the Equation 2.2:

$$\sum_{i=1}^{n} \boldsymbol{n} = \sum \boldsymbol{n} \tag{2.2}$$

As known, the mean and the standard deviation are described by the following equations 2.3 and 2.4:

$$\boldsymbol{\mu} = \frac{\sum_{i=1}^{n} \boldsymbol{x_i}}{\boldsymbol{n}}, \tag{2.3}$$

Where $\boldsymbol{\mu}$ is the simple mean, $\boldsymbol{x_i}$ represents the sample data "$\boldsymbol{i}$" value, n the total number of samples.

$$\boldsymbol{\sigma} = \sqrt{\frac{\sum_{\mathbf{i=1}}^{\mathbf{n}} (\boldsymbol{\mu} - \mathbf{x_i})^2}{\mathbf{n}}}, \tag{2.4}$$

Where $\boldsymbol{\sigma}$ is the standard deviation. The high value for the standard deviation represents a wide spread of data from the mean, whilst a low standard deviation indicates a low dispersion of data points, thus, a better alignment with the mean (Olea, 2008). The variance (Equation 2.5), which is represented as $\boldsymbol{\sigma^2}$, also gives information about the dispersion of values around the mean.

$$\boldsymbol{\sigma^2} = \frac{\sum_{\mathbf{i=1}}^{\mathbf{n}} (\boldsymbol{\mu} - \mathbf{x_i})^2}{\mathbf{n}} \tag{2.5}$$

To better characterize the distribution of the data set, the outliers are frequently eliminated to “clean” the population from discordant values. On the other hand, another option is to work within these values because they express pertinent information about the subjacent population’s characteristics (Geostatistics notes, 2015).

The bivariate analysis presents an understanding about the correlation between two or more distributions. As an example, applied to this project, the bivariate analysis comprises the correlation between the data obtained from hXRF towards the laboratorial results (LAB) when measuring the grades of Cu and Zn. Graphically, this information is presented through the scatterplot and it is possible to retrieve the correlation coefficient from the linear regression. The Pearson correlation coefficient indicates a stronger correlation between the variables if the value is close to 1 whereas it shows a negative correlation if it is close to –1. Values around 0 indicates no existence of correlation (Geostatistic notes, 2015). The linear regression is represented by the following equation 2.6:

$$Y = mx + b, \tag{2.6}$$

Where Y and x are values of the data, which are represented in the y and x coordinate axis, m represents the slope of the linear regression and b is a referenced value on the **y** axis.

2.4 DETERMINISTIC METHODS FOR SPATIAL INFERENCE

Isaaks et al. (1989), stressed the ineffectiveness from the most classical statistical methods within earth science data sets due to their limitation to use the spatial information. The author also referred to the analysis of earth science data, as both frustrating and fraught with difficulty when it is necessary to incorporate spatial correlation and uncertainty.

2.4.1 Thiessen Polygons (Dirichlet or Voronoi diaframs) or the nearest neighbor method

In this approach, each polygon is centered in its sample data value. This is equivalent to say that all points within the polygon undertake the same data value as the sample point, meaning that each point has the same data value as its nearest sample point. This technique is applied to very dense grids of samples or under global estimations where the weighted averages are proportional to the polygon's area (Soares A., 2006).
Burrough and McDonnell (1998), demonstrated the use of the Thiessen polygons method to map the zinc content on a floodplain soil (Figure 8).

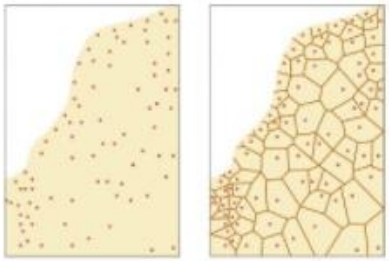

Figure 8 - Location of the sample data points and Thiessen Poligons (Adapted from Burrough and McDonnenell, 1998).

One of the main disadvantages from the estimation is the rough approximation of boundaries between two measured samples.
In the case of spatial continuity intrinsic to the attributes as it is observed in rainfall studies, Tobler, W. (1979) introduced another interpolator namely pycnophylactic interpolation which smooths the variation in the critical limits by converting the original data to a density function.

2.4.2 Triangular Irregular Network (TIN)

In this method, the area of the study is divided by triangles in which each vertice contains one sample data value. In its turn, to estimate non-sampled locals the weighted average is processed between the 3 vertices of the triangle containing the point (Figure 9). This technique is more accurate than the previous one since 3

sample points intervenes in the local estimation based on the plane equation defined by the vertices (Soares, 2006).

Some advantages of the TIN method against some deterministic estimation methods is the possibility of performing many functions (floodplain delineation, storage-capacity curves, etc.) or incorporating other survey data.

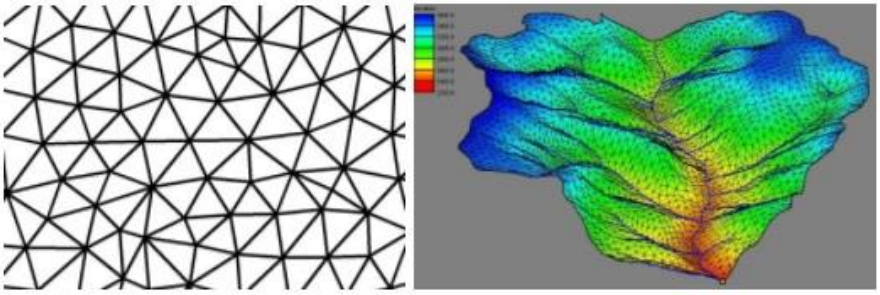

Figure 9 - TIN Method applied to a study on watersheld in Yellowstone National Park (Shaw, E., 2008, AQUAVEO).

2.4.3 Inverse distance weighting, IDW

This technique estimates the value for each point by calculating a distance weighted average of the points within a determined radius depicting a gradual change of the trend surfaces (Burrough and McDonnell, 1998, Soares A., 2006). The inverse distance is elevated to an exponent that represents the influence from the sample nearby the point to estimate. The following Equation 2.7 describes the estimated point, z using IDW:

$$z = \frac{\sum_{i=1}^{N} \frac{\mathbf{1}}{\boldsymbol{d_i}^2} \boldsymbol{z_i}}{\sum_{i=1}^{N} \frac{\mathbf{1}}{\boldsymbol{d_i}^2}}, \qquad \textbf{(2.7)}$$

Where $\boldsymbol{d_i}$ are the distances between the known points from the data, $\boldsymbol{x_i}$, to the point for estimation, $\boldsymbol{x_0}$.

Among others, one of the limitations of the IDW method respects to the grouping of samples, or the presence of clusters. The previous methods of Thiessen Polygons and TIN, do not provide envisaged estimators whilst IDW tends to produce the same weight to the sample located within the cluster and the sample displaced in an isolated point.

However, an advantage is the integration of the different distances into the estimation despite ignoring spatially privileged directions of continuity. This method is undesirable for certain case studies, thus, it is needed to investigate the advantages beforehand.

2.5 GEOSTATISTISTICS

An important contribution of geostatistcs is the assessment to the uncertainty derived from the unsampled values and locations (Goovaerts, 1999). The uncertainty due to the lack of knowledge on natural resources in its extended amplitude leads to constraints when only sustained by the determinist models. The natural resources display different levels of variability and the more it is shown, more uncertainty is associated.

The geostatistical method that is commonly applied to estimate ore resources and reserves was determined by Georges Matheron (1965) through the conceptualization and estimation of regional variables in his publication *"Les variables régionalisées et leur estimation"* (Matheron, 1971; Sinclair & Blackwell, 2004).
In *"The theory of regionalized variables and its applications"*, Matheron (1971) classified the regional variable as an irregular function incorporating 2 fundamental concepts, randomness and structure, due to the origin of the data which is collected within the natural phenomena**.** Thus, geostatistics integrates the spatial structured inference from the regionalization but also the unpredictable variability attached in the variables of study. Between two nearby points with opposite grades, it is possible to observe a gradual transition between the grades after the estimation process.
From the continuous research, geostatistics has evolved from inconsistent applications towards a successful practical utility in the areas of science (Isaaks, 1989). Nowadays, its models are widely used between the mining and oil & gas industry, hydrogeology, soil, ocean and environmental sciences. In the 1980s, the method become popular for oil reservoir characterization due to the lack of the well data (Azevedo, L. and Soares, A., 2017).

Geostatists provides descriptive tools such as the **semivariograms** or as commonly known, the experimental **variograms**. The latest, characterize the spatial pattern of the continuous attributes.
Various interpolation techniques within the estimation process known as kriging, take advantage from the spatial correlation between observations to attribute values at non-sampled locations while using information related to one or other several attributes. Thus, under a discreet and very limited source of data is possible to describe the spatial patterns and build the respective models integrating the uncertainties, which must be quantified to better characterize the natural phenomena.

2.5.1 Variability and variograms

The geostatistical models have been solving different practical problems of natural resources. They lead geostatistics to the next level within the monitoring and sampling methods.
The geostatistical study of the natural phenomena uses the spatial variability towards the metal grades dispersion and is represented by the function $f(x)$ and $f(x+h)$, which represents the measures on site in x and $x+h$ coordinates. The latest functions run the spatial patterns to find the best directions of continuity

and to determine the structural anisotropy. The variograms along different directions within the ore deposit display variations that could mean, as an example, the change in the lithology or other geological features.

Firstly, the experimental variograms are defined and then the estimation follows the interpolating process extending its correlation within the area of study. Expectedly, it is possible to verify the locations characterized by rich grades regarding the minerals of interest.

The variography evaluates the variability of the data set F(X) through a variogram, or also called semi-variogram, represented by the following equation:

$$\gamma(\boldsymbol{h}) = \frac{1}{2N(\boldsymbol{h})} \sum_{\alpha=1}^{N(\boldsymbol{h})} [Z(\boldsymbol{x}_\alpha) - Z(\boldsymbol{x}_\alpha + \boldsymbol{h})]^2 \qquad \textbf{(2.8)}$$

Where $N(\boldsymbol{h})$ is the number of pairs of points for a certain distance,$\boldsymbol{h}$, $Z(\boldsymbol{x}_\alpha)$ is the value of the property measured in the local of study and $Z(\boldsymbol{x}_\alpha + \boldsymbol{h})$ the value of the property measured in a distance $\boldsymbol{h}$ from$Z(\boldsymbol{x}_\alpha)$.

To process the experimental variograms, the following parameters expressed in the Figure 10 (bidirectional reference) are tested by the user: azimuth, $\boldsymbol{\theta}$, inclination, ∅, tolerance for a certain radius, $\boldsymbol{R}$, distance between points, $\boldsymbol{h}$,interval amplitudes, $\boldsymbol{Lag}$, nugget, $\boldsymbol{C_0}$, sill, $\boldsymbol{C_1}$.

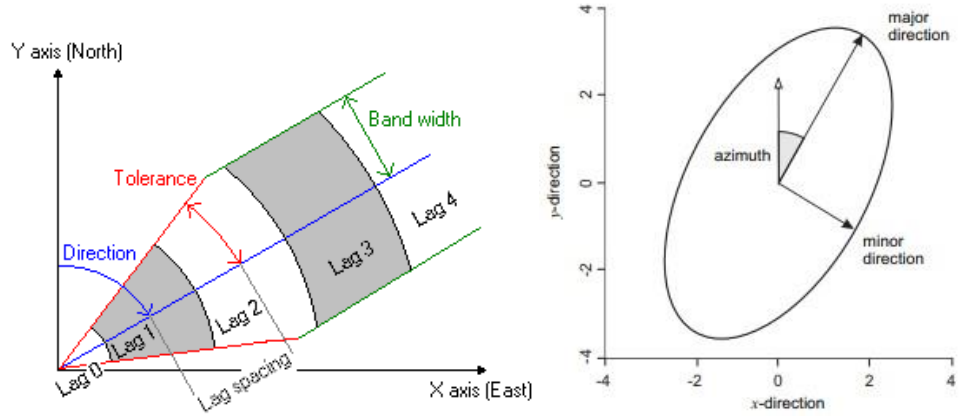

Figure 10 - Schematic representation of the variogram parameters in a bidirectional method (Hengl et al., 2009).

Correlogram

The correlogram is a normalized function from the covariance. It represents the **correlation coefficient** (Pearson's correlation) in a function of $\boldsymbol{h}$ .Its equation describes the degree of dispersion, or continuity between the pairs of points to better understand the behavior of the property (Hengl, Minasny, & Gould, 2009). The following illustration (Figure 11) describes the relation between the variogram $\boldsymbol{\gamma(h)}$, and the covariance $\boldsymbol{C(h)}$, in a graph expressing the correlation as a function of $\boldsymbol{h}$.

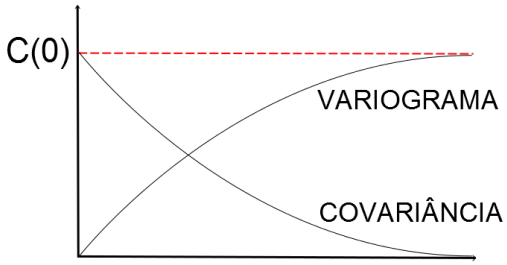

Figure 11 - Illustration of the relation between the covariance and variogram (Hengl et al., 2009).

The equation of the autocorrelation coefficient in a function of the lag h is given by:

$$\boldsymbol{\rho(h) = \frac{C(h)}{C(0)}} \qquad \textbf{(2.9)}$$

Nugget effect

According to the definition used by Clark, I. (2010) in his *Statistics or geostatistics? Sampling error or nugget effect?* Journal paper, the nugget effect $\boldsymbol{C_0}$, refers to the nonzero intercept of the variogram in the y axis. It represents an estimate of errors that might be produced by:

- The measurement inaccuracy and the environmental variability which is occurring at fine scales to be unresolved by the sampling interval,
- The random noise and may represent a short-scale variability, measurement error, sample rate, etc.

Before to proceed with the next phase, some variography exercises where performed to approach the spatial distribution of the hXRF data. The following Figure 12 exemplify the nugget effect. Some values are very erratic because they are different from the others while considering a low distance. The main origins for this type of phenomenon is the human error, regarding the possible misunderstood technical mistakes.

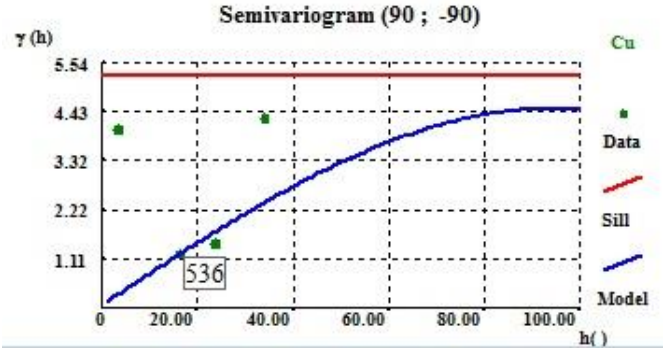

Figure 12 - Variography exercise and the nugget effect (GEOMS).

The variography parameters used for the data modelling within the FC mineralization are described as it follows. For the Cu main direction which expressed the best continuity: 50, -40 and 0. The considered nugget effect was 0,36. The data was modelled through 2 spherical model structures, the first one presented a sill

value of 0.20 and a range of 7,12 and 10. In the second structure, the sill value was 0,44 for a range of 46,40 and 15. Regarding the Zn, the direction was 59, - 38 and 12 with a nugget effect of 0.46. The first structure presented a sill of 0.27 and ranges of 16, 15 and 17. The 2nd structure had 0,26 for the sill and ranges of 112, 55 and 47.

Spherical theoretical model

The spherical model is one of the most commonly applied within various geostatistical applications. It is the adopted model within this study and is defined by 2 parameters, sill $\boldsymbol{C}$ and range $\boldsymbol{a}$, through the following standardized expression:

$$\gamma(\boldsymbol{h}) = \begin{cases} \boldsymbol{C}\,[\,\mathbf{1.5}\,\dfrac{\boldsymbol{h}}{\boldsymbol{a}} - \mathbf{0.5}\left(\dfrac{\boldsymbol{h}}{\boldsymbol{a}}\right)^{3}], & \boldsymbol{h} \le \boldsymbol{a} \\ \boldsymbol{C}, & \boldsymbol{h} \ge \boldsymbol{a} \end{cases} \qquad \textbf{(2.10)}$$

The sill $\boldsymbol{C}$ represents the superior limit in which the variogram values tend to with the increasing $\boldsymbol{h}$ values, the range $\boldsymbol{a}$, represents the distance where the variogram $\boldsymbol{\gamma(h)}$ stop increasing and equals the sill, where the variance of $\boldsymbol{Z(x)}$ is displayed (Soares, A., 2006).

The following illustration (Figure 13) expresses the parameters of the variogram mentioned above in a spherical modelization. Then, it is represented the other common models that are also used.

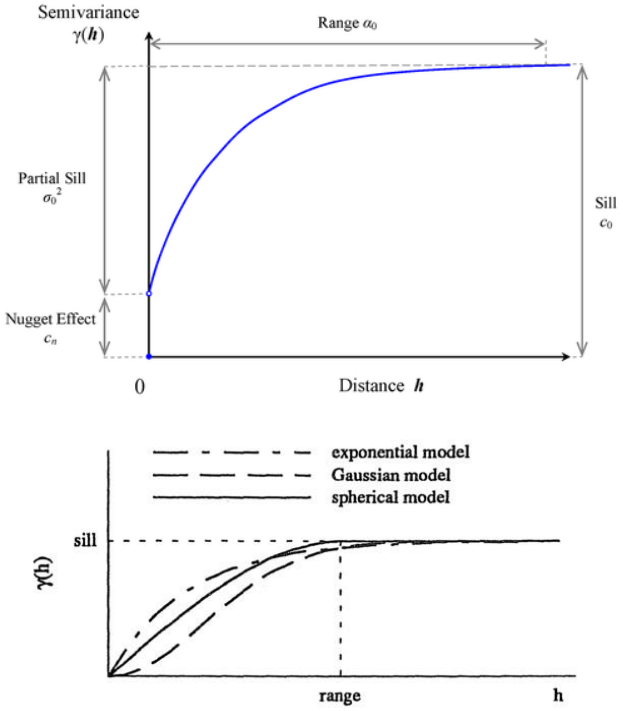

Figure 13 - Spherical model of the variogram with the parameters and its comparison with the common used models (Isaaks, E., 1989).

2.5.2 Estimation by ordinary kriging

In geostatistics, it is assumed that the underlying structure of the data is a stochastic process that leads to the interpolation procedure known as kriging (Scheuerer, Schaback et al., 2013, pag.1).

The kriging estimator was first referred by Matheron G. (1965) in honor of Kridge D. (1951) first approaches (Soares, A., 2006). It includes the following set of estimators which are distinguished by the assumptions taken to determine the optimal weighs. This project uses the ordinary kriging which is the most usual algorithm applied in the geostatistical estimations (Soares, A., 2006).

- Simple kriging,
- Ordinary kriging,
- Universal kriging,
- External Drift Kriging.

After the experimental variogram, which gives the best direction of continuity and preserves the main structural characteristics, it is possible to incorporate the output information plus the original data set values to estimate the non-sampled locals. The following Figure 14 expresses the non-sampled value at x_0 within n neighboring sample points.

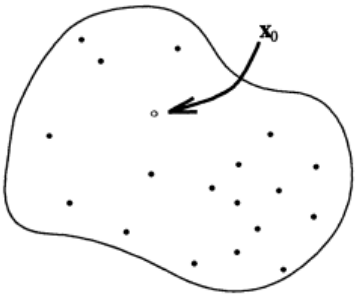

Figure 14 - A domain with irregular spaced sample points (black dots) and the location of interest x_0 (Wackernagel, 2003.

The ordinary kriging estimator (Equation 2.11) describes the point estimation, $[\boldsymbol{z}(\boldsymbol{x}\_\boldsymbol{0})]^*$ through the attribution of weights, $\boldsymbol{\lambda}_{\boldsymbol{\alpha}}$, to each sample,$\boldsymbol{z}(\boldsymbol{x}_{\boldsymbol{\alpha}})$,

$$[\boldsymbol{z}(\boldsymbol{x_0})]^* = \sum_{\boldsymbol{\alpha=1}}^{\boldsymbol{N}} \boldsymbol{\lambda_\alpha}.\boldsymbol{z}(\boldsymbol{x_\alpha}) \qquad \textbf{(2.11)}$$

The estimation uses a linear combination through $\boldsymbol{N}$ neighboring variables $(\boldsymbol{x_0} - \boldsymbol{z}(\boldsymbol{x_\alpha})), \alpha = 1, \dots, N$. Furthermore, the method follows the BLUE's Kridge (as defined in the english literature) for Best Linear Unbiased Estimator) where the following two criteria of Unbiasedness and the Minimum variance estimation (equation 2.13 and 2.14) are verified in terms of the estimation error (equation 2.12),

$$\boldsymbol{\varepsilon}(\boldsymbol{x_0}) = [\boldsymbol{z}(\boldsymbol{x_0})]^* - \boldsymbol{z}(\boldsymbol{x_0}) \qquad \textbf{(2.12)}$$

- Unbiasedness,

$$\boldsymbol{E}\{\boldsymbol{\varepsilon}(\boldsymbol{x_0})\} = \boldsymbol{0} \qquad \textbf{(2.13)}$$

The execution of the process adjusts the results stablishing the mean of the error between the real and the estimated value equal to zero.

- Minimum variance estimation,

$$\mathbf{min}\{var(\varepsilon(x_0))\} \quad \textbf{(2.14)}$$

From the last condition, the estimation errors display a minimum variance.

To mention some of the main advantages of this estimation technique:

- Minimization of the data clustering effects since it gives less weight to the individual points within the cluster,
- Provides the estimation of the error considering the estimation of the variable in study through the kriging variance which may contribute to in the further stochastic simulation.

The distribution of the variable in study will always be influenced regarding the available information that is used throughout the process. Hence, it will be close to the real panorama if it is integrated a greater among of known data (Isaaks e Srivastava, 1989).

2.6 RESOURCES AND RESERVE CLASSIFICATION

Rozman (1998) stated that any resource or reserve estimate is guaranteed to be wrong. Nevertheless, some are less wrong than others *(Beckhoff, B.et al.,2006)*.

To proceed with the valuation of resources and reserves it is mandatory to review the classifications established by the respective entities, to list a few: the JORC code for Joint Ore Reserves Code under the Australian standard for Reporting of Exploration Results, Mineral Resources and Ore Reserves, SAM CODE for South African Mineral Resource Committee and the Canadian standard National Instrument 43-101. The following definition standards presented herein are established by the CIM (Canadian Institute of Mining, Metallurgy and Petroleum) Standing Committee on the Reserve Definitions for Mineral Resource and Reserves adopted in 2000 from the Standards of Disclosure for Mineral Projects, NI 43-101 (Canadian Securities Administrators, 2011; Reserves, 2010). The standards were amended last time in 2014.

Qualified Person: The term defined in the NI 43-101 establish the Qualified Person as the qualified professional able to estimate or provide supporting on the Technical Reports to classify mineral resources and reserves. The experience is mostly associated on commodity markets and accurate technical knowledge to approach different type of deposits and mineralization, sampling, assaying, extraction and processing techniques. Moreover, it is required qualification for Mineral Resource data collection and interpretation as well as for supporting and monitoring Mineral Resource and Reserve estimation documentation (CIM Definition Standards, NI 43.101).

Mineral Resource: The concentration of solid material with an economic interest due to its grade, quality and quantity proposing reasonable prospects for an eventual economic extraction is qualified as Mineral Resource. Formed by different levels on the increasing confidence parameter, the mineral resources are

segmented by the following categories: Inferred, Indicated and Measured. Thus, an Inferred Mineral Resource results in a lower level of confidence once compared to an Indicated Mineral Resource. In its turn, the latest presents a lower level of confidence towards the Measured Mineral Resource *(NI 43-101).*

Mineral Reserve: Formed by different levels on the increasing confidence parameter, Mineral Reserves are segmented by Probable and Proven Mineral Reserves. Thus, A Probable Mineral Reserve results in a lower level of confidence on contrary of the Proven Mineral Reserve.
Mineral Reserves are those parts of Mineral Resources which result in an estimated tonnage and grade which, in the opinion of the Qualified Person(s) executing the estimation, is the basis of an economically viable project under the considerations responsible for converting the Mineral Resources to Mineral Reserves (mining, processing, metallurgical, infrastructure, economic, marketing, legal, environmental, social and governmental factors) known as Modifying Factors (CIM Definition Standards, NI 43-101).

It is needed to pursue better techniques to redefine the existing "generally accepted" or "best" practices to obtain more effective quality assurance policies, guidelines and standards. Hence, it is possible to select better mineral development models and the respective optimal methods to increase the profitability of these activities (Emery et al., 2004). To better describe the measured from the indicated and inferred resources, new developments has been projected to assist the role of the "qualified person". In concordance, the future relies on improvements to minimize the delay between stope sampling and the update of the reserves.
The following Figure 16 illustrates the concepts mentioned above:

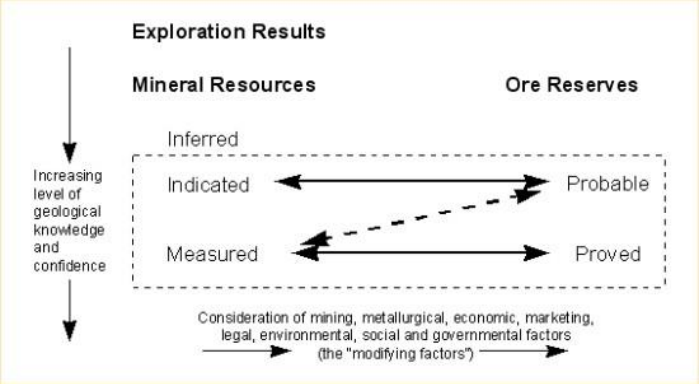

Figure 15 - Resource and Reserve classification (CIM definition Standards, NI 43-101).

Furthermore, the outdated information originated by the discontinuous framework between the grade estimate and decision (after the long-time sampling procedures) easily adds a substantial risk in the mineral valuation since it may produce unexpected operational costs in the further processes towards the mineral beneficiation.

The real-time monitoring and fast updating into the system enables the "qualified person" to work under less substantial bias towards mined resources and reserves.

Through the on site geochemical analysis, it is possible to extend the data collection to cover more areas in less time. The relationship between the hXRF with the international reporting codes and standards for Mineral Resources and Ore reserves, requires the use of these type of equipment supplied with a follow up analysis as well as the integration of more information (device's model, calibration factor, reading times or any other analytical procedures within the unit's hardware).

For instance, when the quantity of data is not sufficient to permit an estimate of the mineral Resources but it is needed to provide a persistent reporting to investors, which occurs in the premature stages of exploration, the portable XRF (hXRF) might deliver a useful data set. A good representativeness and a straightforward strategy are important to integrate the results (Gazley, M., Fisher, L., 2002). Thus, in the reporting of resources the hXRF can give contributions for the understanding of the deposit while supporting the geological model. Furthermore, the production operations require a constant control of the grades, where the hXRF is also a great utility for providing data with a suitable quality.

As performed in this thesis, after the estimation through kriging the ouput files given by SGEMS will provide the MRE regarding the variable Cu. The estimated grades are important for the further calculations.

Hence, the classification will be obtained while suggesting a cut-off grade (COG) which expresses the economic attractiveness of the mineral deposit. The parametric curves of tonnage, mean ore grade and quantity of metal will be presented.

The COG (equation 2.15) is a standard expression that determines which part of the mineral deposit is integrated in the mineral resource estimate (MRE) and depends on the market price fluctuation.

$$COG\ (g\ /\ t))=\frac{ore\ denominated\ operating\ cost\ (€/t)}{Grade\ denominated\ revenue\ (€\ /g)} \quad \textbf{(2.15)}$$

Considering the estimation of resources, the equations expressing the tonnage, average grade and quantity of metal are described in the following Equations 2.16, 2.17 and 2.18.

$$T\ (z) = \sum_{i=1}^{Nt} I_z\ (x_i).t \quad \textbf{(2.16)}$$

$$M(z) = \sum_{i=1}^{Nt} I_z\ (x_i).z(x_i).t \quad \textbf{(2.17)}$$

$$m(z) = \frac{M(z)}{T(z)} \quad \textbf{(2.18)}$$

Where $N(t)$ is the number of blocks, t is the tonnage of each block x_i and $I_z(x_i)\begin{cases}1\ \ if z(x_i) > z\\ 0, otherwise\end{cases}$.

CHAPTER III. METHODOLOGY

This chapter describes and illustrates the workflow and methodologies adopted throughout this work (Figures 16, 17 and 18).

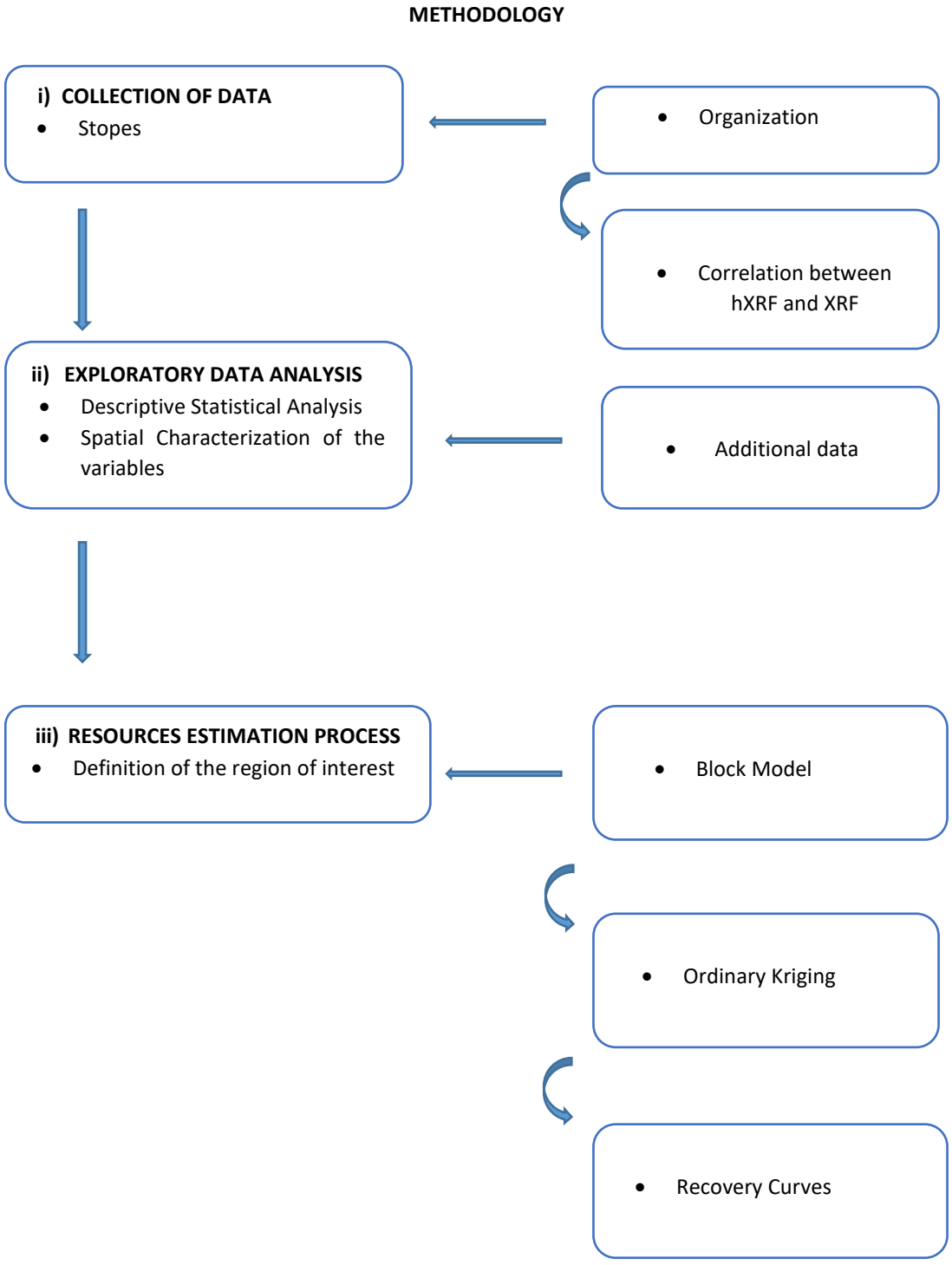

Figure 16 – Thesis workflow.

3.1 WORKFLOW

i) **Collection of data in the mining stopes:** To proceed with the collection of the data, it was firstly required an access to the daily or weekly production mine program as well as the hXRF device's calibration.

Based on the hXRF device's manual, a set of procedures were studied to best adapt the measurements to the environment conditions, during the acquisition of the data.

The mineralization of the Neves Corvo's various mining deposits and the Somincor's method to obtain data through the Face Chips Sampling were studied. Then the procedures for hXRF data acquisition and its validation were defined. This phase is summarized through the following tasks:

- **Organization and study of the data:** The output file obtained from the hXRF device was organized and then it was created a new data file with the readings separated by each type of deposit (domains) and each type of mineralization. The variables of interest, Cu and Zn grades were evaluated throughout the different domains within the mine and it was described the respective extensions of the dataset. The representativeness and the anomalous values of the data were verified. Regarding the absence of the Limits of Detection (**LOD**) in some of the readings or the concentrations bellow this limit, it was followed the indications described in the Technical Report of Lundin Mining for the Neves-Corvo Mine (2017). Duplicated samples were excluded before to proceed with the descriptive uni and bivariated statistical analysis.

- **Additional data:** Additional data was provided by the geological department of Somincor. It consisted in data obtained through the Drill Cole Sampling (ALL) and UGS Face Chip Sampling.

ii) **Exploratory Data Analysis:** A geostatistical modeling software developed by Cerena research department in IST, Geoms, and the SGEMS for Standford Geostatistical Earth Modelling Software, were used throughout the exploratory data analysis and the MRE.

According to the additional data, defined above, the statistical parameters were presented, such as, the mean, maximum, minimum, variance, standard deviation, interquartile range concentrations, coefficient of dispersion and the graphical representations through histograms and bi-plots. The tridimensional spatial data characterization for each one the variables Cu and Zn was verified to detect the trends in the dispersion such as the abnormal behaviors (clusters), distance between samples and directions of continuity/anisotropy.

Through the equation of the regression line between the hXRF and LAB scatterplot, it was tested the prediction for the hXRF measurements (described as hXRF2) regarding the available UGS reference.

The exploratory data analysis gives the first directrices to define the necessary parameters for the further stage of the process, which was the resource estimation through the ordinary kriging interpolator.

iii) **Resources estimation process:** To proceed with the process of estimation by ordinary kriging it was considered the variography parameters estimated for the Cu grade within the FC mineralization in Neves Deposit. The ordinary kriging for the MRE process was applied and the results regarding hXRF2+ALL versus the ALL data (Figure 17) were discussed. The first approach consisted in the definition of the block model.

- **Definition of the block model:** It was defined a block model for the predicted hXRF2 data (obtained in the chapter 5.1.2). Parameters such as the average, minimum and maximum spatial distance between the data (hXRF2, UGS, ALL) were evaluated and the grid calculated. The region for the study was represented through the definition of the grid (number of cells) and the respective dimensions in x, y and z axis.

- **Recovery Curves:** After the estimation process, the resources of copper will be classified under a threshold. The parametric functions will indicate the recovery curves regarding the cut-off grade vs tonnage, mean grade and quantity in metal.

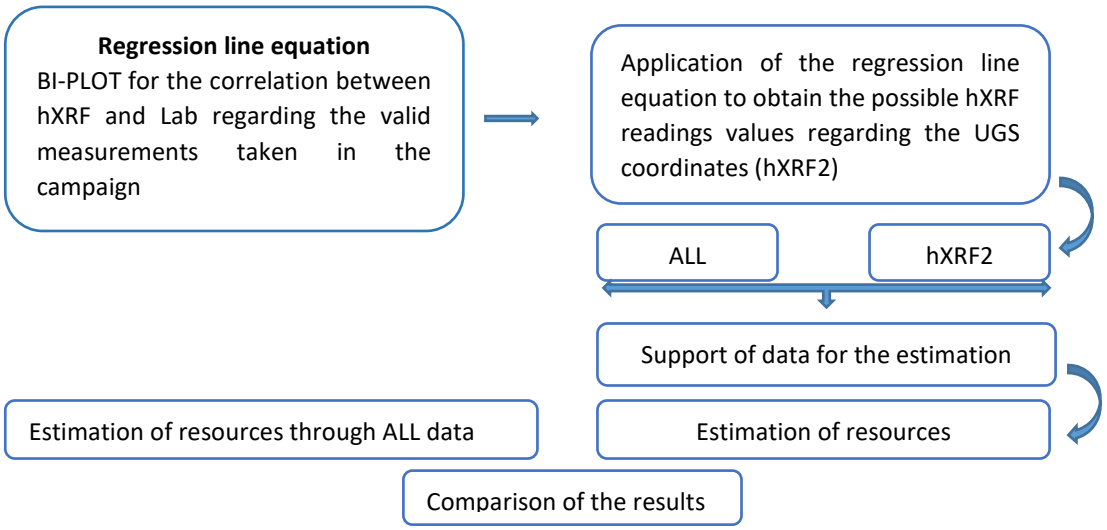

Figure 17 – Schematic description between ii) Correlation hXRF and LAB and iii) Estimation of Resources.

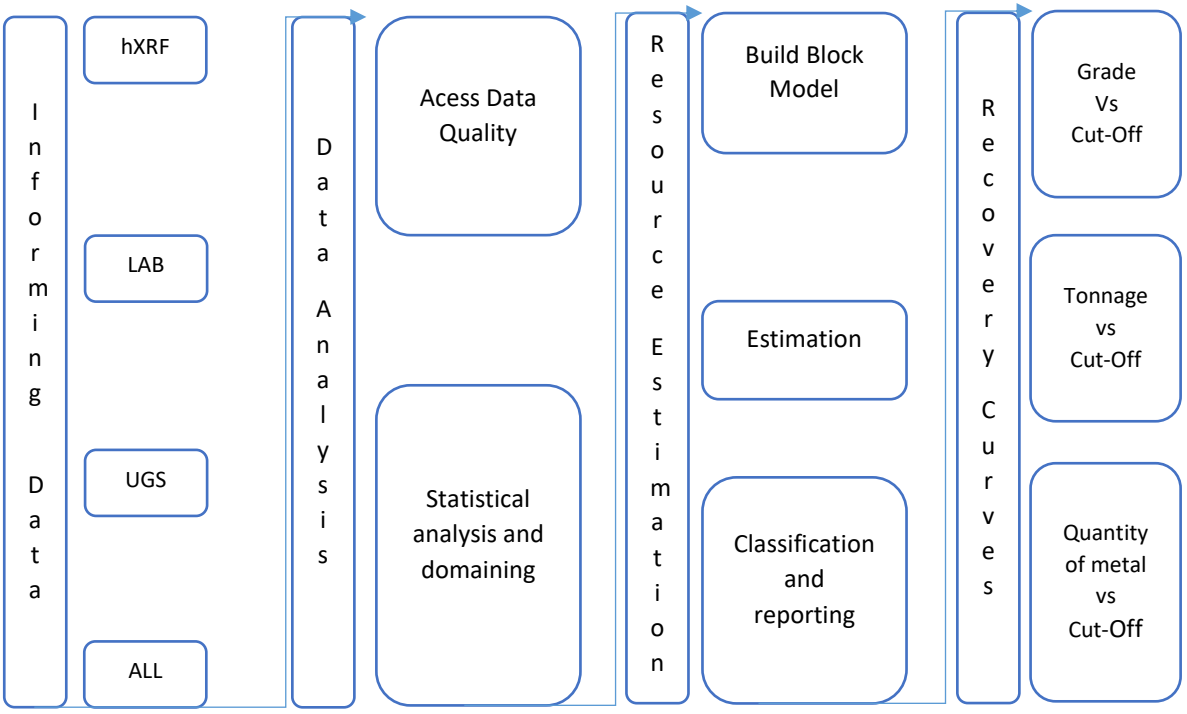

Figure 18 – Brief process flow for the MRE.

3.2 Instrument for the Fast Data collection

This study was carried out through the NITON XL3t 600 device (Figure 19) manufactured by Thermo Fisher Scientific in Germany. The device measures the total elemental metal concentrations. Some procedures were important to follow while the acquisition of data was taking place in order to obtain the best representativeness.

Figure 19 - NITON XL3t 600 produced by Thermo Fisher Scientif.

As it follows, it is presented the instrument specifications. Considering Gazley et al (2011) a complete list should include: device's manufacturer and model, mode of operation, sample container, the correction factor

for each element reported (if applied), the method followed in the conventional analysis data, the sample preparation procedures and the standards used to determine the calibration (if not factory calibration).

The following Table 1 summarizes the device's specifications:

Table 1 - NITON XL3t 600 device's specifications.

Niton XL3t Portable XRF Analyser	**Specifications (Metric/English)**
Dimensions (Lx Wx H)	244 x 230 x 95.5 mm/ 9.6 x 9.05 x 3.75in
Weight	1.3 kg/ 3lb
Display Type	Adjustable angle and touch screen display
Power Consumption	100 µA
Battery	Cell lithium-ion.
--	Spare pack
--	110/220 VAC charger
Tube Type	Au anode 50 kV maximum
--	200 µA maximum
Detector Type	High performance semiconductor
Data Memory	32 Mb Internal System Memory
--	128 Mb Internal user storage

It works under safely temperatures from -10ºC to 50ºC.

3.2.1 Calibration

The device to be used must be well optimized for what is aimed for, since different units fits better in different purposes. Likewise, the unit should be first tested to achieve the best calibration, agreeing with the purpose of the study. It is first suggested to calibrate the device to a given rock matrix already known in the field to be tested or to apply the generic calibration and then proceed with the application of the correction factor. Based on the analysis of the standards that matches the matrix of the samples to be examined, is possible to avoid possible incongruities between the expected and real data (Gazley M. and Fisher L., 2002). Based on the manufacturer's instructions of the hXRF NITON XL3t 600, a minimum of 3 standards are valid to establish the calibration. Nevertheless, more samples improve the quality of the analysis.

The calibration algorithm was calculated using a specific set of well-characterized samples that produces linear calibration curves. The device NITON XL3t 600 provides a slope calibration software (Figure 20) to improve the quality of the data for a single or a suite of elements.

The comparison between the obtained values after the readings and the standardized references creates a linear regression $Y = mx + b$ which expresses the slope,m, and the interception of b on the y axis.

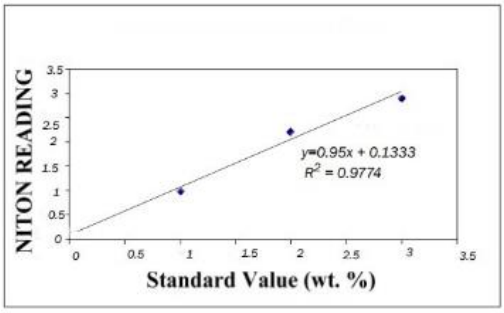

Figure 20 - Calibration factors expressed through the linear regression equation (NITON XL3t user's guide).

It is required to start within the default values set by the manufacturer before any calibration operation and the application of 120 seconds (minimum) for each filter setting, while measuring the standards.

The calibration factor is determined through the comparison between the new readings from the standards and the results obtained before regarding the same standards given by traditional laboratorial essays.
Then, the calibration factor is integrated into the analyzer through the menu (Niton XL3t user's guide).

It is also very important to address that a certain calibration calculated in a specific time cannot be suitable to a future use due to an instrumental drift. Gazley M. and Fisher L. (2002) suggests a set of protocols to lead the analytical drift to be tracked while repeating the same standard samples and plotting the results against time. This procedure allows the understanding of changing the threshold within a determined percentage of the median value.

It was possible to consult the existing calibration factors settled by default for the geology department of Somincor accessing the main menu of the device. The following equations present the calibration factors, regarding the Cu (Equation 3.1) and Zn (Equation 3.2) elements.

$$\boldsymbol{Y = 1,12x - 0,32} \quad \textbf{(3.1)}$$

$$\boldsymbol{Y = 1,20x - 0,39} \quad \textbf{(3.2)}$$

3.2.2 Precision

The precision depends on each hXRF unit as mentioned by Goodale (2012) while testing different units measuring the same sample. Furthermore, the precision is determined by the quality of the device's internal hardware such as the X-ray tube and the detector, the X-ray absorption and emission, the matrix effects of the sample and the efficiency of the unit's software for peak detections (Brand, N. and Brand, C., 2014).

The precision equation is described as it follows:

$$\textbf{Precision (ppm)=2 x } \eth \quad \textbf{(3.3)}$$

3.2.3 Limit of detection

The detection of each element is processed through the validation of the following equation:

$$\textbf{Detected element (ppm)} = 1.5 \times \textbf{precision} \qquad (3.4)$$

For each reading the device gives a measured concentration. However, if the element's sample presents a value that is not even approximated to the minimum of the limit of detection, LOD (Equation 3.5), the LOD may not be indicated.

A non-detected element presents a reading value far below the LOD.

$$\textbf{LOD (ppm)} = 3 \times \eth \qquad (3.5)$$

Where **ð** is the standard deviation.

In the present work, some values were below the LOD and some other measurements did not reach the minimum LOD. The procedure taken in those cases followed the reference provided by the Technical Report of Lundin Mining for Neves Corvo. The values recorded as exactly zero were placed by half of the detection limit and the values below the limit of detection were replaced by the detection limit value. Regarding the non-indicated values, it was given the average mean considering the other readings within the same channel dataset.

CHAPTER IV. REAL CASE APPLICATION

4.1 NEVES- CORVO CASE STUDY

Situated in the province of Alentejo in the Southern part of Portugal, the Neves- Corvo Mining concession is placed within the Iberian Pyrite Belt, IPB (Figure 21). The acessement to Neves-Corvo mine and its facilities is made by the national road network connecting Lisbon and Faro (South).

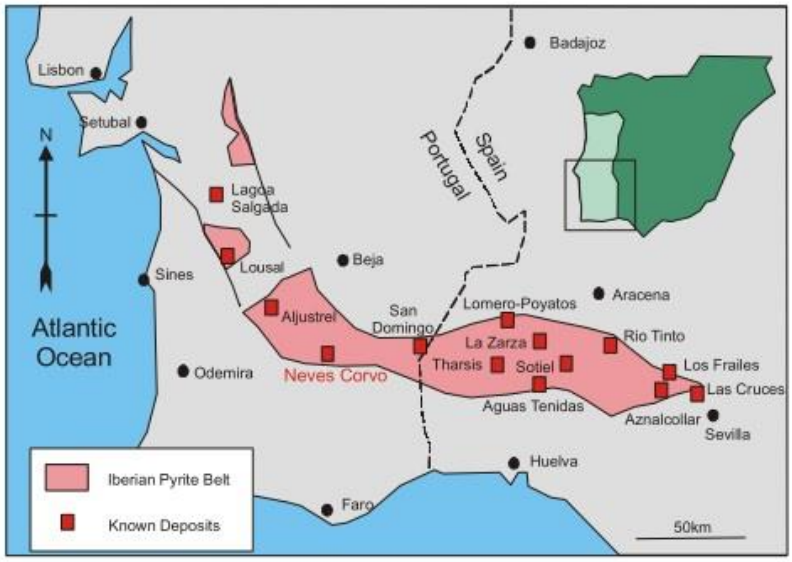

Figure 21 - Location of Neves- Corvo Mining Concession within the IPM (Technical report, courtesy of Somincor).

The latest system consists in a geologic structure integrating various volcano-sedimentary massive sulphide (VMS) deposits originated between the Superior Devonic and carbonic ages. Its extension is through 250 km with 60km of width, from the south of Portugal, Grândola, to the west of Sevile in Spain (Pacheco et al., 1998) and its geological phenomena originated some of the most important massive sulphide deposits in the world (Martins et al., 2006). In 1977 with the works of prospection througout thr IPB, the Neves-Corvo Mine and its reserves were defined based in its extraordinary and anormal concentrations of metals such as copper, zinc and tin. Nowadays, the mine is operated by the portuguese mining enterprise Somincor which is a subsidiary of the Canadian base metals mining company Lundin Mining.

4.4.1 Geological Setting and Mineralization

Due to deformations originated by collisions and subduction effects, the IPB is characterized through a volcanic belt hosting massive sulfide deposits separated by shale units and arenites. The massive sulphide deposits are intercalated with a Volcanic Siliceous Complex (VSC) which presents a 300m of thickness in the Neves -Corvo area and is composed by igneous and sedimentary rocks with a diversified mineralization such as a massive pyrite through a complex base metal sulphides and sulphide stockwork zones. The orebodies within the IPB lie in a succession of layers dated from Upper Devonian and Carboniferous age. An anticline

orientated NW-SE evolves all the mentioned geological settings and the major types of massive sulfide mineralization occur, exposing a high-grade content of copper, tin and zinc widening its deposits as one of the richest within the Iberian pyrite belt (Technical report, 2017). The zone refining is the responsible process in the origin of deposits with such economic interests and consists in the abnormal concentration of certain metals in some regions due to the strong thermal gradient environment within a sulphide lense (high temperatures in the base and colder at the top). This effect led to the precipitation of copper in the base and the dissolution of zinc which moves upwards and concentrates in the exterior of the lense (Folha,2016).

The following Figure 22 illustrates the location of the 7 massive deposits within the Neves -Corvo Mining Concession: the two lenses Neves North and South, Corvo, Graça, Zambujal, Lombador, Monte Branco and Semblana. Integrating this geological complex is a northwest - southwest anticlinal, Rosario-Neves-Corvo,

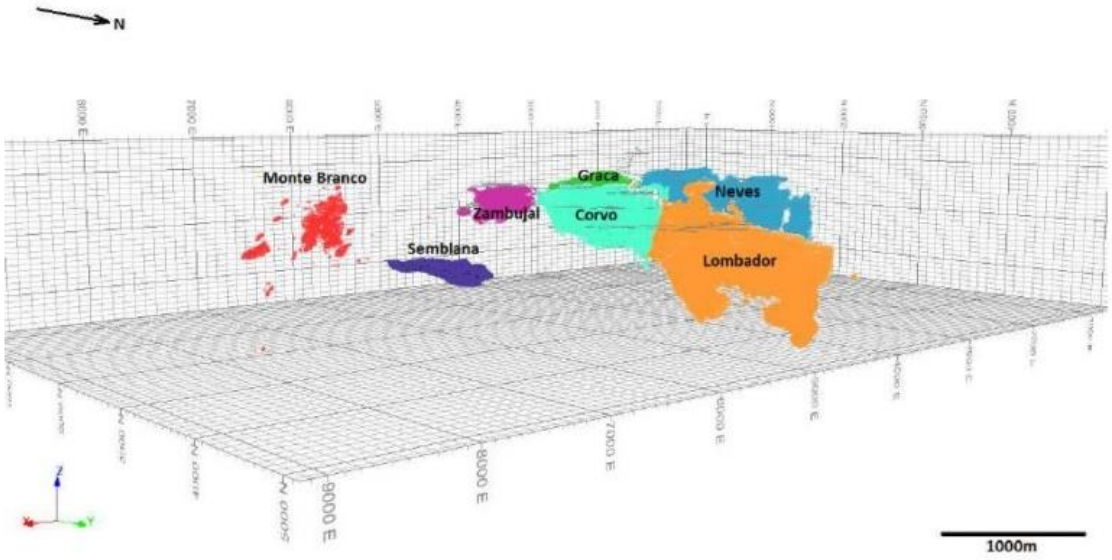

where the mineralization occurs in its both flanks, located below surface between 230-1400 of depths.

The deposits are characterized by regular and continuous features, despite its geological and geometry complexity.

The mineralization approached throughout this thesis is designed as the conventional description used within the mine: MC for Massive Copper with is the major ore mineral (chalcopyrite), MZ for Massive Zinc with sphalerite, FC for stockwork of copper, MCZ for Massive Copper and Zinc, MZP for Massive Zinc and Lead (Sphalerite and galena). Lastly, the FE for Stockwork of Pyrite which is considered as a low grade mineral content characterized by barren.

Figure 22 - Neves -Corvo Mine deposits (Technical report, courtesy of Somincor).

4.4.3 Neves Deposit

This deposit is characterized by two lenses, Neves South and North, that are 0-35º North orientated and connected by a thin bridge. Its dimensions lie between a length of 1 200m and 700m with a thickness of approximately 55m (Technical report, 2017).

The Neves South is characterized by a greater content of zinc with other elements such as lead, copper, silver and pyrite. Furthermore, the copper ore is locally tin-bearing and the mineralization of zinc is classified as very fine, grains <25microns, accusing deleterious elements: Sb, Hg and As.

In its turn, Neves North is copper rich and characterized by the well-developed stockwork and basal massive sulphide.

4.2 DATASET DESCRIPTION

4.2.1 Fast data

Portable XRF measurements (hXRF)

The hXRF equipment device that was used on-the-spot analysis was the NITON XL3 600 (Figure 23). In total, approximately 1167 readings were performed through the various deposits of Neves Corvo Mine. The 120 valid samples were obtained through the calculation of the arithmetic mean in each channel length. The data set consists in the geochemical grade content readings of copper and zinc, among other elements.

Figure 23 - Mining Stopes and the NITON hXRF device.

The hXRF measurements were carried throughout the same points were the fragments of the rock mass were collected for the laboratorial analysis along each 1 m of channel defined by the FC and its mineralization features. The following subchapter 4.2.2 regarding the UGS data describes the sampling procedure that was followed by the geological department.

The total spatial arrangement of the collected data used throughout this thesis follows a random pattern across the Neves-Corvo mine within the deposits of Neves, Corvo, Lombador and Zambujal.

The Table 2 describes the extending dimensions of the dataset within each deposit through its coordinates and the correspondent number of samples.

Table 2 - Description of the data obtained through hXRF in the 2017 Campaign.

Deposits	$x_{min}(m)$	$x_{max}(m)$	$y_{min}(m)$	$y_{max}(m)$	$z_{min}(m)$	$z_{max}(m)$	Nº Samples
Neves	3534.08	4145.88	2647.36	3371.6	751	774.7	66
Lombador	4248.28	4500.68	3354.47	3561.73	396.2	644.6	18
Zambujal	5261.97	5368.84	1922.62	2097.89	722.8	748.9	18
Corvo	5076.49	5081.91	2573.13	3317.36	643.2	646.4	18

The dot separates the integer part from the fractional part of the number written in decimal form.

The extension of the data available through the hXRF device was considered too sparsely located (Figure 24) towards the aim of this project since we could not obtain good results in the estimation process. To tackle this problem, it was defined the best region for the estimation regarding the best representative data and the data support available for the region (Subchapter 4.2.3).

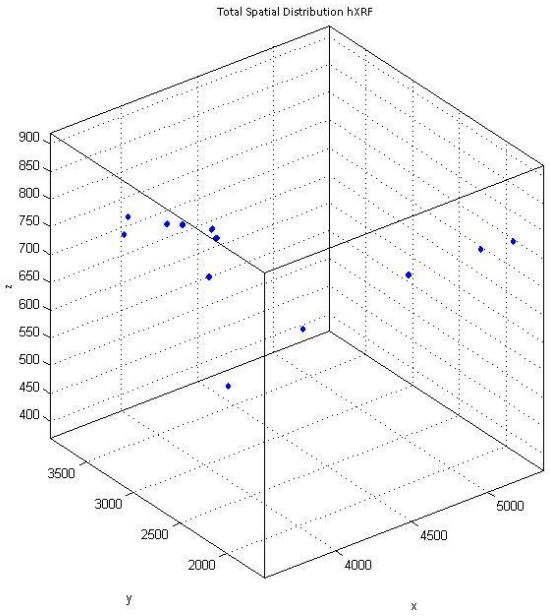

Figure 24 - Total hXRF1 data taken in the 2017 campaign. Each point represents a set of samples.

To guarantee some consistency, we determined that 10 reading points would be measured throughout 1 meter of length of the channel. For each point, the considered reading time was 10 seconds.
To avoid cross contamination, the dust in the window's unit was clean in each measurement. The respective time for the device's warm up was respected according to the Niton's user guide. Also, since the hXRF presents depth limitations It was also assumed that the material on surface is the same as the material beneath the penetration depth of the X-rays. According to *Le* Vaillant et al (2014), this assumption can help to increase the representativeness and consistency of the data.

4.2.2 Slow data

Additionally to the LAB data, two types of data were provided, UGS and ALL. They consisted in the database that was generated in the MRE.
In the Face Chip Sampling**,** the samples comprise fragments, mineral dust or chips that are collected under specific procedures. As mentioned above, two types of Face Chip Sampling are herein referenced: **LAB** and **UGS**. To validate the data provided by the hXRF unit (hXRF1), the face sampling (LAB) was collected by the geological staff of the geological department of Somincor. The **UGS** collection was not executed in the same coordinates as the hXRF. The samples undertaken through Face Chip Sampling were prepared and examined through a geochemical analysis with X-Ray Fluorescence, among other methods, at Neves-Corvo laboratory facilities. The geochemical analysis is realized to detect the elements and reach the respective concentrations of Cu, Zn, As, Pb, Sb, Se, S, Bi, etc. Its results are divulgated to the Resource and Database Geologists (Lundin Mining Technical Report, 2017).

Face Chip Sampling

As mentioned above, the procedures undertaking by the geological staff regarding the face chip sampling were carried out to support the results provided by the hXRF. Thus, this way to check samples is responsible for the data quality since provided enough consistency to verify the results.

- **LAB:** Consists in the chip samples collected in the same coordinates where the campaign 2017 was carried out for this project. In concordance with the hXRF1, the LAB comprises a total of 120 samples. It also consists in additional data provided by the campaigns carried out in the previous years in the various domains of mineralization. The latest, was used to stablish the linear correlation between hXRF and LAB.

- **UGS:** consists in the chip samples collected nearby the coordinates followed in the campaign 2017. It comprises a total of 285 samples and there is no hXRF data collected for these coordinates.

The underground mining stope dimension is $5m\ x\ 5m\ x\ 5m$ which corresponds to the sampling reference to equally divide it into small defined areas that are approached by the geological staff. Each face is sampled

every second or third advance (Technical report). Accordingly, to each style of mineralization the samples can be collect radially through Radial Chip Sampling (massive mineralization) or in Channel (stockwork mineralization). The main style of mineralization that is object of this study is the stockwork of copper, FC. Consequently, the Channel Chip Sampling consists in the face division into a 3x3 grid and the disposal of the channel length depends on the vertical or horizontal alignment of the mineralization feature (Figure 25). Each channel length is 1 m and stands horizontal for the vertical mineralization feature while the horizontal length stands for the vertical veins.

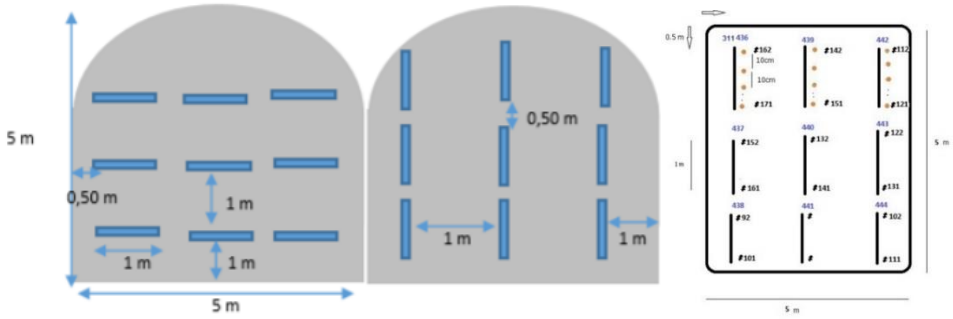

Figure 25 - Scheme of the channel features for the FC (Revês, 2016).

In each channel, fragments of the rock mass were collected in a sample container with the respective label describing the sample location and the respective ID (Figure 26). Finally, the samples were sent to the laboratorial facilities.

Figure 26 - Chip Samples labelled.

The preparation of the samples in the laboratory corresponds to the conventional procedure. The samples are first dried, its grain size is reduced, homogenized, pulverized, fractioned and organized for the further analysis through the x-rays fluorescence laboratorial technique, electro-gravimetric or absorption techniques. One of the procedures for quality monitoring for the assays is to include a non-mineralized sample, which contributes to detect eventual cross contamination between the face samples.

Regarding specific grade intervals of Cu and Zn, the results are re-analyzed through the other techniques (electro-gravimetric or atomic absorption). However, no correction factor is applied regarding the integration of the resultant analysis into the update for the MRE.

Drill Core Sampling

This type of data is referenced with the abbreviation **ALL** and provides information that will be used and compared in the MRE process.

The procedures applied in the underground drill campaigns consist in the removing of the cores from the core barrel and its displacement in boxes where the intervals in depth are signalized and recorded. Then, the material is transported to the on-site logging facilities within the Neves-Corvo Mine and the conventional measurements such as the RQD, texture, color, structures and the grades for each element presented (among others) are executed.

The underground drilling is generally taken on 35 spacing and its orientation is perpendicular to the overall strike characterized by the deposits (Technical report, 2017).

Since the sample intervals in FC were defined along 1m of interval (or even less), it better reflects the variability of the mineralization. The composites are also considered for this length.

The data consists in a set of 9 drill cores within the following coordinates extension (Table 3).

Table 3 - Extension of the Drill Hole Sampling Dataset along the x, y and z coordinates.

Coordinates	*Interval (m)*	*Extension(m)*
X	[4072.42;4169.04]	96.62
Y	[3062.12;3132.43]	70.31
Z	[740.02;779.93]	39.91

The comma separates the integer part from the fractional part of the number written in decimal form.

The following Figure 27 illustrates the variation regarding the Cu and Zn grades along the depth for one of the drill cores.

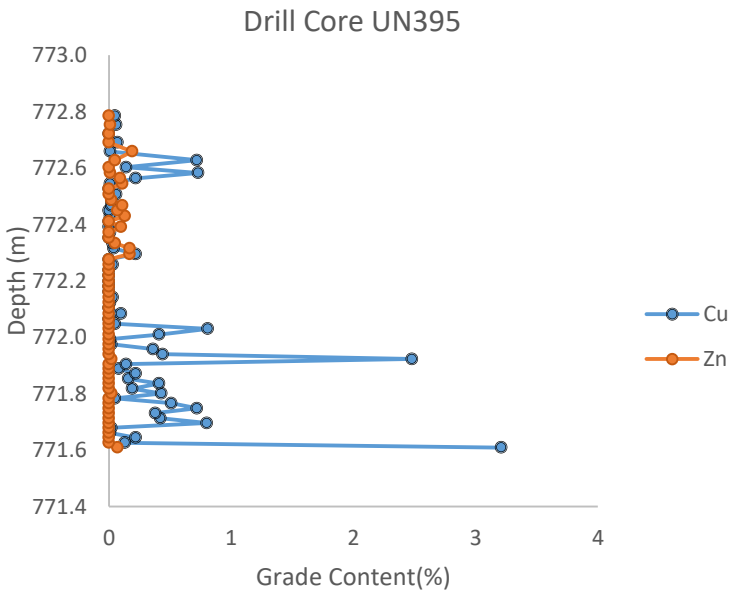

Figure 27 - Cu and Zn grade variation along the depth - Drill Cole Sampling (UN395).

4.2.3 Domain of selection and Support of Data

It was decided to proceed with the study within the domain of Neves deposit which was delimited by the available greater number of samples (hXRF). The deposit of Neves is divided in two lenses where the data was spared and due to the deposit extension and lack of information between the populated regions it was verified where the two other types of data UGS and ALL were localized and could provide additional information.

The chosen region for the MRE was characterized by the FC mineralization. The hXRF and LAB number of samples in Neves deposit were reduced from the initial 66 to 30 available samples since the variability in space from samples displaced along great distances would be bigger. Moreover, the given available additional data was in the surrounding area of this specific region defined by the 30 samples(hXRF1).

The final distribution of the dataset provided by the hXRF1 device and LAB in the FC is shown below (Figures 28 and 29) and comprises approximately $42m$, $10m$ and 24 m along the x, y and z axis (Table 4).

Table 4 - Extension of the hXRF1 and LAB data in Neves deposit- 30 samples.

Coordinates	*Interval (m)*	*Extension(m)*
X	[4103.91;4145.88]	41.97
Y	[3092.65;3103.1]	10.36
Z	[751;774.71]	23.71

The dot separates the integer part from the fractional part of the number written in decimal form.

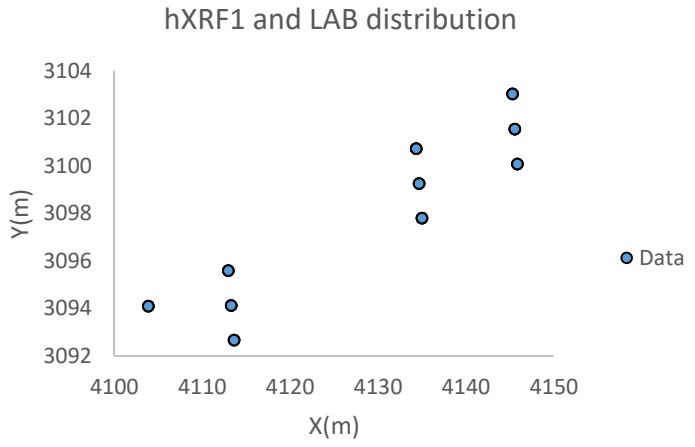

Figure 28 - 2D distribution for hXRF1 and LAB (30 samples).

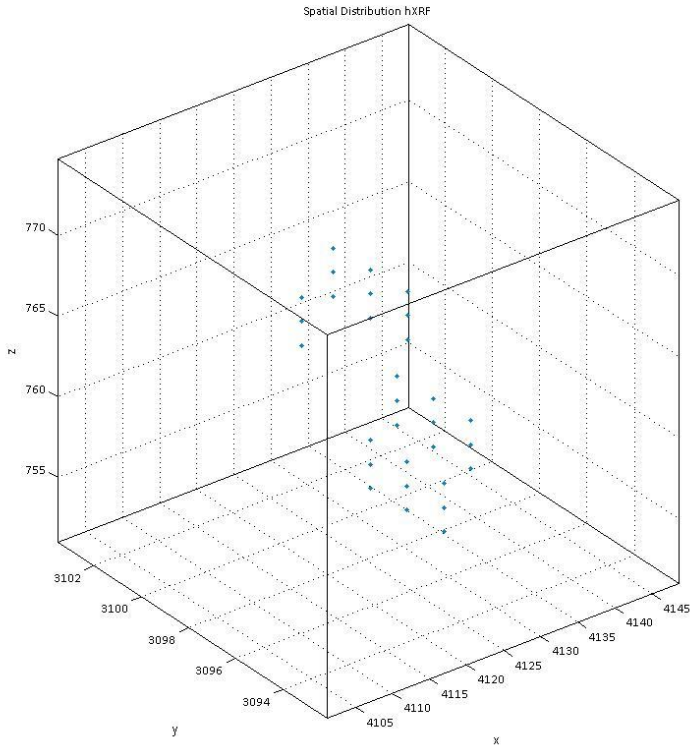

Figure 29 - 3D spatial distribution hXRF1, 30 samples.

The further MRE process will used the UGS and All data obtained in the surroundings regarding the disposal of the 30 available samples hXRF and LAB.

The region where all data could be gathered is described in the Table 5 which represents the final region of interest. Although, the further definition of the block model (subchapter 5.2.1) restricted the estimation to a smaller volume.

These coordinates correspond to the stopes located in the 750 and 770 meters in the topographical elevations.

Table 5 - Domaining and extension of the gathered data (hXRF, UGS and All) – region of interest between the stopes Neves 750 and Neves 770.

Coordinates	*Interval (m)*	*Extension(m)*
X	[4072.42;4169.04]]	96.62
Y	[3046.96;3143.58]	70.31
Z	[711.67;808.29]	39.91

The dot separates the integer part from the fractional part of the number written in decimal form.

.

UGS

The Figure 30 describes the displacement of the UGS data in a 2D graph. The minimum distance between the UGS Face Chip Samples in each mining stope is 0.5m (also the average distance) in the x coordinate, 0.5m for the y axis and the 0,5m for the z axis. The observed maximum distance between UGS total data is approximately 70m, 67m and 24 m for x, y and z respectively.

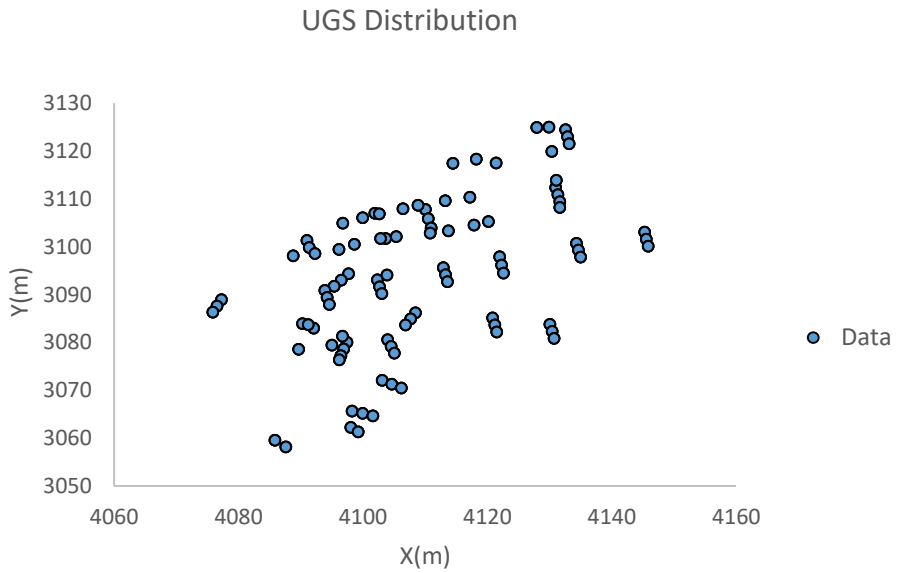

Figure 30 - 2D distribution, UGS.

ALL

Regarding the ALL data, some sample's distance intervals of 2m are shown. However, up to 65% of the major population of the samples were taken under a support of 1m in length, which provides a better understanding on the variability within the FC. The minimum distance between the drills is 5.92m in the x coordinate, 3.76 m in the y axis and 1 m in the z axis. The observed maximum distance between the total drills is approximately 97 m, 70 m and 40 m for x, y and z respectively. Also, the samples are displaced more closely throughout the vertical axis. The drill sections were orientated approximately at N50° accordingly with the inclination of the orebody and are perpendicular to the overall strike of the ore bodies. The following Figure 31 describes the displacement of the ALL data in a 2D graph.

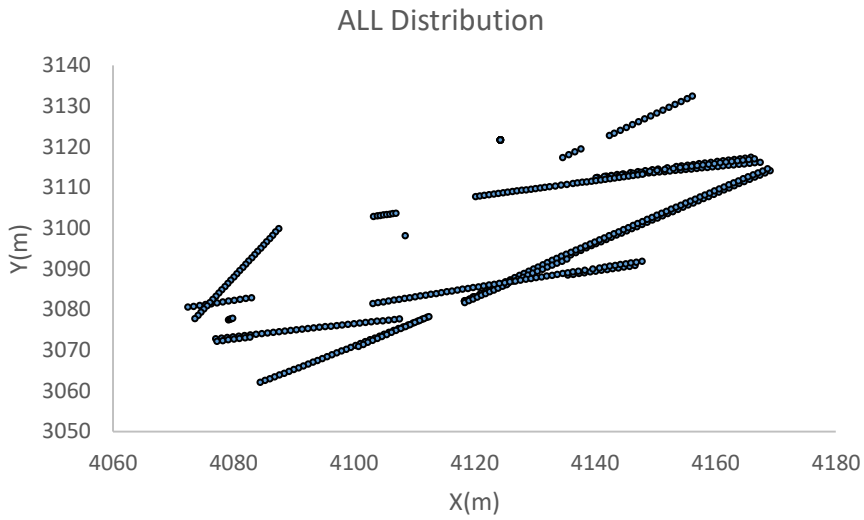

Figure 31 - 2D distribution ALL.

Both data are illustrated in the following Figure 32.

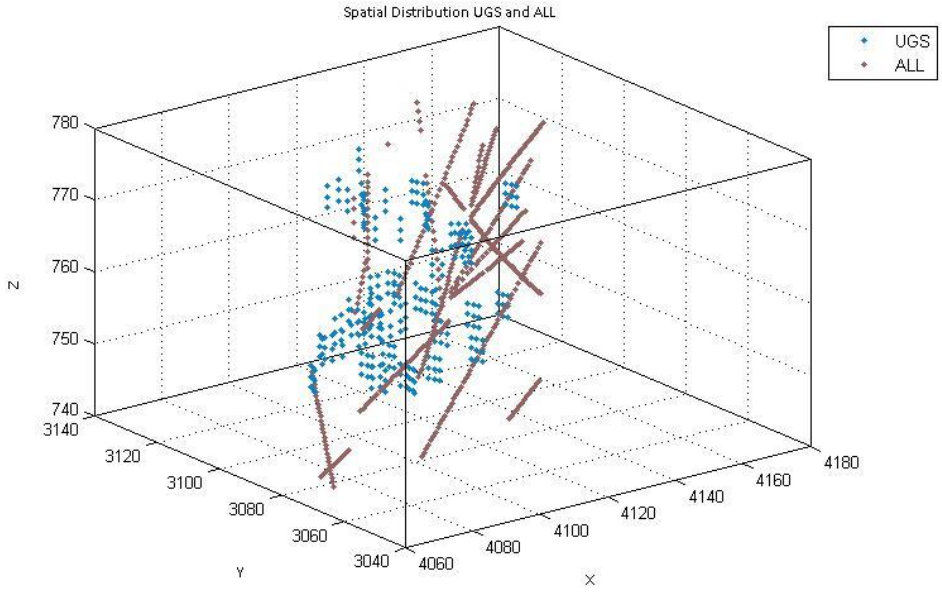

Figure 32 - 3D spatial distribution UGS +ALL (MATLAB).

After the analyzing the data, it was decided to proceed with the estimation using a block model considering a tridimentional grid of $0.5\ m\ x\ 0.5\ m\ x\ 0.5\ m$. Regarding the nature of the ore type within the VMS deposits, the density of the rock per unit volume was considered a homogenous variable of 4, 5 g/cm^3. Accordingly, this density corresponds to the type of mineralization herein approached and the content of sulphide minerals that are present in this type of environments. The chalcopyrite presents an average of 4, 1 g/cm^3 and pyrite shows a specific density about 4.85 g/cm^3 .

CHAPTER V. DISCUSSION OF THE RESULTS

5.1 EXPLORATORY DATA ANALYSIS

This subchapter deals with the statistical description for the variables in study. The description of the statistical features was important to evaluate the performance of the data set acquisition through the hXRF. The collection of 120 samples taken through the hXRF were organized to a new file with the specific ASCII format needed to be uploaded in the SGEMS and GEOMS softwares.
The input data point locates the samples spatially throughout the x, y, and z coordinates expressing the value of Cu and Zn grades.

5.1.1. Univariate Analysis

hXRF and LAB

The adopted region to proceed with the univariate analysis was first demarcated according the 30 samples collected through hXRF in the domain of the Neves deposit (hXRF1), specifically in the 750 and 770m topographic elevations. The ore type defined within this region is FC but also contains FE for stockwork of pyrite, which is considered as a low grade mineral content.

Analyzing the selected dataset between the fast and slow data methods and regarding the Cu variable, 37% of the data present an admissible difference smaller than the unit which means that the other 63% of the data have small variations in the decimal order. It is possible that for the observed higher differences between hXRF1 and LAB, the human errors while displacing the instrument in the irregular surface of the stope or the small sensor from the unit's window may have influenced the readings. Despite this and analyzing the Zn variable, 100% of the data have a difference within the decimal order.
Analyzing the proximity between both data (for Cu and Zn), 65% of the readings present small variations no bigger than 0,5%.

The separated statistical analysis between hXRF1 and LAB for the variables of Cu and Zn are shown in the following Table 6. Three statistical parameters between hXRF2 and LAB present a difference greater than the unit's value: the variance, maximum and the 75 percentile for Cu. Regarding the type of deposit FC, as expected, the mean for Cu is substantial and the variable Zn shows a trivial difference between both data hXRF1 and LAB. Also, the coefficients of variation between Cu and Zn are not dissimilar.

Table 6 - Statistical parameters for the hXRF and LAB results (30 samples for FC) SGEMS.

STATISTICS	hXRF1 (Cu)	LAB (Cu)	Dif (%)	hXRF1(Zn)	LAB (Zn)	Dif(%)
Data Count	30	30	--	30	30	--
Mean	2.03	2.47	0.44	0.13	0.10	0.03
Variance	10.42	7.85	2.57	0.03	0.01	0.02
Maximum	14.29	11.88	2.41	0.70	0.36	0.46
75 Percentile	2.26	3.94	1.68	0.18	0.14	0.02
Median	0.71	1.53	0.82	0.05	0.05	--
25 Percentile	0.31	0.7	0.39	0.04	0.04	--
Minimum	0.01	0.00	0.01	0.02	0.02	--
St. Dev	3.18	2.80	0.38	0.16	0.09	0.07
Coef. Var. (St.Dev./mean)	1.56	1.13	0.43	1.27	0.93	0.34
Coef. Skewness	2.46	1.77	0.69	1.94	1.53	0.41

The dot separates the integer part from the fractional part of the number written in decimal form.

Coef. Var. for Coefficient of variation. St. Dev. for Standard Deviation

The histograms are represented in the Figures 33 and 34.

The histograms present a positive asymmetry in shape (skewed distribution) since the frequencies are not equally distributed. From the box-plots is possible to observe the length from the 1st quartil, which is smaller than the length of the 3rd quartil. From the Table 6 is possible to see the median which is always lower than the mean for both variables.

It is shown more frequency on the left-hand side of the peak meaning that the lower class of values for both hXRF1 and LAB datasets is significant. Despite the data shifting left there was no need to remove the bottom cut results since the data set was not considered has having a very large or even large population. The higher variance value is explained due to the low quantity of the available data set but also regards the distance between the samples, which decreases the autocorrelation between all pairs of data. Furthermore, the Fc presents more variability due to its heterogeneity.

As shown above, the coefficient of skewness is always positive and higher than 1 which indicates the lognormal distribution of the variables in study.

a)

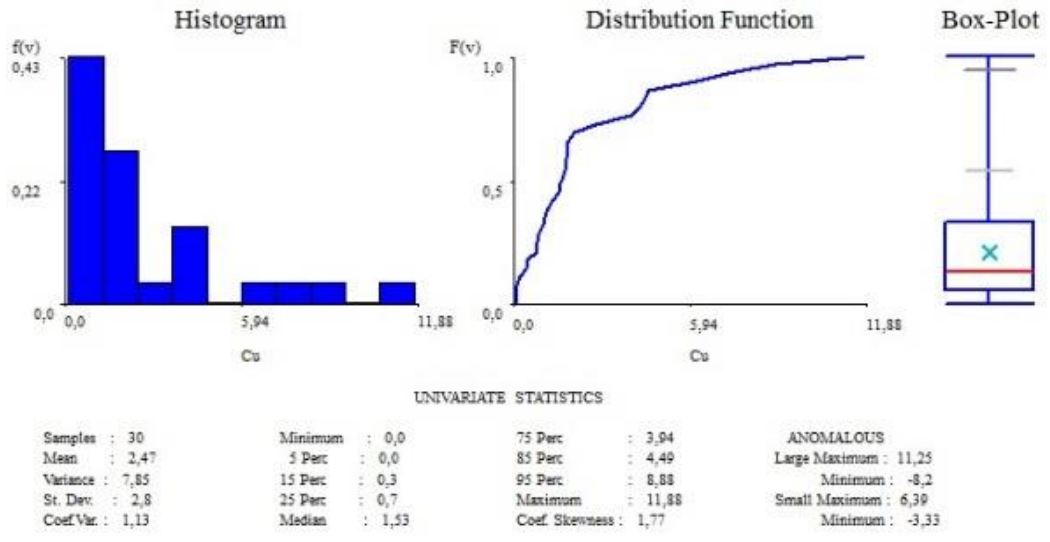

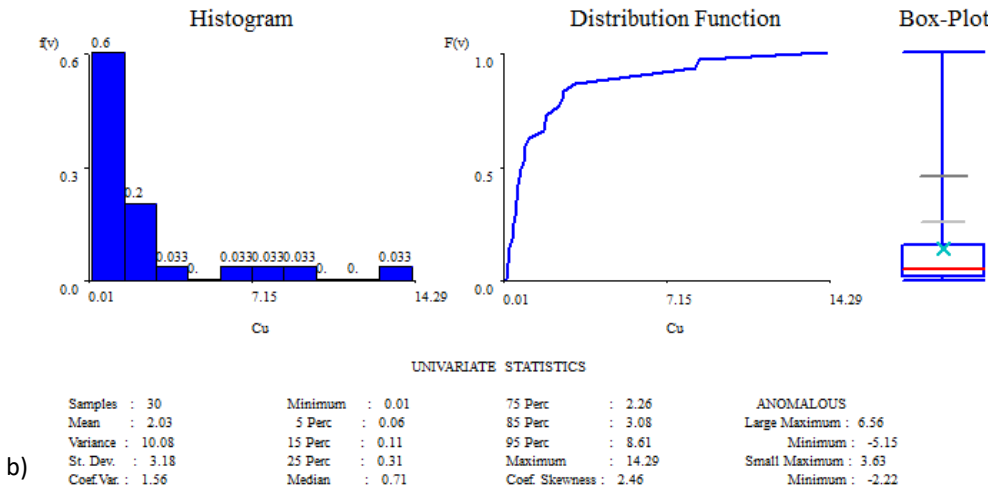

b)

Figure 33 - Cu histogram, probability distribution function and box-plot 30 samples a) hXRF1 b)LAB (GEOMS).

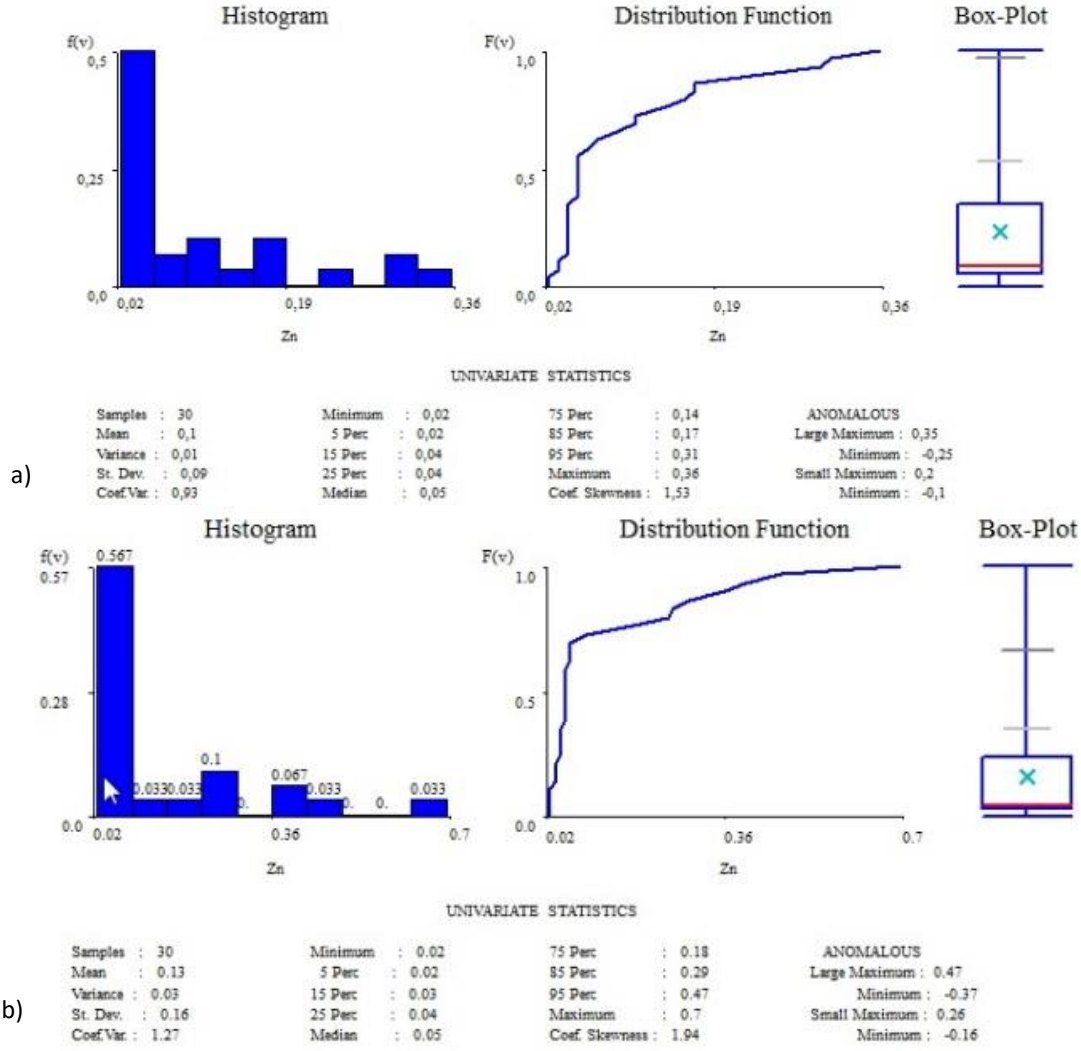

a)

b)

Figure 34 - Zn histogram, probability distribution function and box-plot 30 samples a) hXRF1 b) LAB (GEOMS).

The 3D grade spatial dispersion is shown through the Figures 35 and 36. From the spatial distribution is possible to infer the similar displacement or the positive relationship between the variables of Cu and Zn.

Two regions show higher grades of Cu and Zn, which are equally stressed in both data provided by hXRF1 and LAB.

a) b)

Figure 35 - Cu spatial grade distribution a) hXRF1 b) LAB (SGEMS).

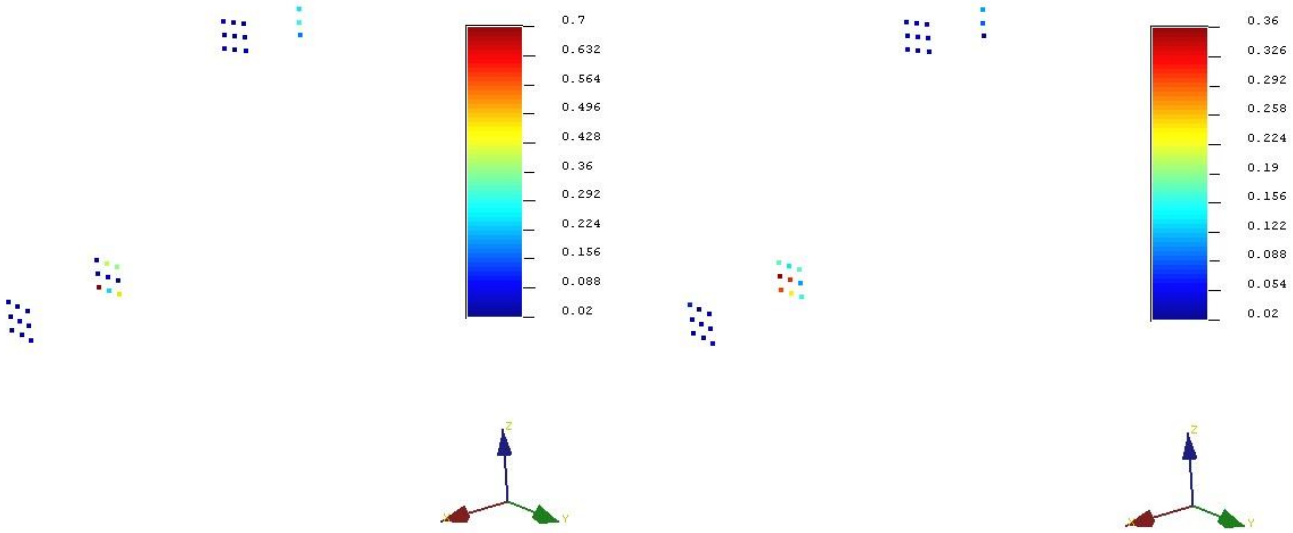

a) b)

Figure 36 - Zn spatial grade distribution a) hXRF1 b) LAB (SGEMS).

*U*GS and ALL

The statistical analysis for UGS and ALL is shown in the Table 7.

Table 7 - Statistics UGS and ALL.

Stockwork of copper	*Number of samples*	*Maximum*	*Minimum*	*Mean*	*Variance*	*Upper Quartile*	*Lower Quartile*	*Median*
UGS(Cu)	285	14.50	0	2.849	8.126	4.27	0.72	1.9
Zn	285	1.76	0	0.149	0.056	0.16	0.04	0.08
ALL (Cu)	515	11.35	0	0.433	1.247	0.34	0.02	0.1
Zn	515	0.63	0	0.032	0.003	0.03	0.00	0.02

The dot separates the integer part from the fractional part of the number written in decimal form.

Regarding the observed statistics it is important to remember the different locations where the UGS and ALL were taken. The UGS respects to Face Chip Sampling (in two topographic elevations) and the ALL, the drilling core sampling. Both cover different coordinates which reflects the different statistical results.

The histograms showing the distribution of the data regarding the Cu and Zn content grades are shown in the Figures 37 and 38.

The histograms for Cu and Zn grades present asymmetry with the tail on the left, which express more frequency of low-grade distribution. The histogram for Cu and Zn shows the tendency for two populations representing different levels of dilution: the values representing more frequency on low grades and the less frequency in high grades. The UGS integrates more variability in the data despite the smaller number of samples when compared with the ALL. The latest, is characterized by a significant low-grade mineral.

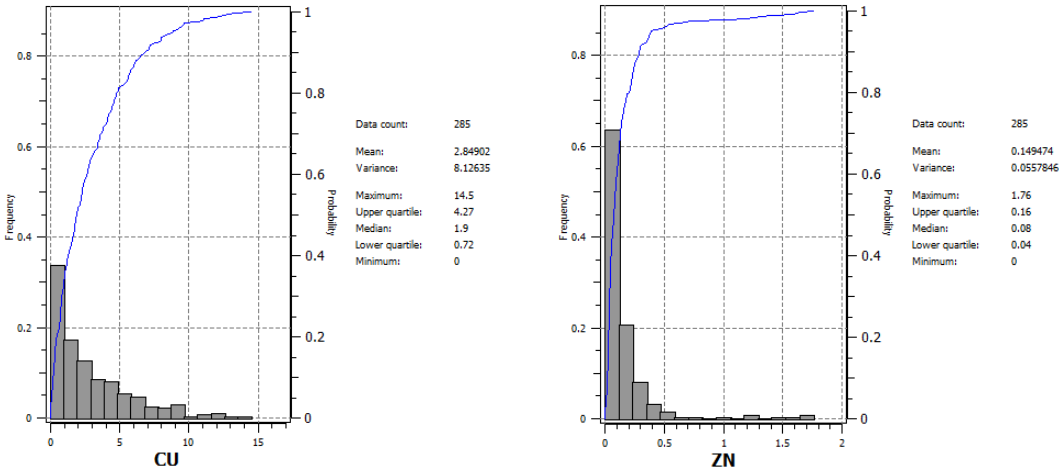

Figure 37 - Histograms and cdf for Cu and Zn, UGS (SGEOMS).

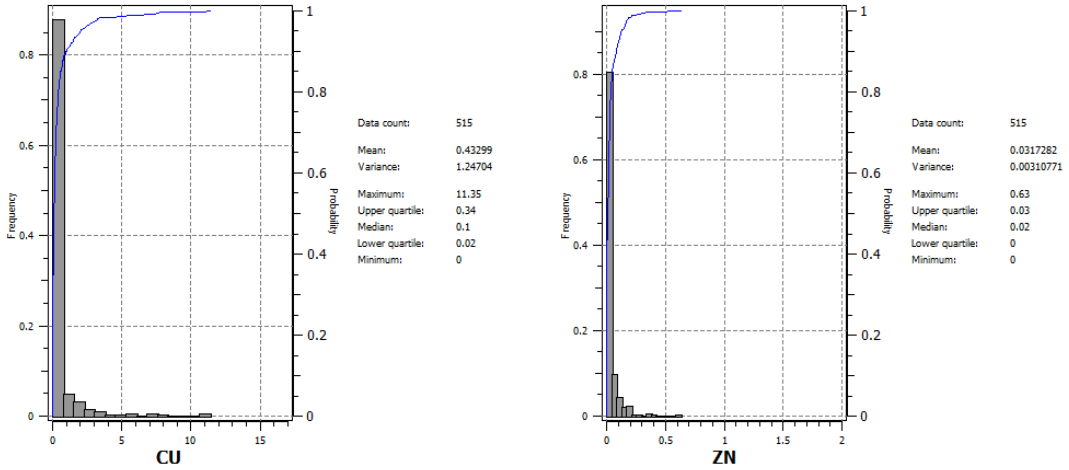

Figure 38 - Histograms for Cu and Zn ALL (SGEMS).

The spatial distribution is presented in the following Figures 39, 40 and 41. It was considered that the UGS and All are well distributed throughout the region.

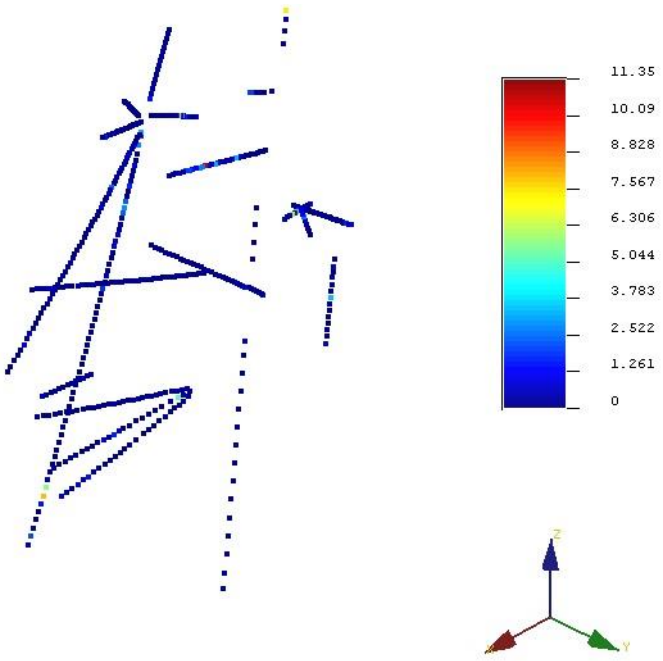

Figure 39 - Cu grade spatial distribution - ALL (SGEMS).

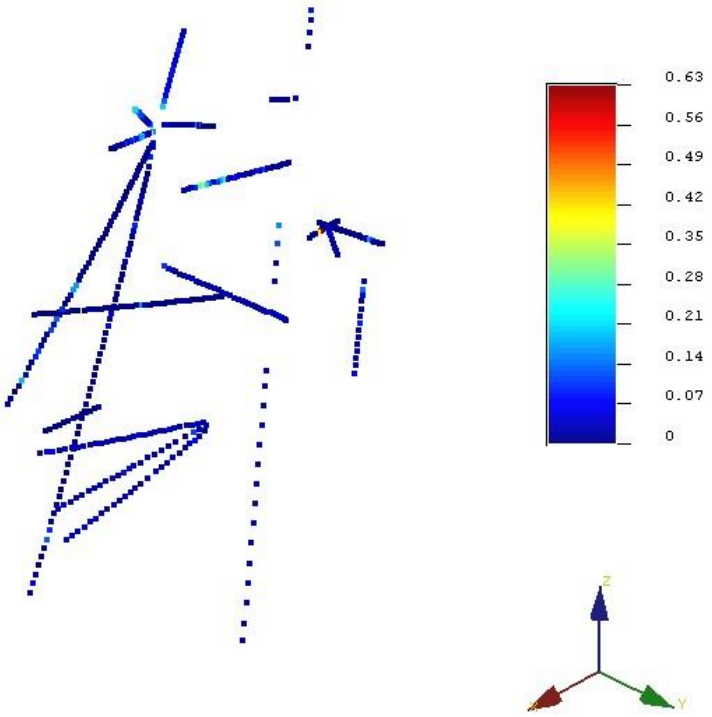

Figure 40 - Zn grade spatial distribution - ALL (SGEMS).

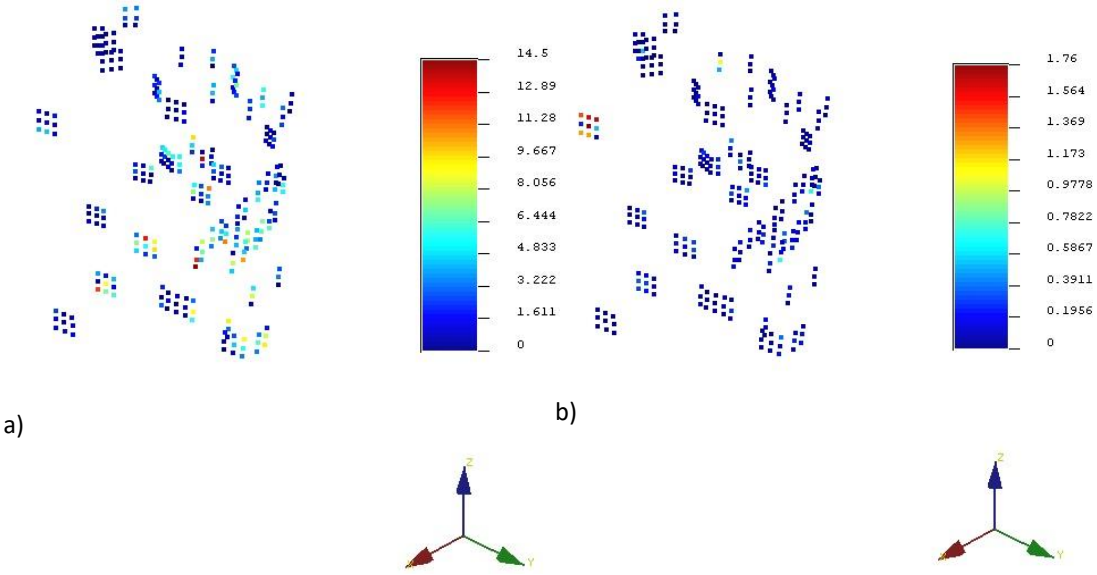

Figure 41 - a) Cu grade spatial distribution - UGS (SGEMS) b) Zn grade spatial distribution -UGS (SGEMS).

5.1.2 Bivariate Analysis

The Pearson's correlation between the data provided by hXRF and LAB is presented in the following figures (Figures 42,43 and 44). The graphs integrated the data obtained through the campaigns done in the previous years of 2015 and 2016, as well as the last campaign of 2017 regarding the FC, MC and MZ mineralization.
The linear correlation between both data are positive for which Y increases (LAB) as X increases (hXRF). The Pearson correlation coefficient, ρ, is approximately 94% for Cu while it is shown 74% for Zn within the FC, 95% and 89% regarding the MC and 97% and 85% respectively for the MZ. Despite the minor number of outlines discordant with the data that may produce a small influence in the equation (Figures 42 b), 43 b)), it is shown a linear dependency between hXRF and LAB. The following table stablish the intervals of correlation.

Both linear regression equations for Cu and Zn considering the FC mineralization (Figure 42) were used in the next subchapter 5.1.3 to predict the data that would be possible taken from the hXRF device in the same coordinates provided by the support of data UGS (hXRF2). In general, the observation of the datasets follows a positive and strong correlation.

Table 8 - Pearson's correlation classification.

Correlation	$\|\rho\|$
Negligible	0 - 0.3
Weak	0.3 – 0.5
Moderate	0.5 - 0.7
Strong	0.7 – 0.9
Too strong	0.9

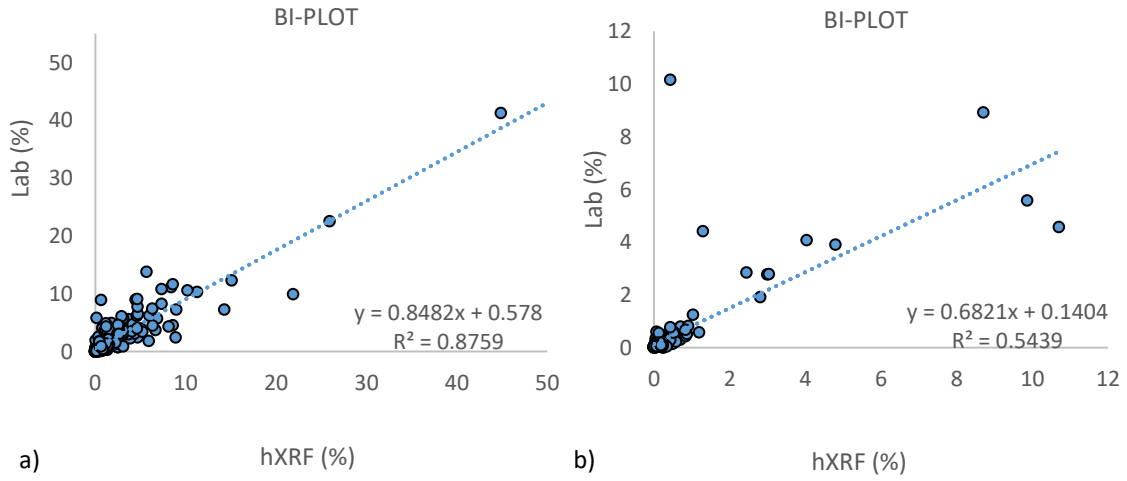

Figure 42 - Correlation between the hXRF and Lab data sets for FC/FE a) Cu b) Zn.

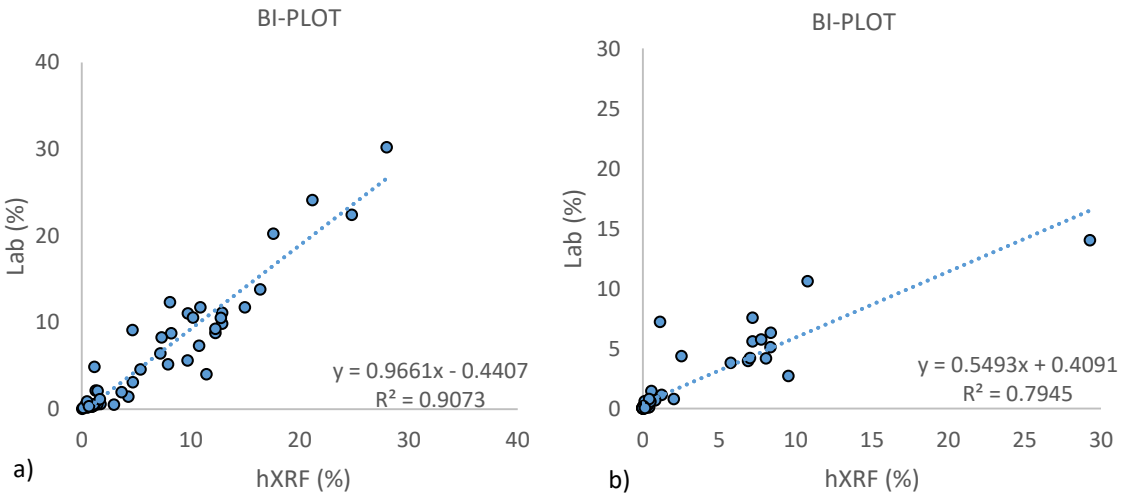

Figure 43 - Correlation between the hXRF and Lab data sets for MC a) Cu b) Zn.

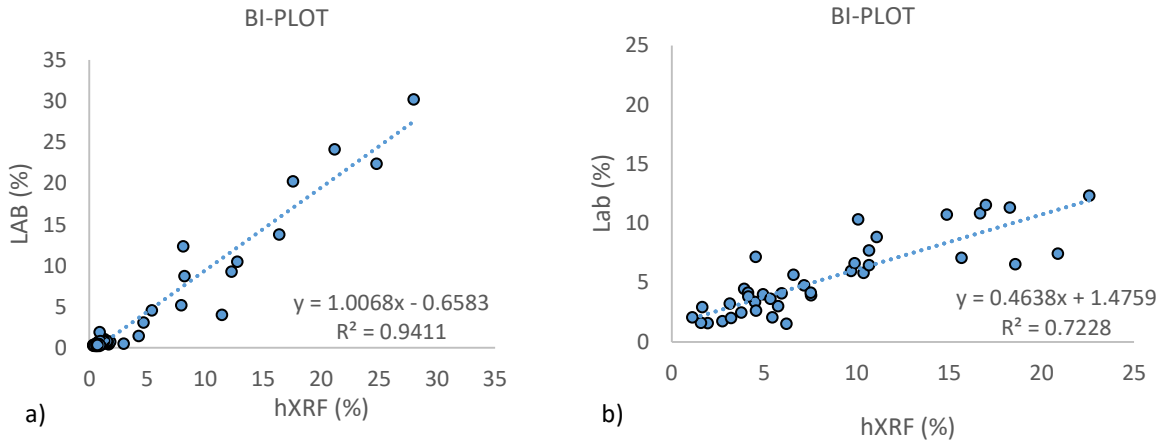

Figure 44 - Correlation between the hXRF and Lab data sets for MZ a) Cu b) Zn.

5.1.3 Forecast hXRF2

The forecast of the possible hXRF data under the UGS coordinates (hXRF2) uses the correlation presented in the bi-plots between the hXRF and LAB for the FC regarding the Cu grade. It is expected to obtain predictions close to the actual values given by the UGS since the R^2 was close to 0,90, as expressed in the Figure 43 a). The forecast data hXRF2 was created through the Equation 5.1 expressing the simple linear model obtained above. It is important to add that this forecast does not integrate the randomness and variability given by the deposit's mineralization features.

$$\widehat{\boldsymbol{y}} = \widehat{\boldsymbol{\beta_0}} + \widehat{\boldsymbol{\beta_1}}\mathbf{x} \qquad \textbf{(5.1)}$$

Where $\widehat{\boldsymbol{y}}$ represents the Cu grade from the hXRF and $\boldsymbol{x}$ is the value of the predictor for which it is required a forecast meaning the Cu grade from the Face Chip Samples UGS. $\widehat{\boldsymbol{\beta_1}}$ represents the slope of the linear regression and $\widehat{\boldsymbol{\beta_0}}$ is a referenced value intersecting the $\widehat{\boldsymbol{y}}$ axis.

The predicted values for hXRF regarding the available UGS data were calculated through the substitution of $\boldsymbol{x}$ by the Cu grade provided from the UGS. Since the values of $\boldsymbol{x}$ where not part of the data used while estimating the linear regression model (Figure 43), the value for the $\widehat{\boldsymbol{y}}$ could be considered a genuine forecast.

The comparison between UGS and hXRF2 is shown as it follows (Table 9).

Table 9 - Statistics between the UGS and the forecast hXRF2.

STATISTICS	*UGS (Cu)*	*hXRF2 (Cu)*	*Difference*	*UGS (Zn)*	*hXRF2 (Zn)*	*Difference*
Data Count	285	285	--	285	285	--
Mean	2.85	2.86	0.01	0.15	0.18	0.03
Variance	8.13	10.28	2.15	0.06	0.09	0.03
Maximum	14.50	16.41	1.91	1.76	2.37	0.61
Upper Quartile(Q3)	4.27	4.35	0.08	0.16	0.16	0.00
Median	1.90	1.56	0.34	0.08	0.13	0.05
Lower Quartile(Q1)	0.72	0.47	0.25	0.04	0.07	0.03
Interquartile range (Q3-Q1)	3.55	3.88	0.33	0.12	0.09	0.03
Minimum	0.00	0.00	0.00	0.00	0.00	0.00

The dot separates the integer part from the fractional part of the number written in decimal form.

The variance and the maximum are higher in the hXRF2 data although the mean between both methods have 1% and 2% of difference for Cu and Zn, respectively.

The cumulative distribution function, CDF is useful to compare UGS and hXRF2 data sets indicating when the probability for an observation is lower or greater than a certain value of grade (Figures 45 and 46). Up to 12 %

and 20% of the population presents more than 1% grade for Cu in the UGS and hXRF2 data sets. Regarding Zn, the values containing more than 1% grade are represented by less than 1% of probability.

The histograms and cumulative distribution functions are shown as it follows.

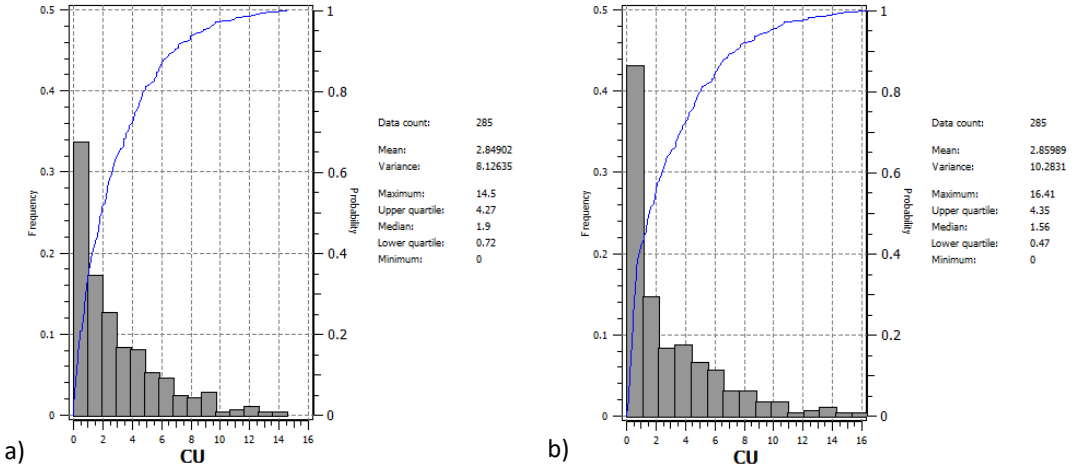

Figure 45 - a) Histogram and cfd for Cu through UGS b) Histogram and cfd for Cu through hXRF2.

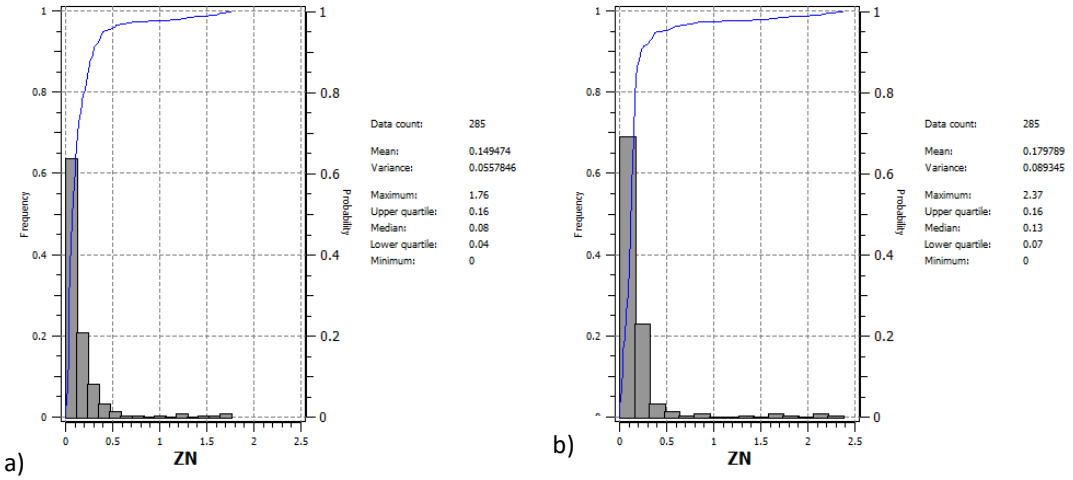

Figure 46 - Histogram and cfd for Zn through UGS b) Histogram and cfd for Zn through hXRF2.

Analyzing the spatial distribution (Figure 47 and 48) is possible to confirm the similarity between both grade distribution results.

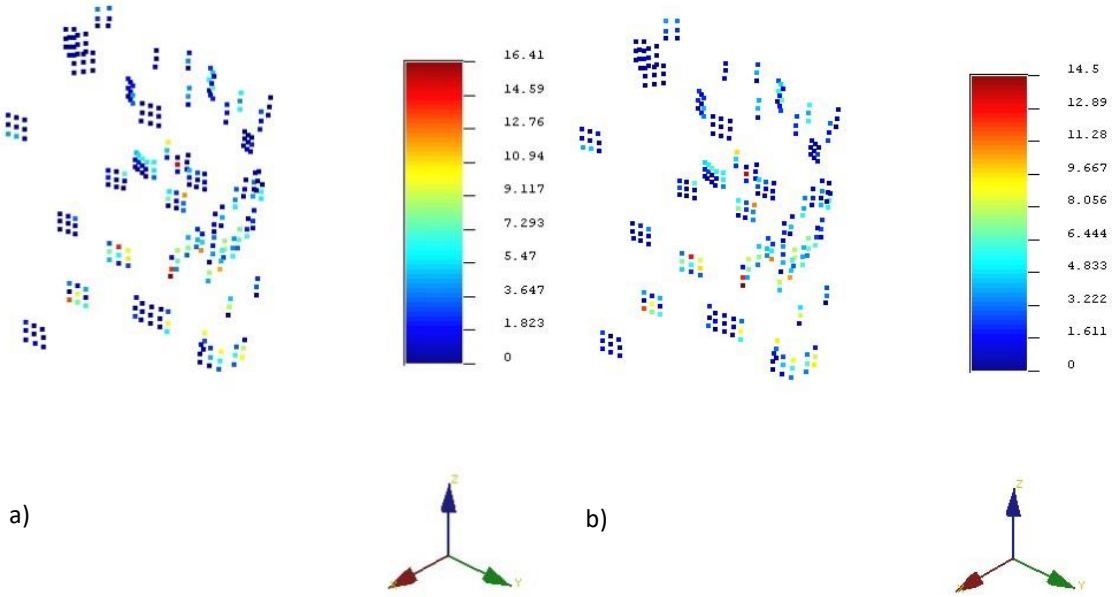

Figure 47 - a) Cu Spatial distribution through UGS b) Cu Spatial distribution through hXRF2.

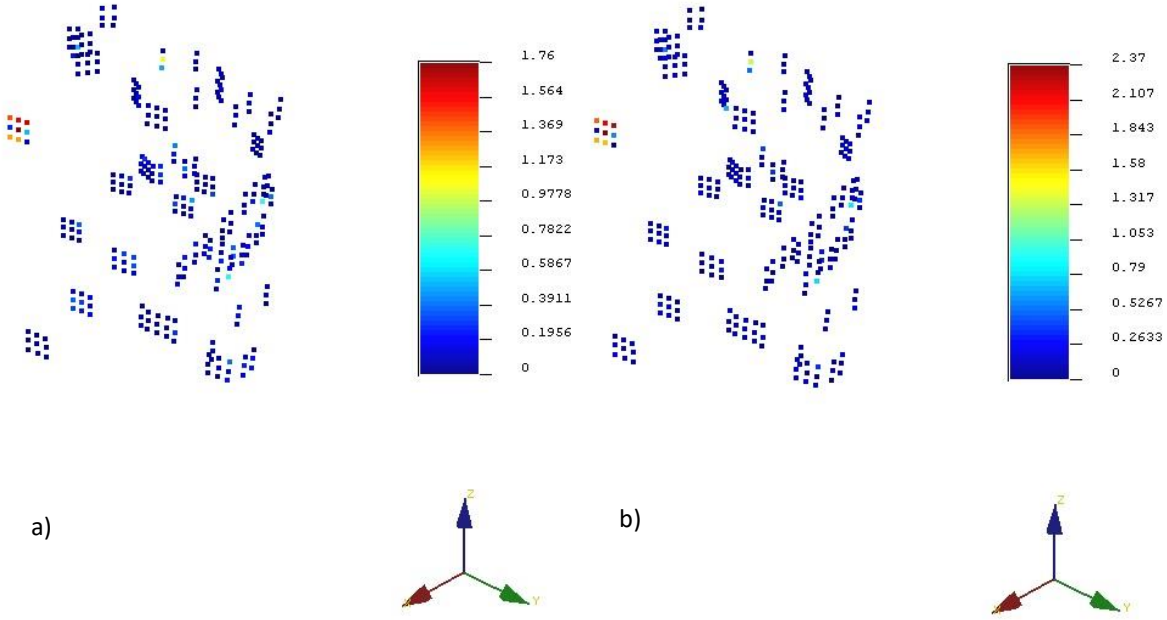

Figure 48 - Zn Spatial distribution through UGS b) Zn Spatial distribution through hXRF2

The MRE will be supported through the comparison between 3 types of data: UGS + ALL, hXRF2 + ALL and ALL. Regarding the type of mineralization FC, the variable in study is the Cu grade which have an economic interest after stating the cut-off grade. The following histograms are shown (Figures 49 and 50), regarding the comparison between the UGS + ALL and hXRF2 + ALL support data for Cu (All histogram was previously presented in the Figure 38).

Table 10 - Statistical parameters for the hXRF2+ALL and UGS+ALL results.

STATISTICS	*UGS+ALL (Cu)*	*hXRF2+ALL (Cu)*	*Difference*	*UGS+ALL (Zn)*	*hXRF2+ALL (Zn)*	*Difference*
Data Count	800	800	--	800	800	--
Mean	1.29	1.30	0.01	0.07	0.08	0.01
Variance	5.03	5.81	0.78	0.03	0.04	0.01
Maximum	14.50	16.41	1.91	1.76	2.37	0.61
Upper Quartile(Q3)	1.50	1.28	0.22	0.08	0.12	0.04
Median	0.27	0.27	0.00	0.03	0.03	0.00
Lower Quartile(Q1)	0.05	0.05	0.00	0.00	0.00	0.00
Interquartile range (Q3-Q1)	1.45	1.23	0.22	0.05	0.12	0.07
Minimum	0.00	0.00	0.00	0.00	0.00	0.00

The dot separates the integer part from the fractional part of the number written in decimal form.

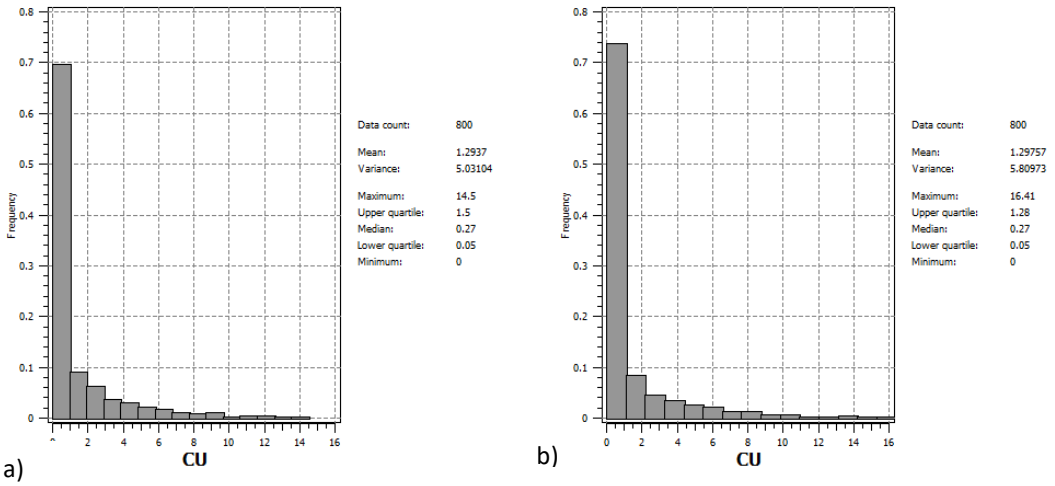

a) b)

Figure 49 - a) Cu Histogram - UGS + ALL b) Cu Histogram - hXRF2 + ALL (SGEMS).

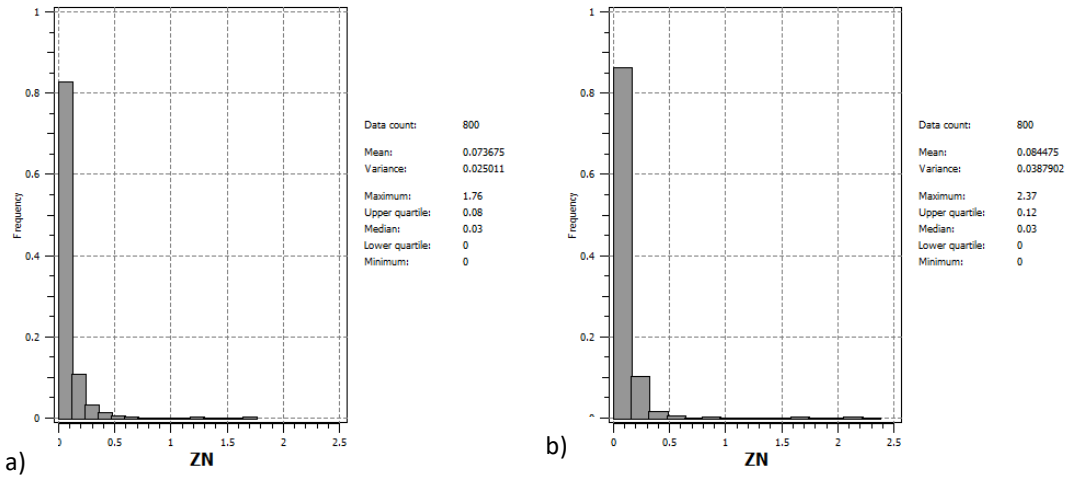

a) b)

Figure 50 - a) Zn Histogram - UGS + All b) Zn Histogram - hXRF2 + ALL (SGEMS).

5.2 ORDINARY KRIGING

This thesis adopted the geostatistical method called ordinary kriging to obtain the MRE.

Regarding the variography, it was decided to perform the kriging estimation under the best directions of continuity given by the Geological Department of Somincor. With this process, it is expected to verify not only the validity of the hXRF2 but also to quantify the advantages from its inclusion as fast data between the drillings hole campaigns (ALL). After the estimates, it will be plotted the recovery curves considering the Cu MRE towards FC. Herein, the estimation of Zn is not significant within this type of mineralization.

5.2.1 Model of Blocks

Regarding the support of data, there are not significant advantages from giving an interval of estimation smaller than the sample intervals. Then, it was decided to proceed with the estimation using 148 (x), 144 (y) and 64 (z) blocks with the dimension of 0. 5 x 0. 5 x 0. 5 m^3 for each mining unit. In total, it corresponds to 1, 363 968 blocks and since each block has 0.125 m^3 , the total volume of the region to be estimated is approximately 170 496m^3. The density was previously considered as 4. 5 t/m^3, thus, the total quantity of mass within the region is about 767 232 t. The block model (Figure 51) regarding the ALL and hXRF2 (or UGS) data sets is described through the coordinates expressed in Table 11. The geostatistical algorithm is not so dubious generating significant errors. However, it is important to stress the errors produced in the extremes of the region in study. For instance, when performing the estimation block by block this information is important since the values located in the extremes will always be attenuated.

From the region of interest (Table 5, subchapter 4.2.3) the coordinates for the estimate were more tailored to restrict the object of study inside the boundary previously defined. Hence, it was expected to minimize the effects from the attenuation in the extremes of the data set.

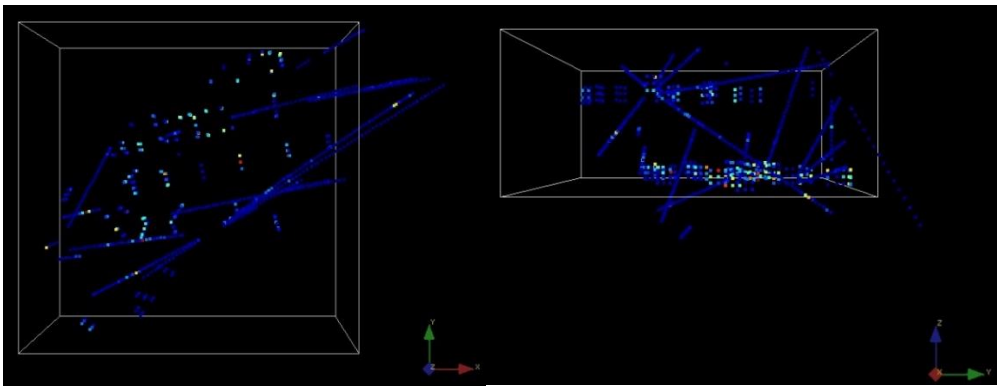

Figure 51 -Block model spatial representation integrating the ALL+UGS data in Y0X and Z0Y planes perspectives.

Table 11 – Extension of the adopted grid.

Coordinates	*Center of origin cell (m)*	*Extension(m)*
x	4074.00	74.00
y	3055.00	66.88
z	750.00	24.15

The dot separates the integer part from the fractional part of the number written in decimal form.

The distribution of UGS and hXRF2 data are inserted in two layers (herein indicated only for a better spatial reference) called down layer and top layer, due to their different topographic elevations (Figure 52).

The following Tables 12 and 13 describe their intervals through the x, y and z coordinates. Between both layers, only the All data is available for the estimation since the UGS was not spread within this region.

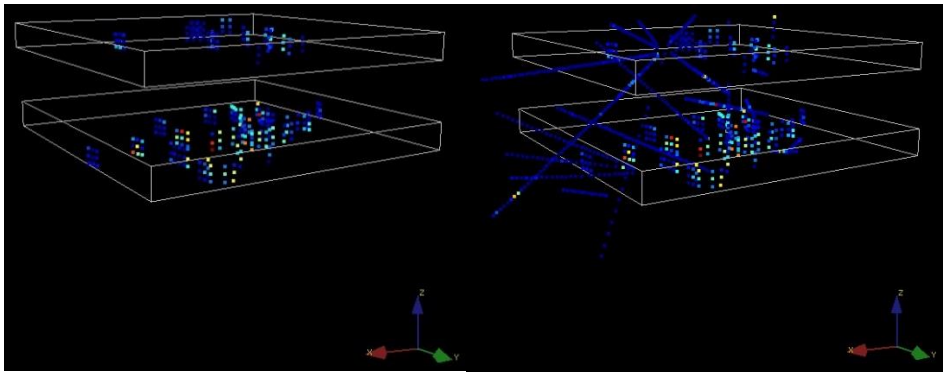

Figure 52 - Distribution of the UGS or hXRF2 distribution throughout the different topographic elevations (SGEMS).

Table 12 - Extension for the down layer

Coordinates	Interval (m)
X	[4074; 4148]
Y	[3055; 3125]
Z	[750; 774.15]

Table 13 - Table 12 - Extension for the upper layer

Coordinates	Interval (m)
X	[4074; 4148]
Y	[3055; 3125]
Z	[770; 776]

5.2.2 Result

The samples were inserted in a small fraction and volume of the mineral deposit and will be used to predict the grades distribution regarding the metal of interest Cu, in the non-sampled locals. Through the ordinary kriging estimate, the global resources will be quantified.

Firstly, within this region, the samples were representative or fairly normally distributed since they were taken in a quasi regular grid. The normal QQ Plot (Annexes A1) was checked to compare how the data hXRF2

and ALL is normally distributed when lined up. Although, an error from the estimation is always considered through the variance of kriging.

The results from the kriging estimator regarding the UGS and hXRF2 data sets show a smoothed spatial inference. The optimal prediction surface obtained from the estimator through the mathematical function or as previously referred, the semi-variogram, is also in concordance with the input data. As illustrated (Figure 53) and tabled (Table 14), the UGS and hXRF2 estimates are similar and can be both considered the same data.

Table 14 - Statistics after ordinary kriging estimation of Cu distribution grade ALL, UGS and hXRF2.

FC Variable Cu	*Number of BLOCKS*	*Maximum*	*Minimum*	*Mean*	*Variance*	*Upper Quatile*	*Lower Quartile*	*Median*
ALL	1363968	4.37	0.00	0.52	0.13	0.68	0.27	0.44
UGS	1363968	10.21	0.19	2.40	0.73	2.70	1.93	2.32
hXRF2	1363968	11.37	0.28	2.37	0.87	2.68	1.86	2.28

The color bars express the higher grades of Cu and Zn through the “warmer” colors and the low grades variation between 0 to 2 are shown in blue. As expected, the hXRF2 and UGS data express similarity and the zonality characterized by an abnormal or higher concentration of Cu. The estimation is gradual and only the maximum values differs in 11% between both data.

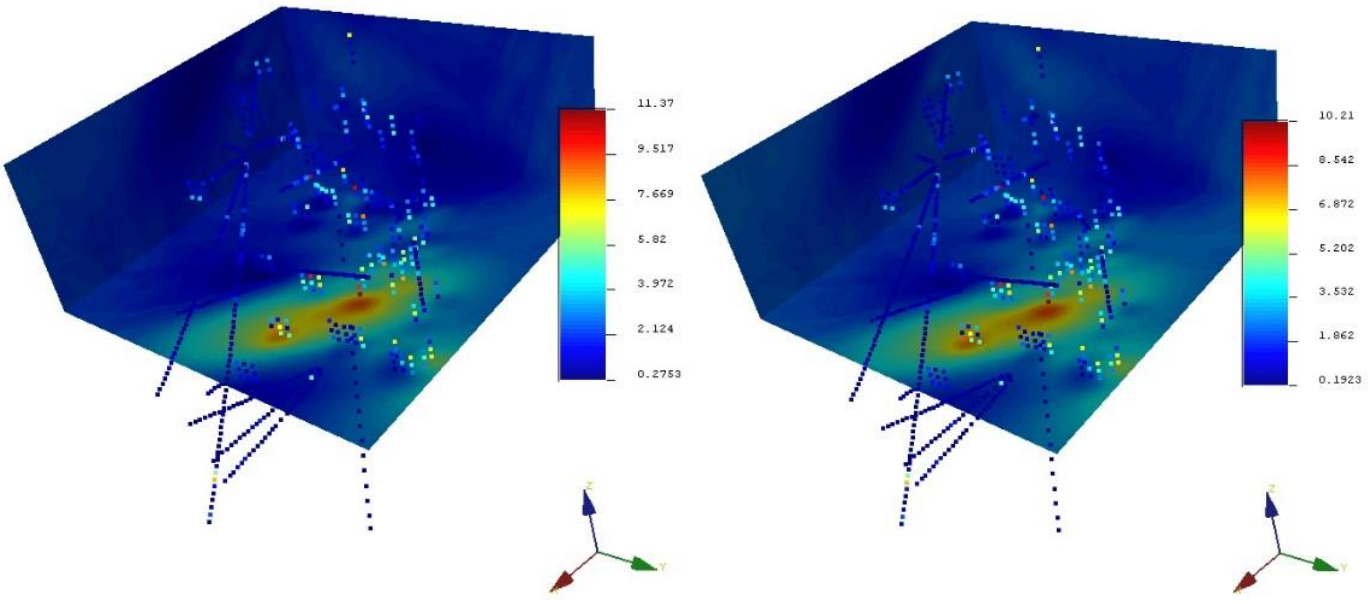

a) b)

Figure 53 - Spatial representation of ordinary kriging results for Cu grades a) UGS b) hXRF2.

The estimation through ALL is represented by the lower grades, showing a small area of Cu concentration.

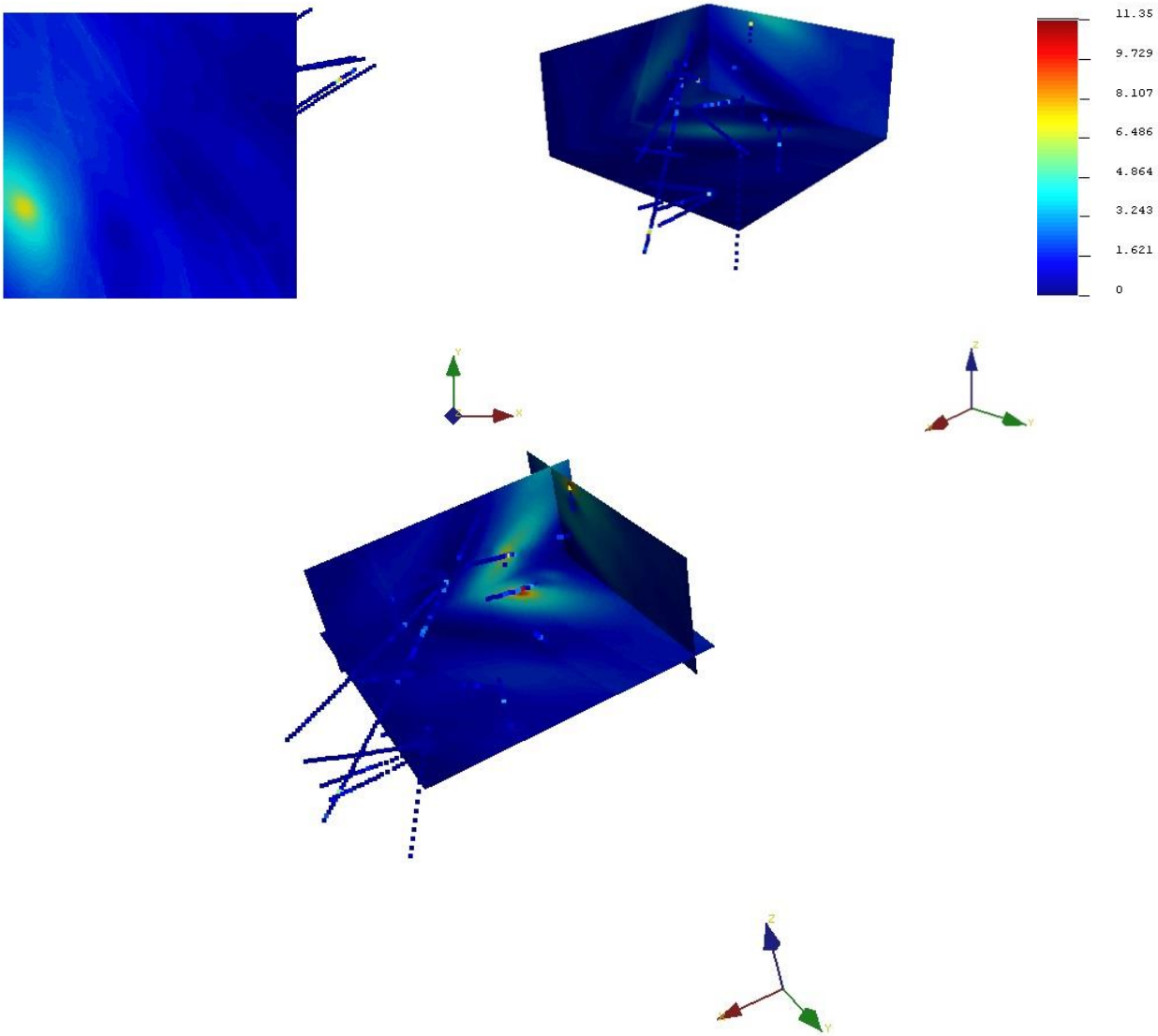

Figure 54 - Spatial representation of ordinary kriging results for Cu grades ALL (GEOMS)

After adding the ALL data in the same support with hXRF2, the results from the estimation are described in the Figure 55 and its statistics presented in the Table 16. In the annexes A2 are illustrated the results regarding the UGS + ALL. Once again, the ordinary kriging estimator reproduced the sampled values. As expected, after adding the ALL data, the mean, maximum and median decreased while the variance increased.

Comparing the statistics between the sampled data and the estimated values after kriging it was observed a reduction of the maximum values and the variance. On contrary, the mean after kriging is increased. After confirmed the approximation between UGS + ALL and hXRF2 + ALL, the further process for the MRE will be compared between the hXRF2 and ALL.

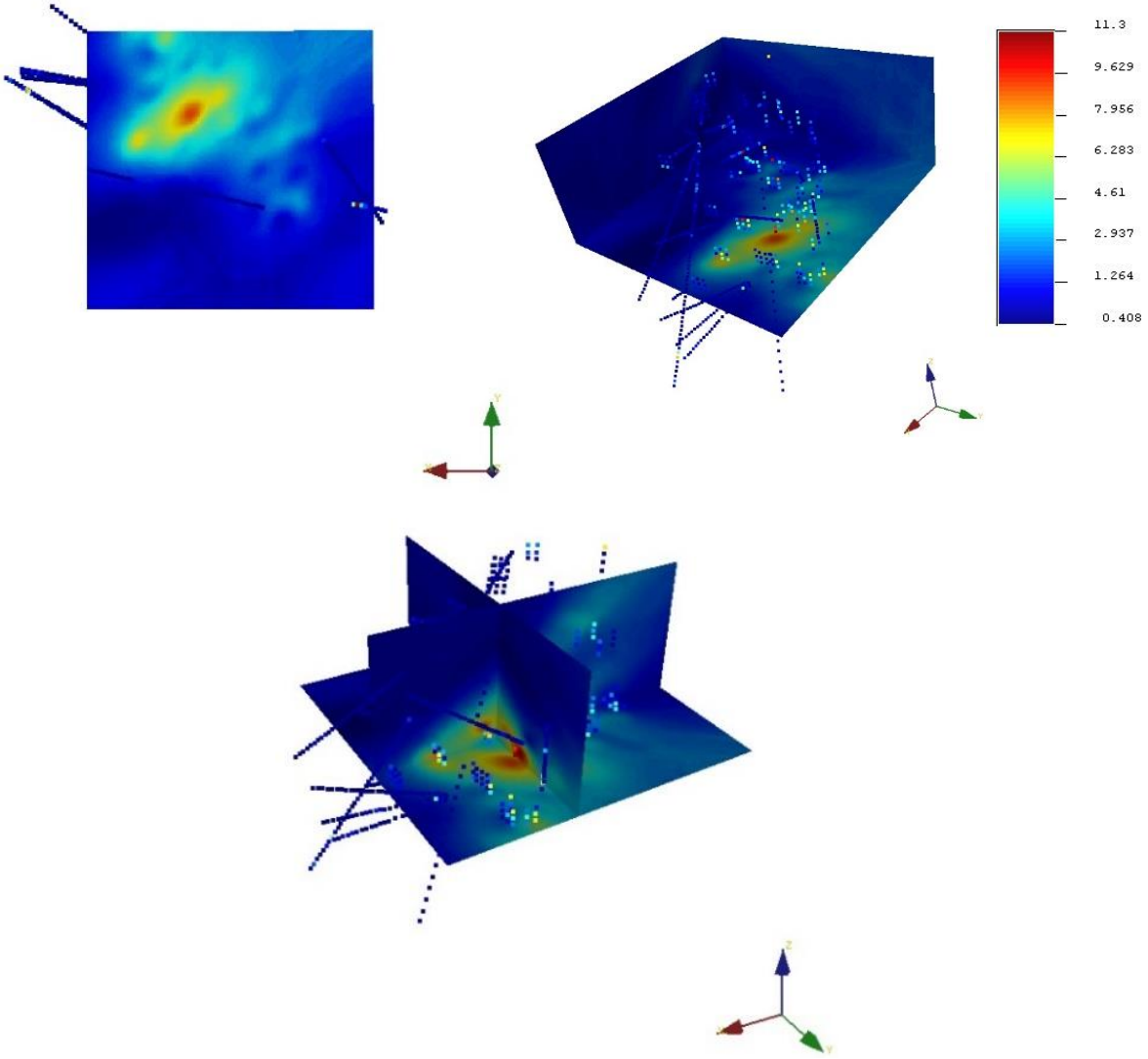

Figure 55 - Spatial representation after ordinary kriging results for Cu grades hXRF2 +ALL (SGEMS).

Table 15 - Statistics after ordinary kriging estimation for Cu grade UGS+ALL and hXRF2+ALL.

FC Variable Cu	*Number of BLOCKS*	*Maximum*	*Minimum*	*Mean*	*Variance*	*Upper Quatile*	*Lower Quartile*	*Median*
ALL	515	11.35	0.00	0.43	1.25	0.34	0.02	0.1
ALL Krig	1363968	4.37	0.00	0.52	0.13	0.68	0.27	0.44
UGS+ALL	800	14.50	0.00	1.29	5.03	1.50	0.05	0.27
UGS + ALL Krig	1363968	10.16	0.00	1.35	1.09	2.01	0.50	1.11
hXRF2+ALL	800	16.41	0.00	1.30	5.81	1.28	0.05	0.27
hXRF2+ALL Krig	1363968	11.30	0.00	1.35	1.70	1.98	0.48	1.08

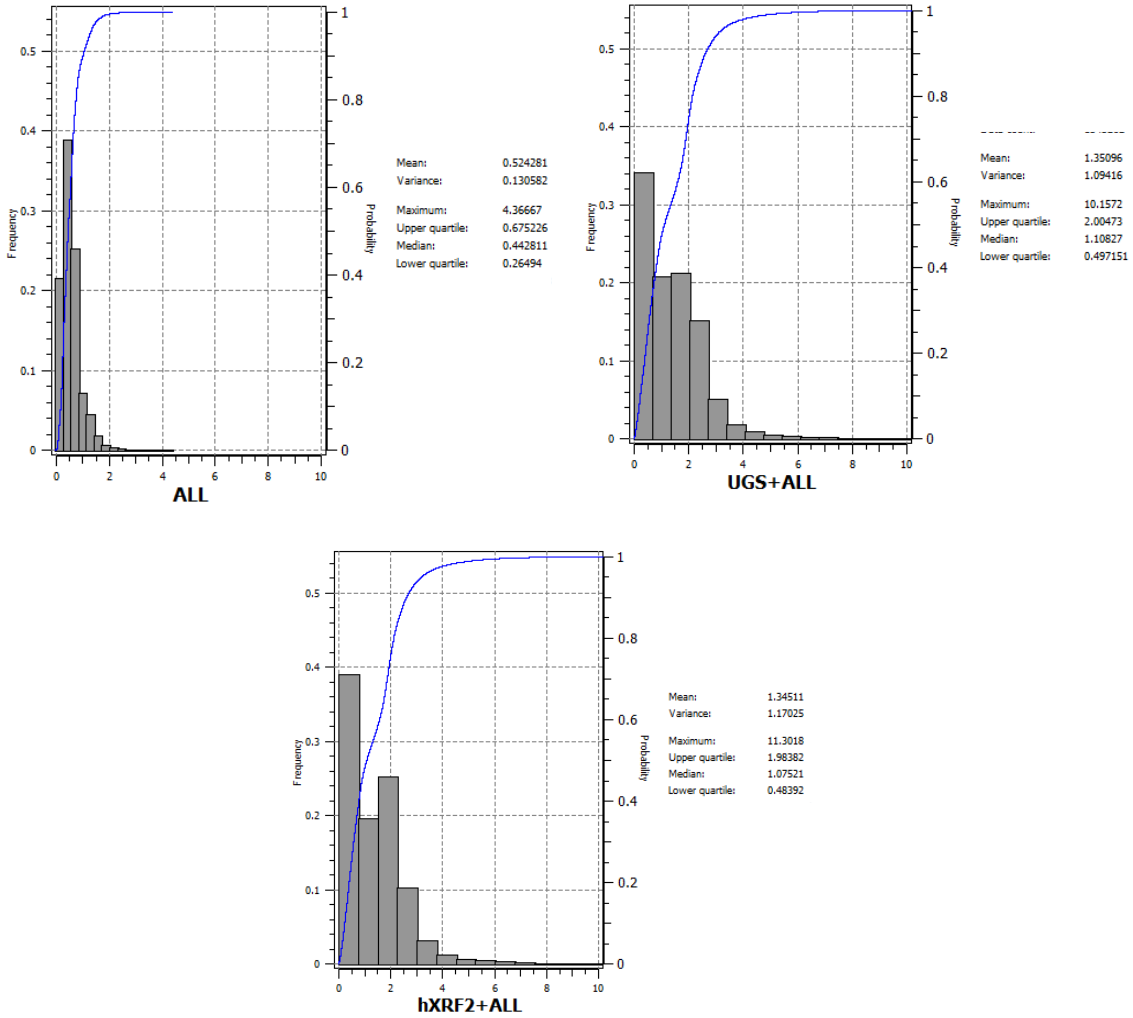

Figure 56 - Histogram and cdf after estimation based on ALL, UGS+ALL and hXRF2+ALL support of data

The variance of kriging is shown in the Annexes A2. As expected, it increases with the increase of the distance between the point to estimate and the sample.

5.3 RESOURCES AND RESERVES

The MRE were parameterized according to a hypothetical Cu cut-off of 0.7g/t within the FC mineralization. The calculations on the parametric curves on Cut-Off vs tonnage, mean grade ($t_{Cu}(\%)$) and quantity of metal ($M_{Cu}(t)$) were previously indicated (subchapter 2.6). The resulting graphs are herein indicated (Figures 57 to 59).

From the initial information regarding the original data samples (UGS and ALL) and the forecast (hXRF2), the recovery of Cu is relatively quantified. Considering the number of data, the maximum value of tonnage refers to the inexistence of the cut-off value (e.g. for hXRF2, $T(z) = 215$, where z =0). Considering a hypothetical cut-off value of 0,7 (z =0.7) then the available tonnage is $T(z) = 83$ in relative terms. This process for the MRE is described in the following Table 16.

Table 16 – Resources and reserves from the sampled data values, apriori and under a Cut-off of 0.7g/t.

FC	N_{data} $_{Resources\ T(z),z=0}$	$N_{data}\mathbf{g_{Cu}} > \mathbf{g_{Cut-off}}$	% $\boldsymbol{Reserves}$ T(z), z=0.7g/t	$t_{Cu}(\%)$	$\%M_{Cu}$
ALL	515	71	13	0.06	8
hXRF2 + ALL	800	250	31	0.41	13
UGS + ALL	800	288	36	0.46	17
UGS	215	189	88	2.51	22
hXRF2	215	179	83	2.38	20

After proceeding with the estimate through ordinary kriging, the obtained results are shown as it follows (Tables 17 and 18).

Table 17 - Resources after the ordinary kriging estimation.

FC	N_{block}	$V_{cell}(m^3)$	$V_{dep}\ (m^3)$	$Tonnes_{Cu}$	$t_{Cu}(\%)$	$M_{Cu}(tonnes)$
ALL					0.52	39 896
hXRF2 + ALL					1.35	103 576
UGS + ALL	1 363 968	0.125	170 496	767 232	1.35	103 576
UGS					2.40	148 136
hXRF2					2.37	148 100

Table 18 - Reserves from the sampled data values, after the estimate and under a Cut-Off of 0.7 g/t.

$\mathbf{g_{Cu}} > \mathbf{g_{Cut-off}}$	N_{block}	$V_{cell}(m^3)$	$V_{dep}\ (m^3)$	$Tonnes_{Cu}$	$t_{Cu}(\%)$	$M_{Cu}(tonnes)$
ALL	312 239		39 030	175 635	1.04	18 266
hXRF2 + ALL	851 701		106 463	479 084	1.90	91 026
UGS + ALL	872 403	0.125	109 050	490 725	1.89	92 747
UGS	1 349 255		168 657	758 956	2.42	138 660
hXRF2	1 345 165		168 146	756 655	2.40	137 597

The total inferred resources of Cu regarding the hXRF2 and hXRF2+ALL is always more conservative once compared with the UGS and UGS+ALL. The MRE for hXRF2+ALL presents a production of 479 084 T with the Cu mean grade of 1.90 and metal quantity of 91 026 T. Comparing the results with ALL, it was provided a

significant additional data and towards the UGS+ALL, the difference does not express abnormal disadvantages.

As the recovery curves comparing ALL, hXRF2 + ALL and UGS+ALL after the estimate process are illustrated in the following Figures 57, 58 and 59. As it is shown in the Figure 57, the ALL trends to reproduce a logarithm curve, the UGS and hXRF2 follows the trend of a polynomial curve and the hXRF2+All and UGS+ALL are attenuated functions. The latest, start to follow a logarithm curve and then present an inflection. The tonnage necessary to produce decreases with the increasing Cut-off and the error between both data increases with the increasing of the cut-off grade.

In general, the curves after the interpolation process express the gradual distribution of the grades and as expected, the ALL is characterized by low grades of Cu and both data hXFF2 and hXRF2+ALL show more conservative models.

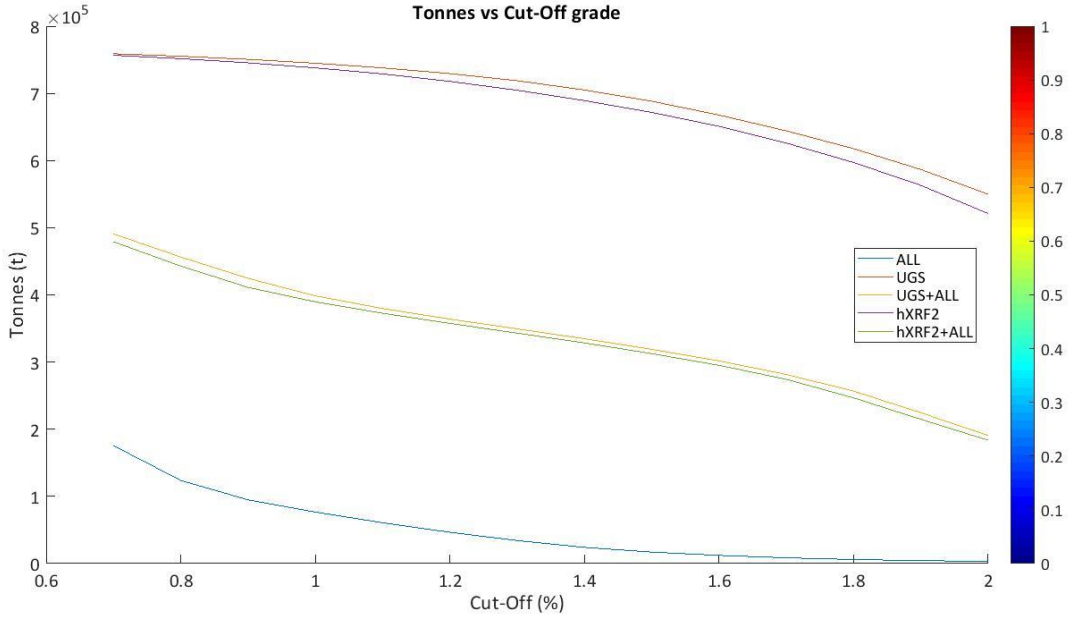

Figure 57 - Parametric Curves after ordinary kriging estimate.

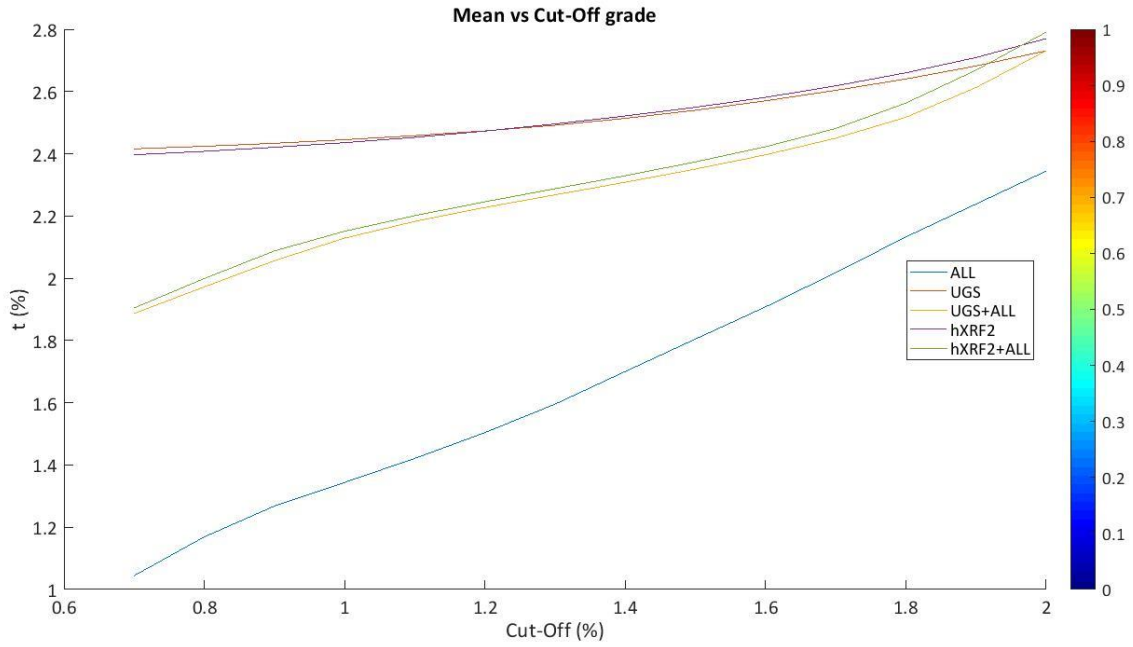

Figure 58 - Mean vs Cut-Off grade after ordinary kriging estimate.

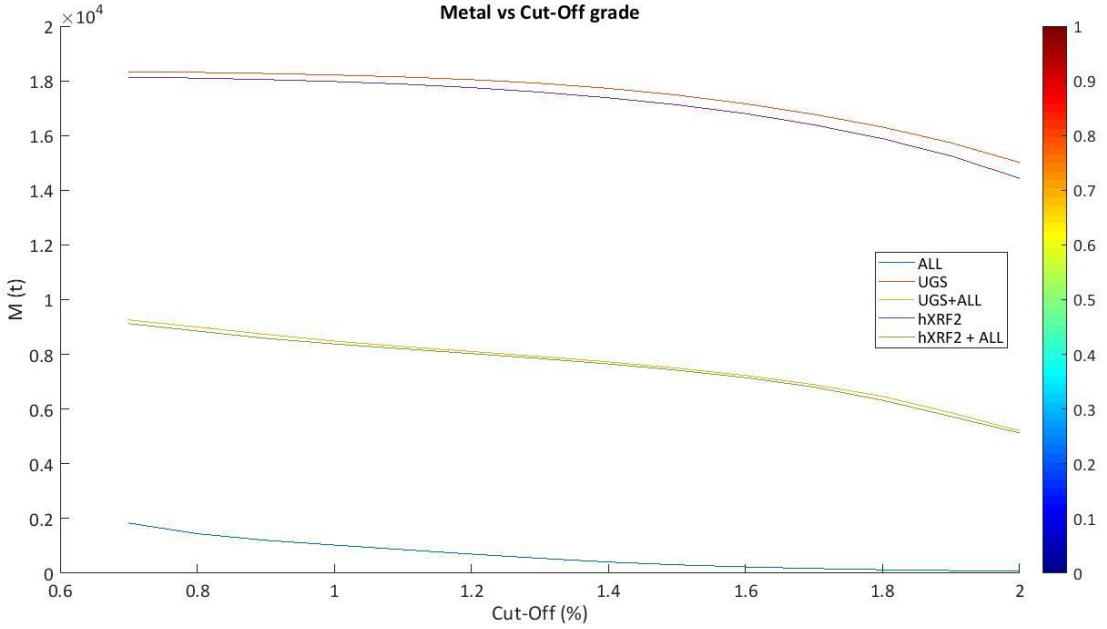

Figure 59 - Metal vs Cut -Off grade after ordinary kriging estimate.

CHAPTER VI. CONCLUSIONS

The aim for this thesis was to explore the validity of integrating fast data into the updating of the resources estimation through the Real Time purpose.

The geochemical analysis executed by the hXRF regarding the grade elements of interest, Cu and Zn, provided good approximations towards the laboratorial results. It was considered that the correlation between both methods are equi-comparable which shows that the hXRF is able to support the drilling hole sampling and face chip sampling campaigns. From the results obtained, and remembering the simplified handling of the instrument, it was shown 88%, 91% and 94% of correlation between hXRF and LAB regarding the Cu grades in the FC, MC and MZ. Hence, the correlation results were classified as strong and too strong.

The equipment is able to be used in the mining stopes to support the UGS and ALL campaigns. When it is not possible to obtain a visual estimate due to the low grade, the hXRF may provide a good support.
However, it is expected the evaluation of the data with the necessary precaution when working with grades nearby the cut-off grade. The device provides operational or instrumental errors associated to its limitations, but the human error has also to be considered.

Some of the measurements taken from the hXRF may be subestimated once compared with the laboratorial references. The subestimation may be due to the unit's window's area. In the other hand, the laboratorial assays prepare the samples until obtain a homogeneous and representative material which improves the incidence of the beans and the correspondent efficiency in the measurements while detecting the elements.

It was also verified that the portable XRF presents an increase of the error with the higher grades. For this reason, it is considered its best performance towards the FC mineralization when is needed to decide between to leave or to continue the production.

It should be noted the need to work in a new campaign considering an extended timetable and the collection of a great among of data in each of the deposits. The massive of copper and zinc deposits should be target as the next domaining to test. The next chapter will better reinforce the aspects to consider regarding a new campaign.

Applying a hypothetical cut-off grade of 0.7%, for the global MRE and regarding the Cu, the hXRF2+ALL has shown a production of 479 084Mt for an average grade content of 1.90 % and quantity in metal of 91 250t. It clearly adds more information in comparison with the available ALL data but also expresses a more conservative model towards UGS+ALL. The possibility to obtain the previous resources and reserve estimate is one of the main advantages of the RTM framework.

It is concluded that there are advantages such as the minimization of operational costs, increasing safety and a better resources management while adding real time data into the system through the portable x-rays fluoresce devices, which is an innovative sampling method proposal in the near future of the mining operations.

CHAPTER VII. WAY FORWARD

Rozman (1998) stated that any resource or reserve estimate is guaranteed to be wrong. Nevertheless, some are less wrong than others *(Beckhoff, B., Langhoff, N. et al.,2006)*. The work to be done concerning the update of mineral resources through fast data provided by hXRF devices could be improved in many stimulating perspectives.

It would be very important the execution of a good planning prior to any other campaign and an extended timetable in order to guarantee the acquisition of representative data. The collection of several data through the hXRF device is not made in one day since it depends on the production works.

Thus, the synergy between a new research and the mining company main interests should be established. The study could be better done if the region of interest and type of mineralization are previously well defined before to start the measurements. Therefore, a great among of data would be valid for the estimation and provide more accurate and reliable results.

Some adaptations could be considered regarding the parameters of reading time and the calibration factors. It is recommended to guarantee the calibration of the equipment with the same standards used in the laboratory before starting with the campaign. It would be also very interesting to integrate the behavior of the penalty elements such as As, Sb and Hg.

Despite the precision of the hXRF readings shows a better behavior when measuring low grades it is also important to motivate the study in the massive of copper and massive of zinc, where the equations provided in the bi-plots models shows values up to 90% of correlation.

In the second stage of the study, a simulation should be performed so it would be possible to obtain various scenarious with the same probability of occurrence. The stochastic simulation would quantify the local uncertainity through different levels while maintaining the initial data. The direct sequential simulation would be an interesting approach while integrating a reclassification according to the minor or major levels of uncertainity. After this process, the further step would be performing the reconciliation through the comparison between the created grade models through hXRF and the grades entering in the process plant.

CHAPTER VIII. BIBLIOGRAPHY

Azevedo. L. Soares. A. (2017) Springer. *Geostatistical methods for reservoir geophysics*. Page 1-141

Beckhoff, B., Kanngiber, B., Langhoff, N., Wedell, R., Wolff, H., (2006). *Handbook of Practical X-ray Fluorescence Analysis*. Springer. Germany. Page -1-783

Benndorf, J., Buxton, J., MWN, Nienhaus,K., Rattmann, L., Korre, A., Soares, A., deJong, A., Jeannee, N., Graham, P., Buttgereit, D., Gehlen, C., Eljkelkamp,F., Mischo, H., Sandtke,M. &Willsnack,T. (2015). Real-time mining. Moving towards continuous process management in mineral resource extraction. *Future Mining Conference*, page 1-10.Sidney

Benndorf, J., Osterholt, V. , (2015) Real-time optimization of extraction and the logistic process in highly complex geological and selective mining settings. Real-Time Mining under Horizon 2020 Grant Agreement.

Benndorf, J., Mike Buxton (2017). Proceedings of Real -Time Mining International Raw Materials Extraction Innovation Conference.

Brand, N. W., Brand, C. J., Perth, W. (2014). PERFORMANCE COMPARISON OF PORTABLE XRF INSTRUMENTS : A MINERAL EXPLORATION INDUSTRY This document was presented at the Denver X-ray Conference (DXC) on Applications of X-ray Analysis . Sponsored by the International Centre for Diffraction Data (ICDD).

Brown, T., Idoine, N., Hobbs, F., Mills, J. (2014). *European Mineral Statistics 2008-2012*.

Burrough and McDonnell. (1998). Principles of Geographical Information Systems. Oxford: Oxford University Press. Chapters 5 and 6.

Chales, C. (2017) Principles of rockbolting design. Journal of Rock mechanics and geotechnical Engineering. Vol. 9 Pages 396-414

Clark, I.. (2001). *Practical Geostatistics. Scotland* page 1-115

Clark, I. (2010) in his *Statistics or geostatistics? Sampling error or nugget effect?* Journal paper.

Canadian Securities Administrators. (2011). Rules and Policies. *National Instrument 43-101 Standards of Disclosure for Mineral Projects*, *2011*, 7043–7086.

Cannell, R. (2016). *Prospecting the Physicochemical Past. Three dimentional geochemical investigation into the use of space in Vicking Age sites in southern Norway using portable XRF.*Bournemouth University. United kingdom

Dogget, M. (1999). Global Mineral Exploration and Production- The Impact of Technology 50-Year Trends in Base-Metal and Gold Exploration Costs 50-Year trends in base-Metal and Gold discovery costs and Gold Production values 50-Year trends.Page 63-68

Dreibus, G. et al. (2003). refined data of Alpha Proton X-ray Spectrometer analyses of soils and rocks at the Mars Pathfinder site: Implications for surface chemistry.Vol.108

Emery, X., Ortiz, J., Rodriguez, J. (2004). Quantifying Uncertainty in Mineral Resources with Classification Schemes and Conditional Simulations. *Center for Computational Geostatistics Annual Report Papers*, *531*, 1–13.

Eurostat, European Commision. Sustainable development in the European Union. *2009 monitoring report of the EU sustainable development strategy.*

Le Vaillant. M. et al. (2014). Use and calibration of portable X-ray fluorescence analysers; applications to

lithogeochemical exploration for komatiite- hosted nickel-sulphide deposits, Geochemistry : Exploration, Envrionment Analysis

Freiberg, B. et al. (2017). *Proceedings of Real-Time Mining International Raw Materials Extraction* Innovation Conference 10th & 11th October. The Netherlands

Longoni, A. et al. (1998) A portable XRF spectrometer for non- destructive analysis in archaeometry. 409, Page 407-40

Fisher, B., Schnittger, S. (2012). *Autonomous and Remote Operation Technologies in the Mining Industry Benefits and Costs*. Page 1-53

Folha, 2016. *Avaliação das reservas mineiras do jazigo de Lagoa Salgada. Um contributo da Simulação Geostatística.* IST. Portugal

Gazley, M., Fisher, L. (2011). A Review of the Reliability and Validity of Portable X-ray Fluorescence Spectrometry (pXRF) Data. Page 1-14

Gazley et al. (2011). *3D Visualization of portable X-ray Fluorescence data to improve geological understanding and predict metallurgical performance at Plutonic Gold Mine*, Western Australia, Institute of Mining and Metallurgy, vol.120.

GEOMS user's guide

Goovaerts, P. (1999). Geostatistics in soil science: State-of-the-art and perspectives. *Geoderma*, *89*(1–2), 1–45.

Henckens, M., Ierland, Van, Driessen, P., Worrell, E. (2016). Mineral resources : Geological scarcity , market price trends , and future generations. *Resources Policy*, *49*, 102–111.

Hengl, T., Minasny, B., & Gould, M. (2009). A geostatistical analysis of geostatistics. *Scientometrics*, *80*(2), 491–514.

Holley, *S. (2017)Technical report Lundin Mining for the Neces Corvo Mine, Portugal. 2017*

Holler, S., Richardon, S. (2017)*. Energy and climate change environment infrastructure and utilities land and property mining and mineral estates waste resource management.*

International Copper Study Group*. Copper Market Forecast 2017/2018.* ICSG Press Release

Isaaks et al. (1989). *Applied Geostatistics*. OXFORD UNIVERSITY PRESS. New York.

Isaaks, E., Srivastava, M. (1991). An introduction to applied geostatistics. Oxford University Press. USA

Karaś, H. (2015). Robotics in mining. KGHM Polska Miedź. SPARC Topic Group, (June).

Karl, N., Wilburn, D. (2016) Annual *Exploration Review 2015.* U.S. Geological Survey. Mining Engineering Journal. Page 30-51

Kesler, B.(2002). Mineral Supply and Demand into the 21st Century.

Kelsey E., Evans C. et al. (2016). A review of the handheld X-ray fluorescence spectrometer as a tool for field geologic investigations on Earth and in planetary surface exploration. Applied Geochemistry. Vol 72. Pages 77-87

Kevin, L., A. 2008. *Tutorial introduction to autonomous systems. Vol. 41.Page 11720-11731*

Marques. R. (2016). Dissertação *Metodologia para controle de qualidade de minério e destinação de blocos de lavra usando raios-X.* Universidade Federal do Pampa.page 1-96

Martins (2006). Reabilitação ambiental de áreas mineiras do sector português da Faixa Piritosa Ibérica: estado de arte e perspectivas futuras. IGME. V.117. Page 289-304

Matheron, G. (1971). The theory of regionalized variables and its applications. *Les Cahiers Du Centre de Morphlogie Mathematique*.

Olea, R. A. (2008). Basic Statistical Concepts and Methods for Earth Scientists. *U.S. Geological Survey, Open-File Report 2008-1017*, 191.

Minnitt. R. (2007). The Southern African Institute of Mining and Metallurgy Analytical challenges in Metallurgy. *The impact on costs and decision making. 1-73.*

Moya, J., Boulamanti, A. (2016). European Commission, Joint Research Centre, Institute for Energy and Transport. Elsevier. *Production costs of the non-ferrous metals in the EU and other countries: Copper and zinc.1-7*

Olea, R. (2008). *Basic Statistical Concepts and Methods for Earth Scientists*. U.S. Geological Survey, Open-File Report 2008-1017, 191.

Scheuerer, M., Schaback, R.,Schlather, M. (2013). Interpolation of spatial data – A stochastic or a deterministic problem? *European Journal of Applied Mathematics*, *24*(4), 601–629.

Sinclair, A., Blackwell, G. (2004). *Applied Mineral Inventory Estimation*. *Cambridge University Press*.

Soares, A. (2006). *Geostatística para as ciências da terra e do ambiente.* IST Press. Page 1-210

SGEMS user's guide

Somarin A. K. (2013) *Using Thermo Scientif Portable XRF instruments for analyzing ore concentrates and grade control.* Thermo Scientif Portable Analytical Instruments Aplication Note.

Thermo Scientif Niton user's guide

Thrybom, L., Neander, Hansen, E., Landernäs, K. (2015). ScienceDirect Future Challenges of Positioning in Underground Mines Future Challenges of Positioning in Underground Mines. *IFAC-PapersOnLine*, *48*(10), 222–226.

Tobler. W. (1979). “Lattice Tunning”. Geographical Analysis. XI. 1. 36-44

Tobler. W. (1979). Journal of the American Statistical Association. Volume 74. Number 367. 519-536

United Nations Department of Economic and Social Affairs, P. D. (2017). World Population Prospects The 2017 Revision Key Findings and Advance Tables. *World Population Prospects The 2017*, 1–46.

Van Neuss, L. (2015). Why did the Industrial Revolution Start in Britain? *Available at SSRN 2696076*, 1–54. https://doi.org/10.13140/RG.2.1.2542.4721

Yusuf, A., Halima, S., Zakir, A., Abdullahi, M., Sani, K. (2014). *X-ray fluorescence: An accessible and effective technique for evaluation of hazards and economic potential associated with important mineral deposits in Nigeria*, Journal of Geology and Mining, Vol.6.

Not published documents:

Revês, I. (2016). *Relatório de estágio no departamento de Desenvolvimento Mineiro da Somincor*. Page 19-30

Soares E., (2017). *Proyeto de control de la dilución operativa*. Page1-31. Internship, Mexico.

Websites:

http://www.xmswiki.com/wiki/GSDA:TIN)

http://spatial-analyst.net

https://support.sas.com/

http://somincor.pt/pt

www.mine-engineer.com

www.realtime-minig.eu

www.nasa.gov

ANNEXES

A1. Exploratory Data Analysis

1st – Track

Neves deposit
FC/FE/MC/ME/MCZ/MZP
66 samples
box: 724.24 * 724.24 * 724.24
X - 3477.86;4202.1
Y - 2647.36;3371.6
Z - 459.98;1184.22

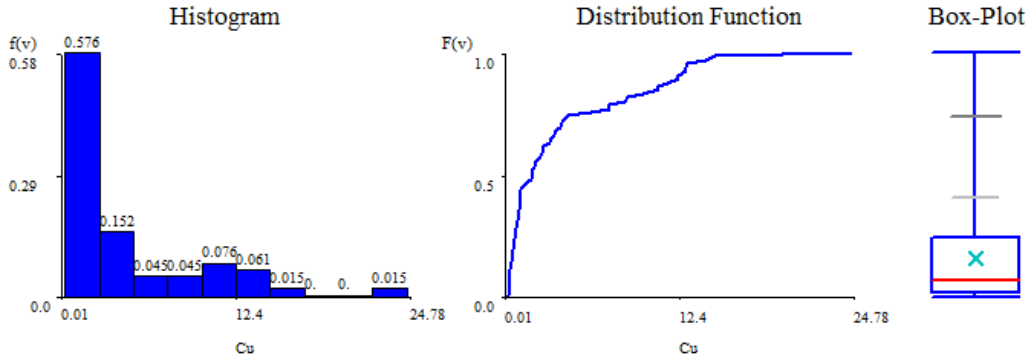

UNIVARIATE STATISTICS

Samples	: 66	Minimum	: 0.01	75 Perc	: 6.01	ANOMALOUS	
Mean	: 3.97	5 Perc	: 0.06	85 Perc	: 10.86	Large Maximum :	18.3
Variance	: 25.89	15 Perc	: 0.25	95 Perc	: 12.93	Minimum :	-14.82
St. Dev.	: 5.09	25 Perc	: 0.49	Maximum	: 24.78	Small Maximum :	10.02
Coef.Var.	: 1.28	Median	: 1.74	Coef. Skewness	: 1.71	Minimum :	-6.54

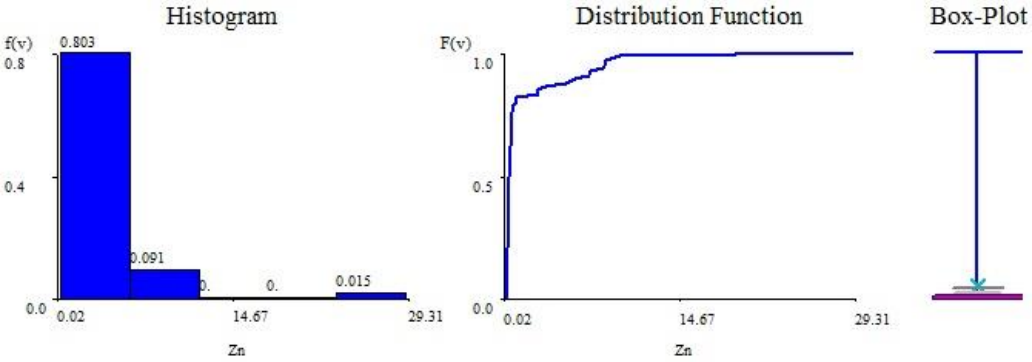

UNIVARIATE STATISTICS

Samples	: 66	Minimum	: 0.02	75 Perc	: 0.42	ANOMALOUS	
Mean	: 1.61	5 Perc	: 0.02	85 Perc	: 3.26	Large Maximum :	1.28
Variance	: 17.69	15 Perc	: 0.04	95 Perc	: 8.37	Minimum :	-0.94
St. Dev.	: 4.21	25 Perc	: 0.05	Maximum	: 29.31	Small Maximum :	0.72
Coef.Var.	: 2.62	Median	: 0.17	Coef. Skewness	: 4.67	Minimum :	-0.38

Figure 57 – Statistics for the 66 total samples within the Neves deposit though hXRF (GEOMS).

A2. Ordinary Kriging

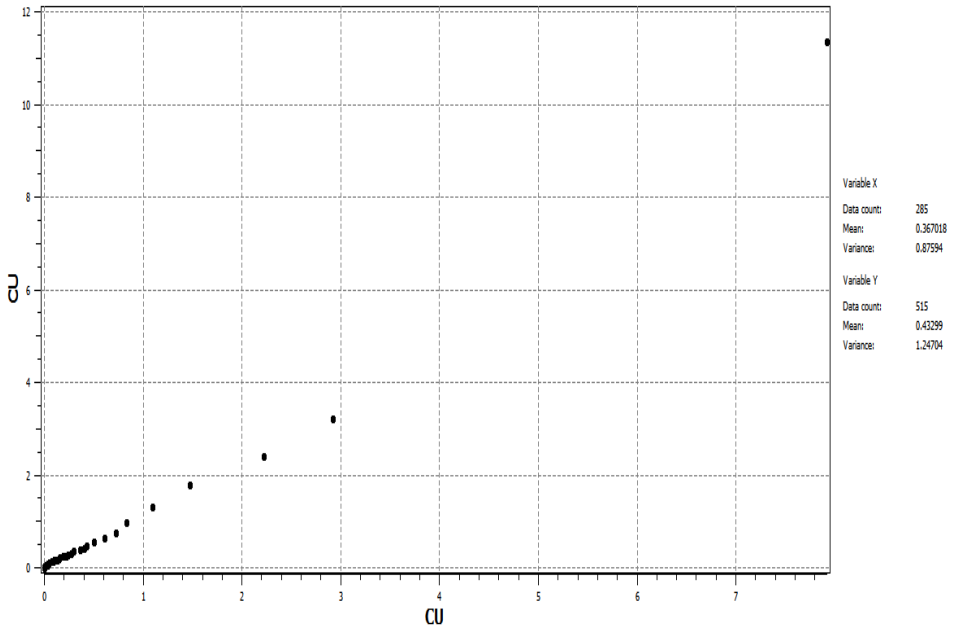

Figure 58 - Normal QQ plot between hXRF2 (x axis) and ALL (y axis)

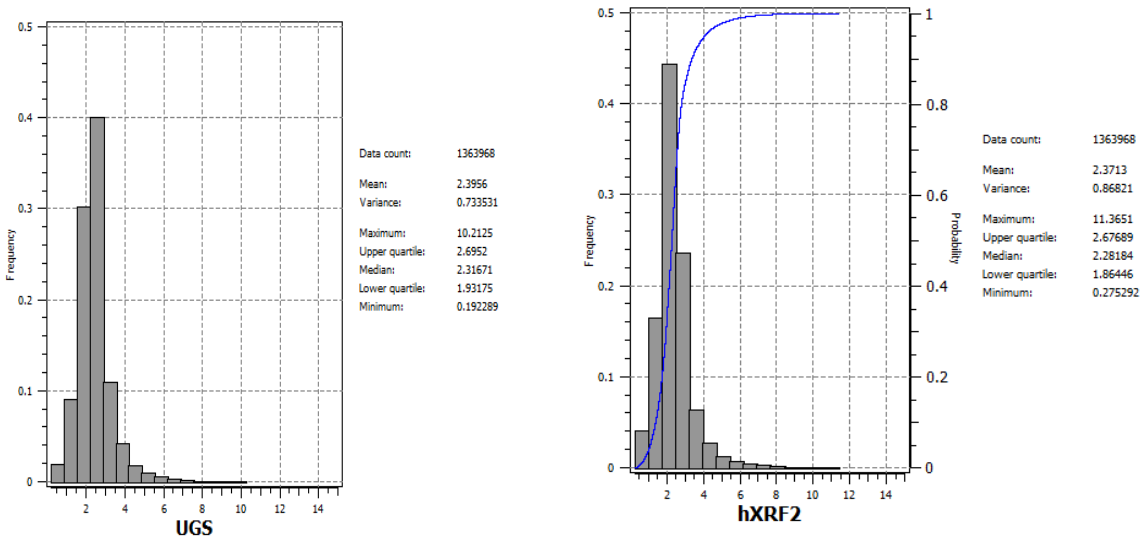

Figure 59 - Histograms for UGS and hXRF2 (SGEMS).

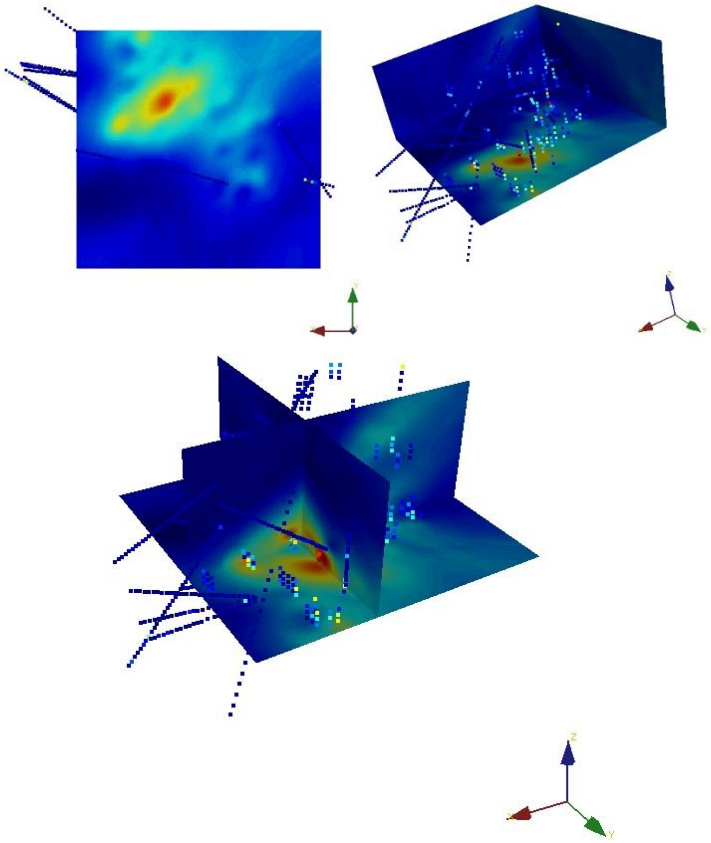

Figure 60 - After ordinary kriging results for Cu grades UGS + ALL (SGEMS).

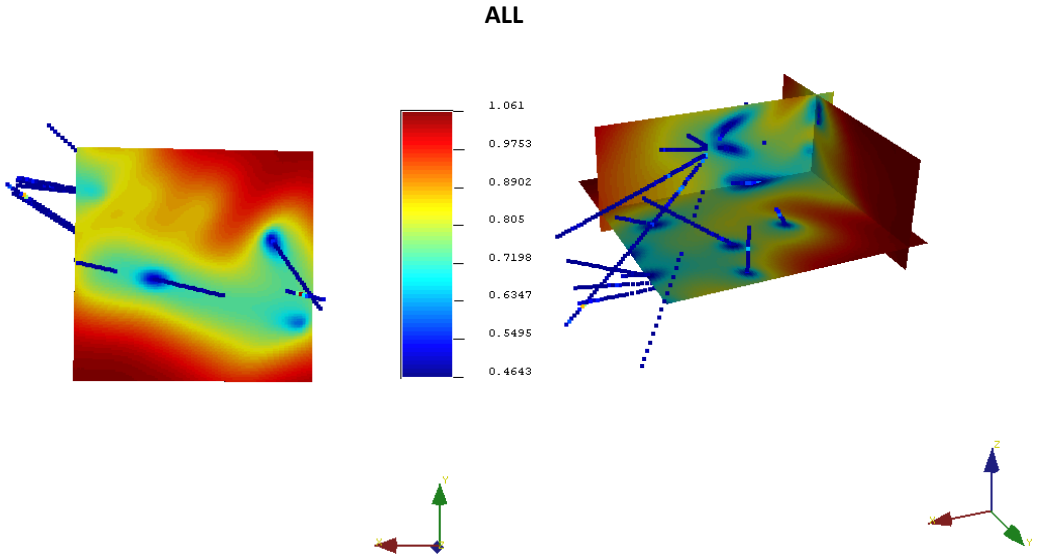

Figure 61 - After ordinary kriging results for ALL - variance of kriging (SGEMS).

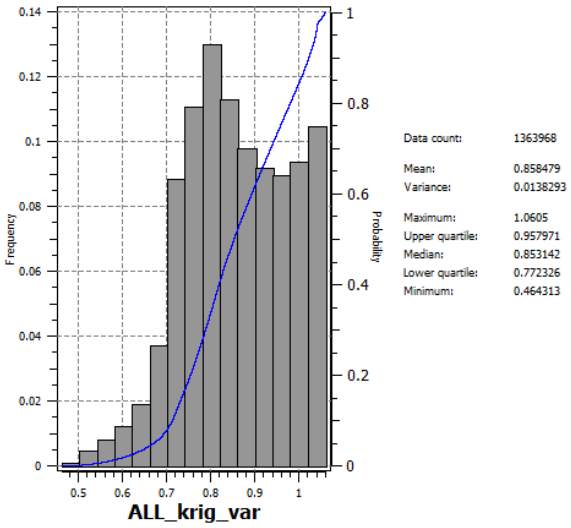

Figure 62 - Histogram variance of kriging for ALL (SGEMS)

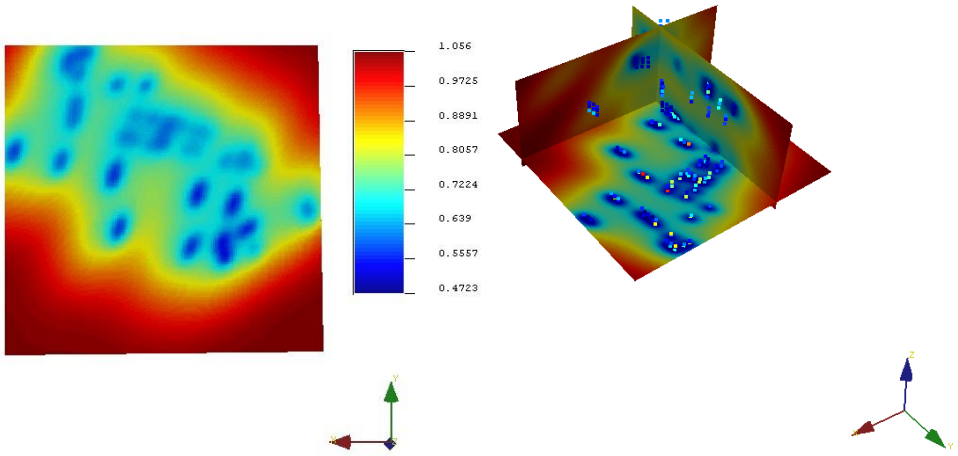

Figure 63 - After ordinary kriging results for UGS - variance of kriging (SGEMS).

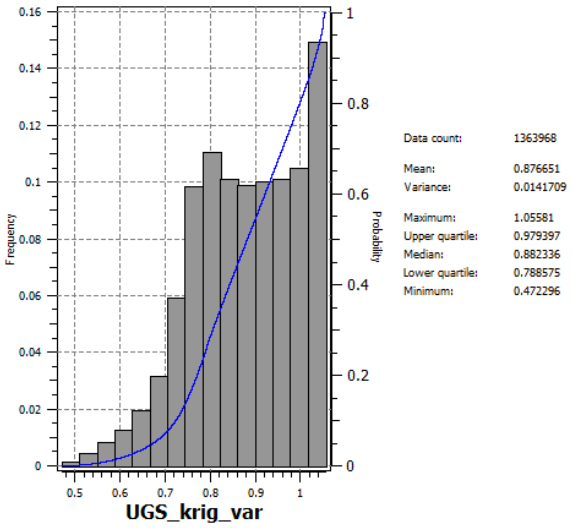

Figure 64 - Histogram variance of kriging for UGS (SGEMS)

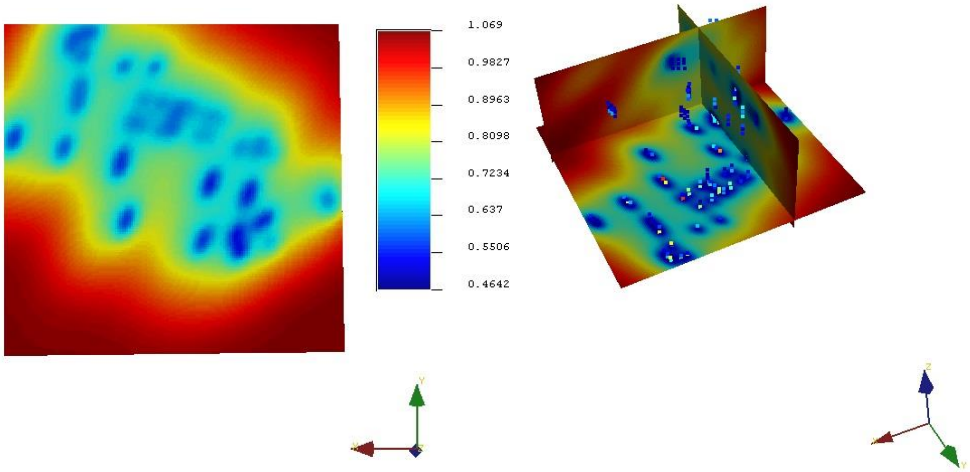

Figure 65 - After ordinary kriging results for hXRF2 - variance of kriging (SGEMS).

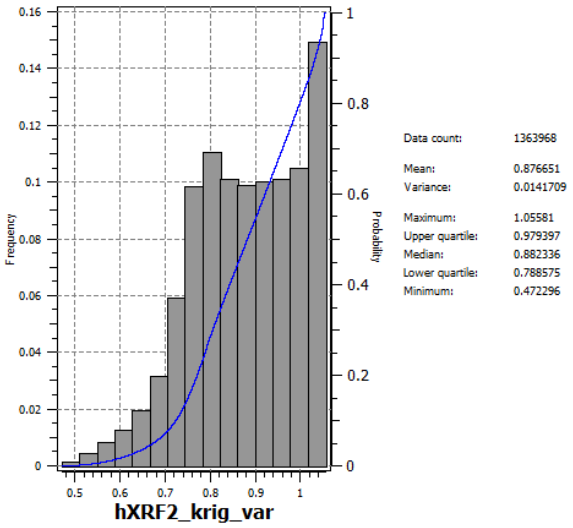

Figure 66 - Histogram variance of kriging for hXRF2 (SGEMS)

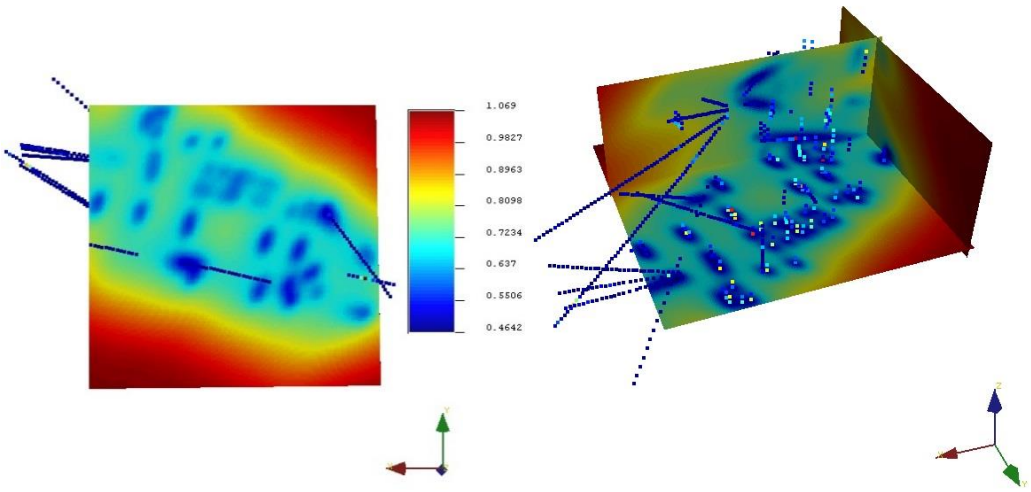

Figure 67 - After ordinary kriging results for UGS+ALL - variance of kriging (SGEMS).

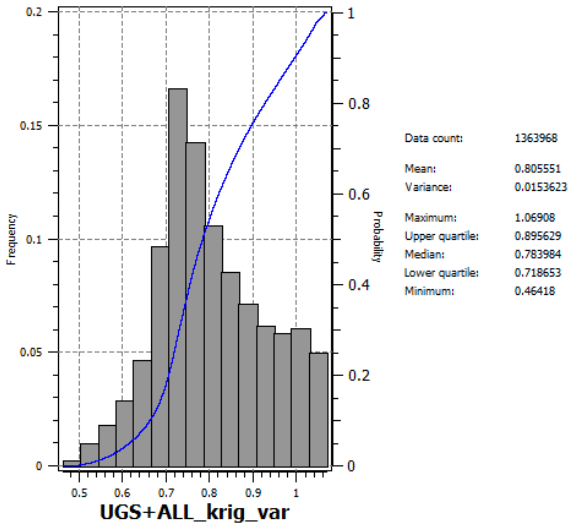

Figure 68 - Histogram variance of kriging for UGS+ALL (SGEMS)

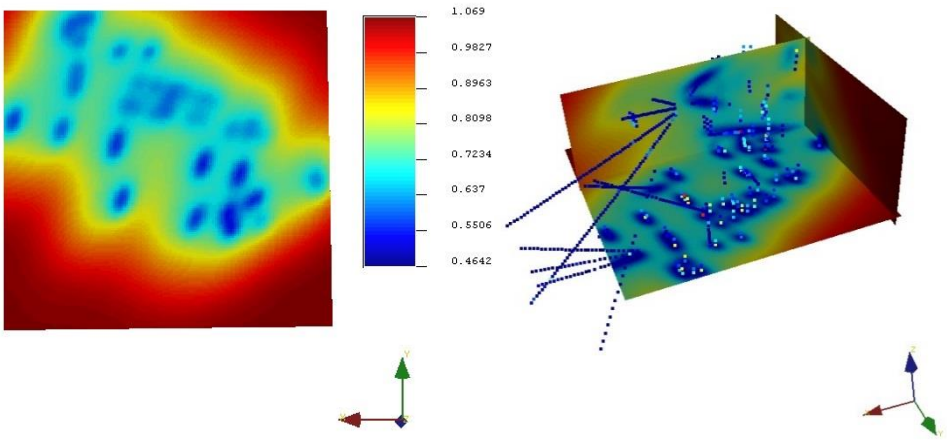

Figure 69 - After ordinary kriging results for hXRF2+ALL - variance of kriging (SGEMS).

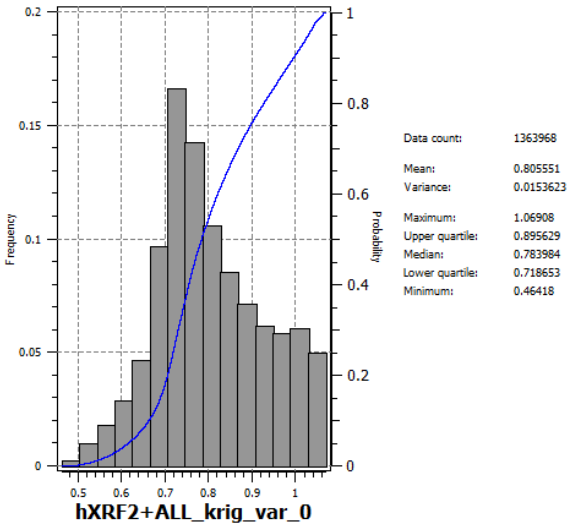

Figure 70 - Histogram variance of kriging for hXRF2+ALL (SGEMS)

A3. Resources estimation

Matlab

```
>> vars=who;
fMean = figure; %Figure 1
fTonnes = figure; %Figure 2
fMetal = figure; %Figure 3

tc = 0.7 : 0.1 : 2;
for j = 1 : length(vars)
   eval(['data = ', vars{ j },';']);


   lmask= repmat(data,1,numel(tc))>=repmat(tc, numel(data),1);
   for i = numel(tc):-1:1, mtc( i ) = mean( data( lmask( :, i ) ) ); end
   figure(fMean)
   hold on
   m( j )=plot(tc', mtc');
   hold off

   nb(j,:)=sum(lmask,1);
   vtc(j,:) = sum( lmask*0.5*0.5*0.5 );
   figure(fTonnes)
   hold on
   t( j ) = plot(tc', sum( lmask*4.5*0.5*0.5*0.5 )');
   hold off

   figure(fMetal)
   hold on
   qm( j ) = plot(tc', sum( (lmask*4.5*0.5*0.5*0.5).*repmat(data/100,1, numel(tc) ) )');
   hold off
end
```